Characterization of DnaJB6: a molecular chaperone implicated in LGMD type 1D

Frederik Emil Thomasen
St John's College
University of Oxford

A thesis submitted for the degree of
MSc by Research in Biochemistry
August 2019

Acknowledgements

A special thank you to Jason Schnell for supervision and Justin Benesch for co-supervision.

Thank you to Felipe Ossa for guidance on the project and day-to-day supervision in the laboratory.

Thank you to Shane Chandler for helping with mass spectrometry work.

Thank you to Tim Nott, Maike Bublitz and Christina Redfield for guidance in thesis committee meetings and transfer of status.

Thank you to all the people in the Schnell and Benesch groups for support.

Abstract

To maintain protein homeostasis, life has developed highly conserved networks of molecular chaperones and degradation machinery to assist in protein synthesis, quality control, maintenance, localization and degradation. J-proteins (HSP40s) are a family of co-chaperones that specifically bind misfolded target proteins for the HSP70 chaperone machinery. DnaJB6 is a human J-protein shown to suppress aggregation of misfolded disease-related proteins such as huntingtin, aβ42 and α-synuclein, either through the HSP70 pathway or independently. Mutations in DnaJB6 are associated with limb-girdle muscular dystrophy type 1D (LGMD1D). DnaJB6 contains a substrate binding domain (SBD) with low sequence complexity, especially enriched in S/T/G/F-residues, and possibly a separate C-terminal domain (CTD), but these regions of the protein remain largely structurally uncharacterized. DnaJB6 is also known to form polydisperse oligomers, but the mechanism and function of oligomerization remains unknown. In this work, DnaJB6 was recombinantly expressed, purified and characterized with focus on the properties of oligomerization, the effect of LGMD1D-associated mutations and structural features of the SBD and CTD. Native mass spectrometry indicated that the polydisperse oligomer-distribution is populated from 10-mer to 15-mer with both odd and even oligomers populated, excluding a homodimer as the smallest subunit of oligomerization. The mutation of 6 phenylalanines in the SBD resulted in a significant decrease in oligomerization propensity, while mutation of a positive charge-block of arginines only resulted in a small decrease, as determined by dynamic light scattering. At ionic strength shown to dissociate the DnaJB6 oligomer, holdase chaperone activity for aggregating insulin was lost, indicating that oligomerization is necessary for chaperone function. ^{1}H-^{15}N correlation NMR spectroscopy of DnaJB6 at oligomeric conditions indicated that regions of the protein remain flexible in the oligomer. Chemical shift perturbations from LGMD1D-associated mutations F89I, F91L and F93L, determined with a DnaJB6 residue 1-130 truncation construct, revealed that these mutations structurally perturb the J-domain of DnaJB6. Helix II and the HPD-motif of the J-domain, known to be important for binding to HSP70 and stimulation of HSP70 ATPase activity, were least structurally perturbed, and stimulation of HSP70 ATPase activity was not significantly affected by LGMD1D-associated mutations.

Contents

List of Figures **xi**

List of Tables **xiii**

Abbreviations **xv**

1 Introduction **1**
1.1 Proteostasis and chaperones 1
1.2 The HSP70 chaperone machinery 2
1.2.1 HSP70 substrate binding cycle 3
1.3 J-proteins 5
1.4 J-protein HSP70 interaction 6
1.5 DnaJB6 9
1.5.1 Domain architecture 10
1.5.2 Chaperone activity 11
1.5.3 Limb-girdle muscular dystrophy 12
1.5.4 Oligomerization 14
1.5.5 Structural modelling of DnaJB6 16
1.6 Aims 17
1.6.1 Structural characterization by NMR 17
1.6.2 Oligomerization 18
1.6.3 LGMD1D-associated mutations 18
1.6.4 Research questions 18

2 Materials and methods **21**
2.1 Constructs and cloning 21
2.1.1 Plasmid and constructs 21
2.1.2 Cloning 22
2.2 Protein expression and purification 24
2.2.1 Protein expression 24
2.2.2 Full length DnaJB6 purification 26
2.2.3 HSC70 and DnaJB6 residue 1-130 purification 27
2.2.4 SDS-PAGE 28

2.3 Protein characterization 28
2.3.1 Circular dichroism spectroscopy 28
2.3.2 Holdase activity assay 28
2.3.3 Dynamic light scattering 29
2.3.4 Native mass spectrometry 31
2.3.5 Nuclear magnetic resonance spectroscopy 31
2.3.6 ATPase activity assay 32

3 Results **35**
3.1 Expression and purification 35
3.1.1 Full length DnaJB6 35
3.1.2 DnaJB6 residue 1-130 37
3.1.3 HSC70 37
3.2 DnaJB6 is folded and active 39
3.3 Oligomeric full length DnaJB6 by NMR 40
3.4 Oligomerization 45
3.4.1 Native mass spectrometry 45
3.4.2 Mutational study of interactions in oligomerization 49
3.4.3 The effect of 1,6-hexanediol on oligomerzation 54
3.4.4 Oligomerization and holdase activity 55
3.5 LGMD1D mutations and the G/F-rich region 57
3.5.1 Chemical shift perturbations in the J-domain 57
3.5.2 Stimulation of HSP70 ATPase activity 64

4 Discussion **67**
4.1 Structure 67
4.2 Oligomerization 69
4.2.1 Populated oligomeric species 69
4.2.2 Oligomerization interaction 70
4.2.3 Oligomerization and holdase activity 72
4.3 LGMD1D mutations and the G/F-rich region 73
4.3.1 Correlation with clinical severity 75
4.3.2 The functional effect of LGMD1D-associated mutations . . . 75
4.4 Future work 76
4.4.1 Improvement of preliminary results 76
4.4.2 The functional effect of LGMD1D-associated mutation . . . 77
4.4.3 Oligomerization 78
4.4.4 Structural characterization 79
4.5 Conclusion 79

5 Appendix **83**

Bibliography **87**

List of Figures

1.1 Functional substrate binding/release cycle of HSP70 4
1.2 Structure of the human DnaJB1 (Hdj1) substrate binding domain homodimer 7
1.3 Structure of the *T. thermophilus* DnaJ2 homodimer 7
1.4 Conservation of J-domain structure 8
1.5 Structure of *E. coli* DnaK (HSP70) bound to the J-domain of DnaJ based on molecular dynamics simulation with NMR restraints . . . 9
1.6 Cartoon figure of DnaJB6 domain architecture 11
1.7 Sequence based disorder prediction and sliding net charge of DnaJB6 15
1.8 Structure of DnaJB6 dimer based on Robetta modelling with chemical crosslinking mass spectrometry restraints 17

2.1 Protein constructs 23
2.2 Mutational constructs of DnaJB6 24

3.1 SDS-PAGE gels of DnaJB6 purification 37
3.2 Size exclusion chromatography (SEC) traces and SDS-PAGE gels of DnaJB6 1-130 and HSC70 purifications 38
3.3 Far-UV circular dichroism (CD) spectrum of DnaJB6 39
3.4 Holdase activity assay with DnaJB6 40
3.5 ^{1}H-^{15}N BEST-TROSY spectrum of ^{15}N-labelled DnaJB6 43
3.6 Overlay of ^{1}H-^{15}N BEST-TROSY spectra of ^{15}N-labelled DnaJB6 full length and DnaJB6 1-130 44
3.7 Native mass spectrometry (MS) of DnaJB6 polydisperse oligomers . 46
3.8 Native mass spectrometry (MS) of DnaJB6 with collision induced dissociation (CID) 48
3.9 Example of dynamic light scattering to measure DnaJB6 oligomerization 49
3.10 Mutational study of DnaJB6 oligomerization by dynamic light scattering (DLS) 51
3.11 Oligomerization propensity of DnaJB6 mutant constructs by dynamic light scattering (DLS) 52
3.12 Effect of 1,6-hexanediol on DnaJB6 oligomerization by dynamic light scattering (DLS) 54

3.13 DnaJB6 holdase activity as a function of NaCl concentration 56
3.14 Overlay of ^{1}H-^{15}N BEST-TROSY spectra of ^{15}N-labelled DnaJB6 1-130 wild type and with LGMD1D-associated mutations F89I, F91L and F93L introduced 59
3.15 Zoom of peak shifts from overlay of ^{1}H-^{15}N BEST-TROSY spectra of ^{15}N-labelled DnaJB6 1-130 wild type and with LGMD1D-associated mutations F89I, F91L and F93L introduced 60
3.16 Chemical shift perturbations (CSPs) from LGMD1D-associated mutations F89I, F91L and F93L in DnaJB6 1-130 61
3.17 Chemical shift perturbations (CSPs) from LGMD1D-associated mutations (figure 3.16) plotted on homology model of DnaJB6 1-130 . 63
3.18 Effect of LGMD1D-associated mutations on DnaJB6 stimulation of HSC70 ATPase activity 64

4.1 Summary of results 74

5.1 Amino acid sequence of protein constructs with Strep-tag and TEV-cleavage site labelled 84
5.2 DnaJB6 amino acid sequence with secondary structure prediction (PSIPRED) 85
5.3 Protein sequence alignments 86

List of Tables

2.1 Protein constructs 22
2.2 Primers for generation of DNA constructs 25
2.3 Expression and purification buffers 26

3.1 Oligomerization propensities for DnaJB6 wild type and mutant constructs 53

5.1 Alignments % sequence identity 85

Abbreviations

ADP	Adenosine diphosphate
ATP	Adenosine triphosphate
BEST-TROSY	Band-selective excitation short-transient transverse relaxation optimized spectroscopy
CD	Circular dichroism
CHIP	C-terminus of Hsp70-interacting protein
CID	Collision induced dissociation
CSP	Chemical shift perturbation
CTD	C-terminal domain
DLS	Dynamic light scattering
DTT	Dithiothreitol
EDTA	Ethylenediaminetetraacetic acid
HEK293 cells	Human embryonic kidney 293 cells
HEPES	4-(2-hydroxyethyl)-1-piperazineethanesulfonic acid
HOP	Hsp70-Hsp90 Organizing Protein
HPD-motif	His-Pro-Asp-motif
HSP	Heat shock protein
HSQC	Heteronuclear single quantum coherence
IPTG	Isopropyl β-D-1-thiogalactopyranoside
LB media	Lysogeny broth media
LGMD1D	Limb girdle muscular dystrophy type 1D
MD	Molecular dynamics
MES	2-(N-morpholino)ethanesulfonic acid
MS	Mass spectrometry
Native-PAGE	Native polyacrylamide gel electrophoresis

NEF . . . . . Nucleotide exchange factor

NMR . . . . . Nuclear magnetic resonance

NOE . . . . . Nuclear Overhauser effect

NPC . . . . . Nuclear pore complex

PCR . . . . . Polymerase chain reaction

PRE . . . . . Paramagnetic relaxation enhancement

RBS . . . . . Ribosome binding site

SAXS . . . . . Small angle x-ray scattering

SBD . . . . . Substrate binding domain

SDS-PAGE . . Sodium dodecyl sulfate–polyacrylamide gel electrophoresis

SEC . . . . . Size exclusion chromatography

sHSP . . . . . Small heat shock protein

TEV . . . . . Tobacco Etch Virus

1 Introduction

Contents

1.1 Proteostasis and chaperones 1
1.2 The HSP70 chaperone machinery 2
1.2.1 HSP70 substrate binding cycle 3
1.3 J-proteins 5
1.4 J-protein HSP70 interaction 6
1.5 DnaJB6 9
1.5.1 Domain architecture 10
1.5.2 Chaperone activity 11
1.5.3 Limb-girdle muscular dystrophy 12
1.5.4 Oligomerization 14
1.5.5 Structural modelling of DnaJB6 16
1.6 Aims 17
1.6.1 Structural characterization by NMR 17
1.6.2 Oligomerization 18
1.6.3 LGMD1D-associated mutations 18
1.6.4 Research questions 18

1.1 Proteostasis and chaperones

Almost all biological processes involve proteins. In order to survive, cells must maintain protein homeostasis (proteostasis), ensuring the correct synthesis, quality control, maintenance, localization and degradation of its proteome [1].

One challenge the cell faces when maintaining proteostasis is the misfolding and aggregation of proteins. Proteins sample a complex free-energy landscape when folding, with kinetic barriers resulting in the population of intermediate folding states [2, 3]. Such kinetically trapped proteins may form non-native interactions that result in misfolding and aggregation [4].

To deal with the challenge of maintaining proteostasis, all domains of life have an integrated proteostasis network of molecular chaperones and protein degradation machinery. Molecular chaperones aid client proteins in acquiring their functionally active conformation. They assist newly synthesized proteins in folding correctly and efficiently in the crowded cellular environment, and also prevent and sometimes reverse aggregation of proteins [1]. Chaperone systems may also help in transfer of substrate proteins to cellular compartments or to the degradation machinery [1, 5].

Chaperones usually function in a cycle of substrate binding and release. This process can involve caging the substrate protein to allow for folding protected from the cellular environment. It can also involve binding of hydrophobic patches to prevent aggregation-causing interactions and to reverse misfolding [6]. Many chaperones are upregulated as a stress responses to for example increased temperature or oxidative stress, which may increase protein misfolding and aggregation [7].

Decline of the proteostasis network is thought to be a cause of aging, and many neurodegenerative diseases are associated with aggregates of amyloid-forming proteins, such as amyloid-β and Tau in Alzheimer's disease, α-synuclein in Parkinson's disease and huntingtin in Huntington's disease [1, 8].

1.2 The HSP70 chaperone machinery

Heat shock protein (HSP) 70s are a family of molecular chaperones with a wide array of functions in both cellular house-keeping and stress-response. HSP70 is a hub in the proteostasis network, with many modes of interaction with other chaperone

systems and degradation machinery [5]. One function of HSP70 is assisting the folding of newly synthesized proteins, after which substrate may be handed over for further folding assistance by the HSP90 system or the chaperonins [5,9]. HSP70 can also transfer substrate protein to the ubiquitin proteasome system or autophagy for degradation [5, 10]. In stress response, HSP70 has antiaggregation activity and can cooperate with small heat shock proteins (sHSPs) and HSP100 in protein disaggregation [11,12]. HSP70 does not only target unfolded, misfolded or aggregated protein, but also has roles in assisting functional protein. For example, HSP70 assists in translocating substrates across membranes to their targeted organelle and in disassembly of protein complexes, such as in clathrin-coated vesicles [13, 14].

In order to target diverse client proteins for a variety of possible functions, the HSP70 machinery makes use of co-chaperones. Co-chaperones are proteins that assist the HSP70 machinery in its function. For example, the co-chaperone HOP facilitates substrate handover to HSP90 and the co-chaperone CHIP is an E3 ubiquitin-protein ligase that assists in targeting substrates for degradation [9, 10, 15].

HSP70s are highly conserved across species from bacteria to eukaryotes. The human genome encodes 13 HSP70 homologs, with differences in tissue specificity, cellular localization, substrate recognition, target site localization (e.g. ribosomes or membrane translocons) and cooperation with co-chaperones [5].

1.2.1 HSP70 substrate binding cycle

Client binding by HSP70 functions as an ATP-dependent cycle of substrate binding and release mediated by co-chaperones with many coordinated allosteric conformational changes (figure 1.1). In the resting state, HSP70 exists in an ATP-bound state with a low basal level of ATPase activity. The ATP bound state has a low substrate binding affinity. A J-protein co-chaperone delivers substrate to HSP70; the association of substrate and J-protein promotes the ATPase activity of HSP70 by inducing a conformational change, freeing the nucleotide binding domain of

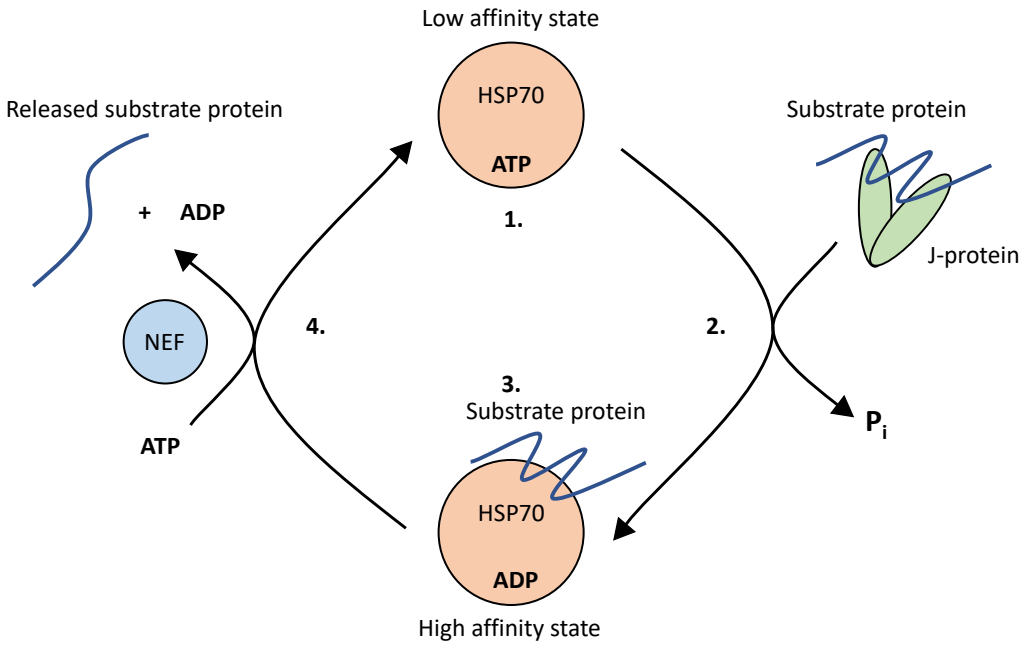

Figure 1.1: Functional substrate binding/release cycle of HSP70. **1.** HSP70 exists in an ATP-bound low substrate affinity state. **2.** Binding of a J-protein carrying misfolded/unfolded substrate protein results in increased ATPase activity. ATP is hydrolyzed and HSP70 undergoes a complex allosterically controlled conformational change. **3.** HSP70 is now in an ADP-bound high substrate affinity state with substrate protein bound. **4.** A nucleotide exchange factor (NEF) exchanges ADP for ATP and HSP70 undergoes a conformational change back to the low substrate affinity state resulting in release of substrate protein [5, 16].

HSP70 from a clamping mechanism. The presence of the J-protein is important, as substrate alone does not fully stimulate ATPase activity. Upon ATP-hydrolysis, the substrate protein is locked in place by a lid mechanism; HSP70 is now in its high-affinity substrate-bound state. To mediate the release of bound substrate, a nucleotide exchange factor (NEF) co-chaperone associates with HSP70 in the high-affinity state and exchanges ADP for ATP, resulting in a conformational change back to the low affinity-state and substrate release. The ATP-dependent cycling between affinities allows HSP70 to bind client proteins with high affinity but retain fast on/off rates. The co-chaperone activity of J-proteins allows for dynamic specificity towards diverse substrates [5, 16].

1.3 J-proteins

J-proteins, also known as HSP40s, are a diverse family of proteins that function in the HSP70 chaperone machinery. They are classified by the highly conserved J-domain, which is N-terminal in most J-proteins [17]. J-proteins function as co-chaperones for HSP70; they bind client proteins and pass them to HSP70, with specificity depending on the J-protein variant. Thus, J-proteins provide functional specificity to the HSP70 chaperone machinery [17]. J-proteins stimulate ATPase activity in HSP70 [18]. Upon ATP hydrolysis, HSP70 undergoes a conformational change, increasing its affinity for substrate [5]. J-proteins can also have antiaggregation activity independent of HSP70 [17]. This antiaggregation activity is independent of ATP hydrolysis, involving only the binding and "holding" of substrate, and has been coined holdase activity.

J-proteins are divided into three subfamilies: A, B and C. Type A has an N-terminal J-domain followed by a G/F-rich region of unknown function, a Cys-rich zinc-finger containing region and a C-terminal dimerization domain. Type A are considered the canonical J-proteins and have the strongest resemblance to the bacterial J-protein, DnaJ. Type B also consists of an N-terminal J-domain followed by a G/F-rich region, but has variable C-terminal regions. Type C is the most diverse category, as it simply consists of J-proteins that do not meet the requirements of type A or B. It should be noted that the subfamilies are distinguished only by these features, and as such do not describe function or substrate-specificity, which may be diverse within subfamilies [17].

The J-domain structure is highly conserved across species, overlaying well from bacteria to higher eukaryotes (figure 1.4). It is around 70 residues long and consists of four α-helices. A conserved HPD-motif in the loop between helix II and III in the J-domain is necessary for stimulation of HSP70 ATPase activity [17, 19, 20].

Despite being grouped within the same subfamily, there is still quite large variation in sequence between B-type J-proteins. This is evident from sequence alignment of DnaJB6 with DnaJB8 and DnaJB1 (appendix figure 5.3). DnaJB6 and 8 seem to have similar SBDs and CTDs, while DnaJB1 has less similarity in the SBD and C-terminus. In 2008, the structure of the substrate binding region of human DnaJB1 (then named Hdj1) was solved by X-ray crystallography (figure 1.2). The crystal structure revealed a homodimeric U-shaped structure of elongated monomers, with the dimer interaction at the C-terminus [21]. The structure overlays well with the previously solved structure of the B-type J-protein Sis1 from yeast [21, 22]. However, due to the variation in sequence discussed above, this structure may not be relevant to all B-type J-proteins; a distinct DnaJB6/8-like SBD and CTD may exist [17].

In 2013, the first structure of a full length and dimeric bacterial DnaJ, DnaJ2 from *T. thermophilus*, was solved by X-ray crystallography (figure 1.3). The structure agreed with the U-shaped structure of J-proteins previously determined. The crystal structure revealed that the G/F-rich region following the J-domain, previously expected to be flexible, is ordered and packing against the J-domain. This contact with the J-domain consists mainly of hydrophobic interactions with Phe residues in the G/F-rich region [23].

1.4 J-protein HSP70 interaction

The interaction between J-protein co-chaperones and HSP70 has been investigated in the bacterial DnaJ (J-protein) DnaK (HSP70) system. Nuclear magnetic resonance (NMR) spectroscopy revealed that helix II and the HPD-motif in the DnaJ J-domain comprise the binding site for interaction with DnaK [27]. Mutational study of residues in this region confirmed this finding [28]. A later study involving NMR and molecular dynamics simulations revealed that the interaction is of a

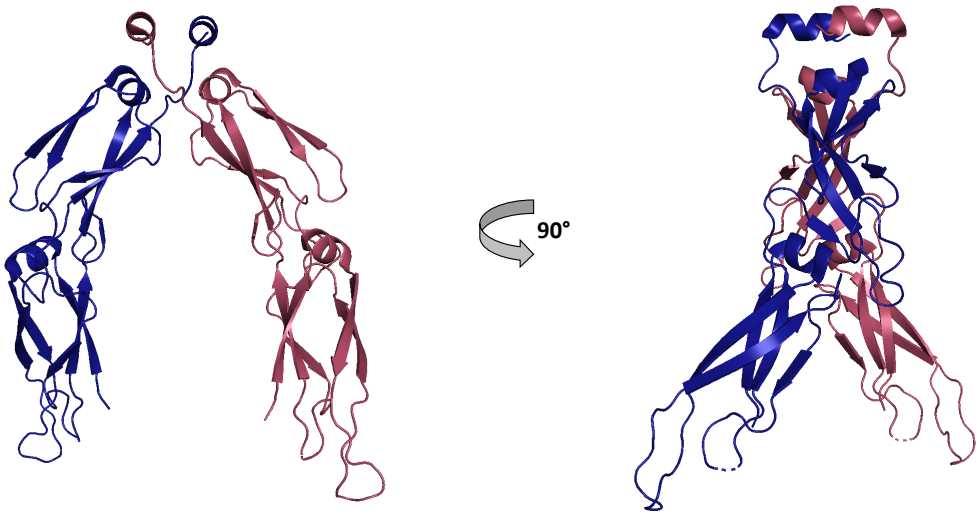

Figure 1.2: Structure of the human DnaJB1 (Hdj1) substrate binding domain (SBD) homodimer. The construct consists of residue 162 to 335 of DnaJB1 (Hdj1), with the exception of a short loop region (residues 228 to 230). The structure was solved by X-ray crystallography to a resolution of 2.7 Å. The dimer of elongated monomers form a U-shaped SBD, with the dimerization site at the C-terminus. A distinct DnaJB6/8-like SBD and C-terminal domain may exist. (PDB: 2QLD) [21].

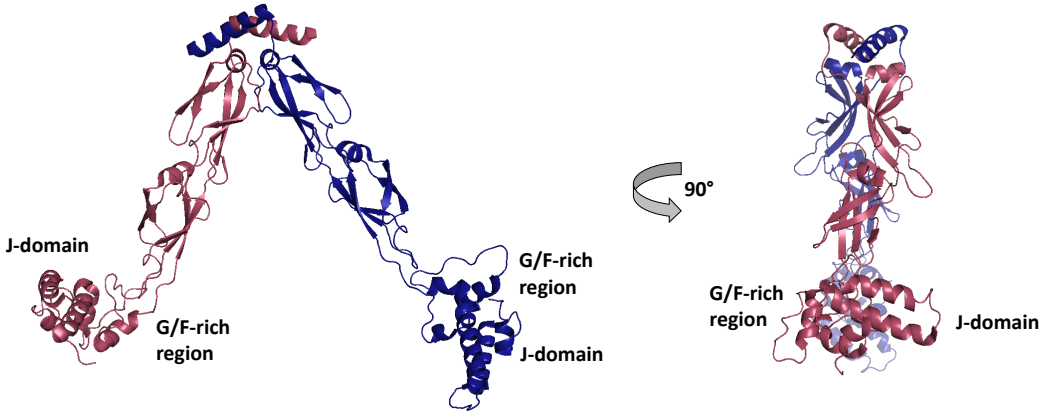

Figure 1.3: Structure of the *T. thermophilus* DnaJ2 homodimer. The structure was solved by X-ray crystallography to a resolution of 2.9 Å. The dimer of elongated monomers forms a U-shape, with the J-domains and G/F-rich region at the N-terminus (labelled), followed by the substrate binding domain (SBD) and C-terminal dimerization domain. While the structure of the J-domain and G/F-rich region are likely similar in DnaJB6/8, a distinct DnaJB6/8-like SBD and C-terminal domain may exist. (PDB: 4J80) [23].

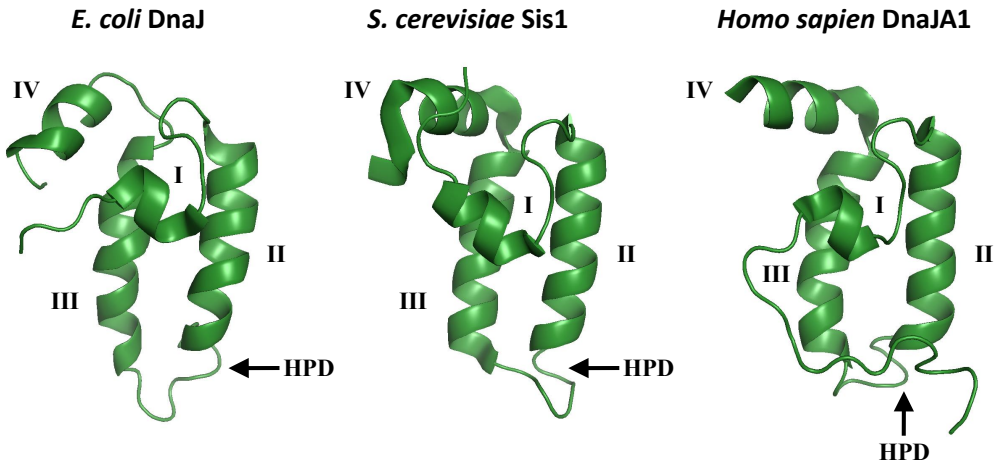

Figure 1.4: Conservation of J-domain structure. Cartoon representation of J-domains from *E. coli* DnaJ (PDB: 1BQ0) [24], *S. cerevisiae* Sis1 (PDB: 6D6X) [25] and *Homo sapien* DnaJA1 (PDB: 2M6Y) [26]. J-domains are the classifying feature of J-proteins and are highly conserved across species. α-helices are numbered and conserved HPD-motif is labelled. Backbone RMSDs between shown structures are: 2.61 Å between *E. coli* DnaJ and *Homo sapien* DnaJA1, 1.43 Å between *S. cerevisiae* Sis1 and *Homo sapien* DnaJA1, 2.58 Å between *E. coli* DnaJ and *S. cerevisiae* Sis1. Backbone RMSDs were determined with the "super" command in PyMOL.

dynamic character, with helix II of the J-domain scanning the surface of ADP and peptide-bound DnaK, and with the HPD-motif not being directly bound in the interaction [29] (figure 1.5).

In a study of *E. coli* HscA (HSP70) and HscB (J-protein) by NMR, the HPD-motif was shown to directly bind to HscA. Binding was observed to the ATP-bound state of HscA, but was abolished for the ADP-bound state. The nucleotide binding domain of HscA alone did not bind to HscB, indicating that the substrate binding domain (SBD) of HscA is also necessary for this interaction. Additionally, a second binding site for HscB was identified in the C-terminal region of HscA. Binding to this site was independent of whether HscA was in the ATP or ADP-bound state [30]. This illustrates the complexity of the J-protein-HSP70 interaction. The current model of J-domain interaction with HSP70 consists of the negatively charged helix II of the J-domain binding to the positively charged surface of the

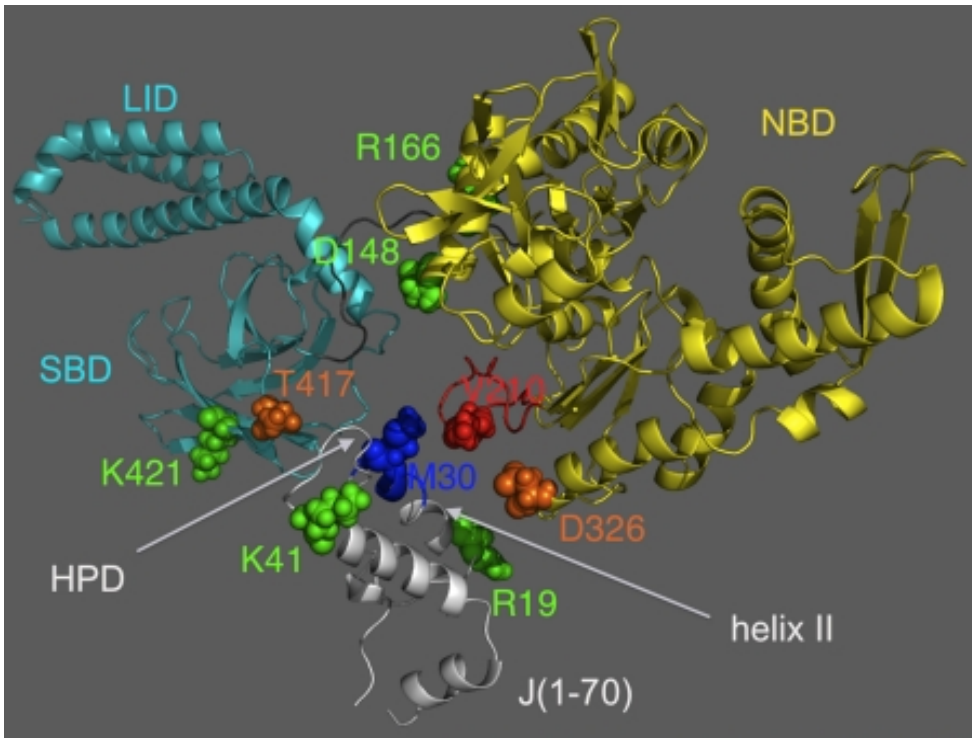

Figure 1.5: Structure of *E. coli* DnaK (HSP70) bound to the J-domain of DnaJ based on molecular dynamics (MD) simulation with NMR restraints (figure from Ahmad et al. 2011 [29]). The shown structure is the average position in an MD simulation with distance restraints determined by paramagnetic relaxation enhancement (PRE). The HSP70 binding site of the J-domain consists of helix II and the HPD-motif (labelled). The structure is colored as follows: DnaK nucleotide binding domain: Yellow, DnaK substrate binding domain with lid: Cyan, DnaJ J-domain (residue 1–70): white. Colored residues shown as spheres indicate PRE spin-labelling sites.

nucleotide binding domain of HSP70 in a dynamic manner with multiple contact points. The HPD-motif of the J-domain is necessary for this interaction, but is not necessarily directly bound to HSP70 [31].

1.5 DnaJB6

DnaJB6 is a human B-type J-protein co-chaperone functioning in the HSP70 chaperone machinery. It was first cloned in 1999 and was shown to be ubiquitously expressed in humans [32]. In 2002, it was discovered that expression of DnaJB6 (then named MRJ) is enriched in the central nervous system and inhibits the

toxicity of aggregation-prone huntingtin polyglutamines [33]. It was also discovered that DnaJB6 stimulates ATPase activity in HSP70, confirming its role as a co-chaperone [33].

DnaJB6 and its homolog DnaJB8 seem to have features distinct from the J-proteins for which the structures have been solved. They *do* contain the conserved J-domain and G/F-rich region, but they form polydisperse oligomers as opposed to dimers and they have a SBD distinct from the canonical bacterial DnaJ-type SBD for which structures are solved (appendix figure 5.3). Additionally, deacetylation of certain C-terminal Lys-residues by histone deacetylases (HDAC) is required for activity [17, 34].

DnaJB6 is found in two isoforms, a and b. Isoform a is 241 residues long and isoform b is 326 residues long. Isoform a contains a nuclear localization signal from residue 241-326 and differs in sequence from isoform b in residue 232-241. Otherwise, the sequences are identical. The shorter isoform b has been used for all experiments in this project.

1.5.1 Domain architecture

DnaJB6 consists of an N-terminal J-domain, followed by a SBD, predicted to be mostly disordered, and a C-terminal domain (CTD), predicted to contain β-strand (figure 1.6). The SBD has low sequence complexity; 67% of residues in the SBD and 81% of residues in the S/T-rich region (a subregion of the SBD) are either Ser, Thr, Gly or Phe, with the region following the J-domain being especially G/F-rich and the more C-terminal region being especially S/T-rich. The demarcation of a CTD is based on the prediction of β-strand content (appendix figure 5.2) and conservation between DnaJB6 and its homolog DnaJB8 (appendix figure 5.3).

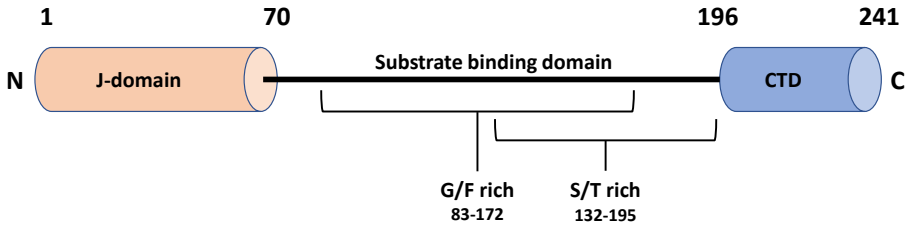

Figure 1.6: Cartoon figure of DnaJB6 domain architecture. Residue 1-69 is the conserved J-domain characteristic of J-proteins (orange). Residue 70-195 is the substrate binding domain (SBD). This domain has low sequence complexity with a region enriched in G/F-residues and a region enriched in S/T-residues. The SBD is predicted to be disordered from around residue 100. Residue 196-241 is possibly a separate C-terminal domain (blue), based on secondary structure prediction and conservation in DnaJB8.

1.5.2 Chaperone activity

DnaJB6 and its homolog DnaJB8 were identified as the most potent suppressors of polyglutamine aggregation in a screen of the HSP70 machinery proteins [34]. It has since been shown *in vitro* that DnaJB6 inhibits polyglutamine aggregation at low substoichiometric concentrations, even in the absence of HSP70 [35]. Deletion of the residues 149-186 in the S/T-rich region causes loss of chaperone activity for polyglutamines, and S/T-to-A mutations in the S/T-rich region (residue 132-195) also results in loss of chaperone activity in a dose dependent manner [34, 36]. This effect has also been shown with overexpression of polyglutamines in HEK293 cells [36]. As such, the residue 132-195 S/T-rich region has been identified as the substrate binding site of DnaJB6. It has been suggested that the large number of hydroxyl groups participate in hydrogen bonding with the target substrate in a cooperative manner, resulting in the dose dependence of chaperone activity on S/T-residues [36, 37].

In vivo, it has been shown that DnaJB6 reduces polyglutamine huntingtin-induced toxicity in *Xenopus laevis* [34]. DnaJB6 has also been studied in a mouse

model, where it was discovered that brain-specific overexpression could reduce huntingtin aggregation and delay disease onset [36].

Polyglutamine peptides are not the only client of DnaJB6. Knock-out of DnaJB6 in HEK293 cells resulted in higher levels of α-synuclein aggregation, and the phenotype could be rescued by reintroduction of DnaJB6 [38]. As opposed to what has been observed for polyglutamines, suppression of α-synuclein aggregation is dependent on the presence of HSP70, indicating that the mechanism of DnaJB6 chaperone activity could depend on the substrate [38].

DnaJB6 also inhibits aggregation of aβ42 amyloid fibril formation *in vitro*. Mutational study of the S/T-rich region again revealed that antiaggregation activity depends on S/T-residues in a dose-dependent manner, as it does for polyglutamines [37].

Aggregation of huntingtin, α-synuclein and aβ42 is associated with Huntington's, Parkinson's and Alzheimer's disease respectively [39]. The specificity of DnaJB6 towards these substrates and its potential role in decreasing their toxicity makes the protein an important target for study.

1.5.3 Limb-girdle muscular dystrophy

Mutations in the DnaJB6 gene are associated with the disease limb-girdle muscular dystrophy type 1D (LGMD1D). Multiple missense mutations and a splice site mutation causing LGMD1D have been discovered by genetic sequencing of patients. The mutations include F89I, F91I, F91L, F93I, F93L, P96R, F100V and a splice site mutation in exon 5 of DnaJB6. The missense mutations are located in the G/F-rich region following the J-domain and the splice site mutation results in deletion of this region (residue 79-115) [40].

Studies in various animal models have revealed that both knock-down of DnaJB6 and introduction of LGMD1D mutations result in muscle pathology. Morpholino knock-down of DnaJB6 in zebrafish resulted in loss of muscle integrity, but the

phenotype could be rescued by reintroduction of DnaJB6 [41]. In a *Drosophila melanogaster* model, disease-linked protein aggregation could be rescued by co-expression of wild type MRJ (fly homolog of DnaJB6) but not LGMD1D associated MRJ [42]. Finally, expression of DnaJB6 F93L in a transgenic mouse model resulted in pathological features similar to LGMD1D [43].

Clinically, the phenotype of LGMD1D is variable in age of disease on-set, muscle involvement and overall disease severity. There seems to be a correlation between the LGMD1D genotype and clinical presentation [40]. In order to represent a variety of clinical severities, the mutations F91L, F89I and F93L - ordered from most to least severe clinical severity - have been chosen for study in this project.

The function of the G/F-rich region in DnaJB6 is poorly understood. Because these mutations are located in the G/F-rich region and have a detrimental effect on healthy DnaJB6 activity, they provide a framework for studying the function of the G/F-rich region. A number of possible functions necessary for healthy DnaJB6 activity could be impaired by LGMD1D mutations. These include substrate recognition and binding, interaction with HSP70, substrate passing to HSP70, stimulation of HSP70 ATPase activity, oligomerization, localization, expression level, protein stability or an entirely different unknown function.

A likely candidate seems to be that LGMD1D mutations interfere with binding to HSP70 and stimulation of HSP70 ATPase activity. As previously mentioned, the G/F-rich region of bacterial DnaJ packs against the J-domain with hydrophobic contacts made by Phe-residues [23]. It is possible that the LGMD1D-implicated mutations disrupt this interaction, subsequently perturbing helix II and the HPD-motif of the J-domain and disrupting the interaction with HSP70 and/or stimulation of HSP70 ATPase activity.

1.5.4 Oligomerization

DnaJB6 forms polydisperse homo-oligomeric complexes. Oligomerization has been observed by dynamic light scattering (DLS), size exclusion chromatography (SEC), native PAGE [35] and SEC-coupled small angle x-ray scattering (SAXS) [44], with which oligomers as large as 1.48 MDa have been observed. One sub-species of DnaJB6 oligomer has been analyzed by negative stain electron microscopy, revealing a spherical, cage-like structure [44].

In DnaJB8, a homolog of DnaJB6, deletion of residues 149-186 removes oligomerization [34]. This region corresponds to the S/T-rich region of DnaJB6, indicating that this may be the site of the oligomerization interaction. Additionally, in a study using intersubunit chemical crosslinking in the DnaJB6 oligomer, the crosslinks K189-K189 and K232-K232 were identified [44]. As the cut-off of these crosslinking restraints is 40 Å, this does not exclude the S/T-rich region as the oligomerization site. However, the exact oligomerization site of DnaJB6 and the interactions responsible for driving the association of oligomers remains unknown.

Interaction-types in oligomerization

Analysis of the amino acid sequence of DnaJB6 reveals that there are two blocks of negative charge and two blocks of positive charge from around residue 100 to the C-terminus. The charge-blocks are organized in a sequence motif of negative-positive-neutral-positive-negative (figure 1.7b). Additionally, this region has low sequence complexity, with a high content of Ser, Thr, Gly and Phe. It has been shown that mutation of Ser- and Thr-residues in this region of DnaJB6 does not affect oligomerization [36], but the role of Gly and Phe sequence content has not been investigated. The region is predicted to be disordered (figure 1.7a) and overlaps with the suspected oligomerization site based on study in DnaJB8 [23].

The SBD of DnaJB6 has characteristics associated with proteins that function in liquid-liquid phase separation. A main identifier is intrinsic disorder [46].

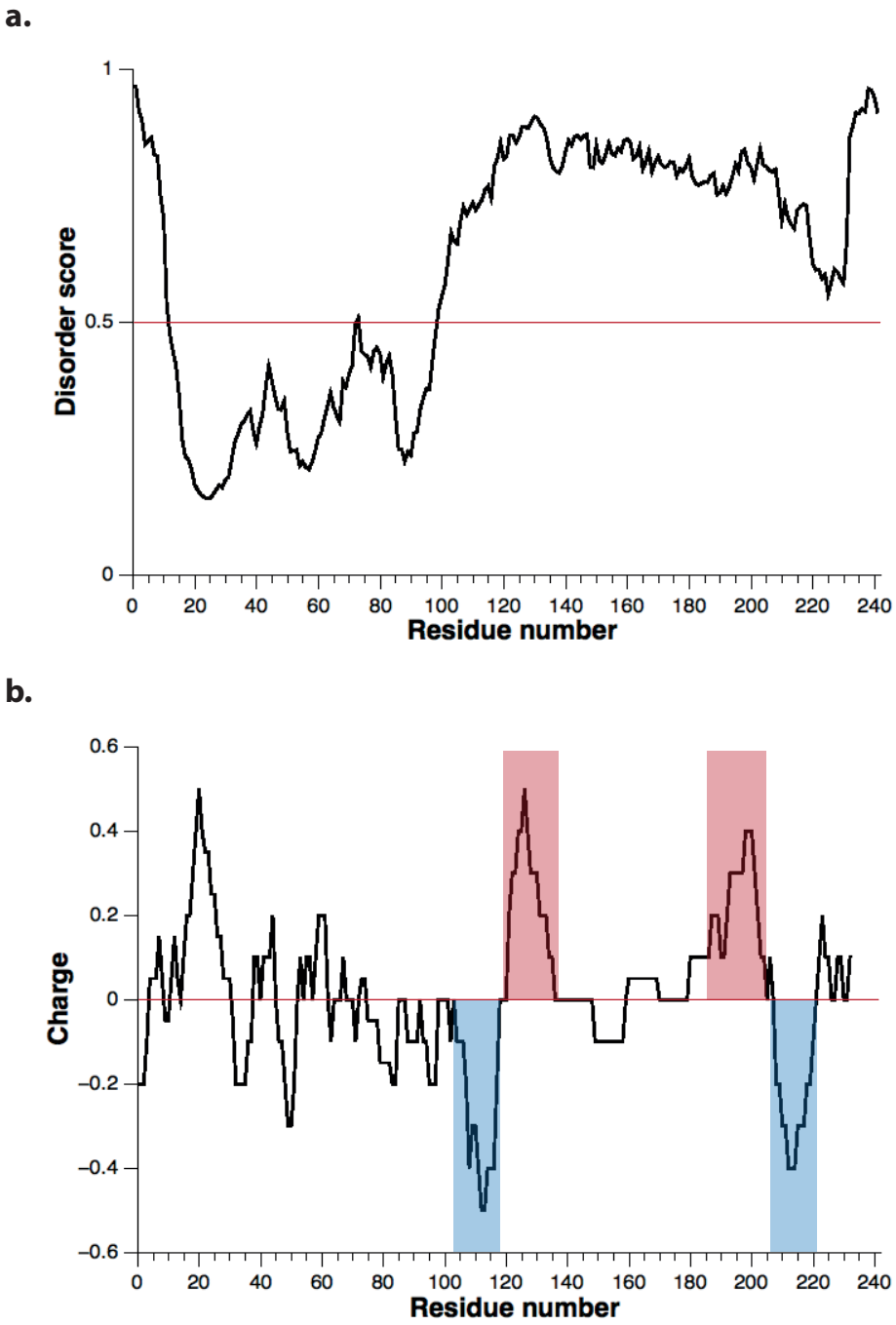

Figure 1.7: Sequence based disorder prediction and sliding net charge of DnaJB6. **a.** Prediction of intrinsic disorder in DnaJB6 using PONDR-FIT [45], a meta-predictor of intrinsic disorder based on cross-validation from eight disorder predictors. **b.** Sliding net charge in the DnaJB6 sequence, with a sliding window size of 10 residues. In the substrate binding domain, positive and negative charge-blocks are marked in red and blue respectively.

Additionally, blocks of electrostatic charge in the amino acid sequence have been shown to be important for phase separation [46, 47]. Cation-pi and pi-pi interactions have also been identified as important interaction-types in driving phase separation [46, 48], implicating the high Phe sequence content and electrostatic charge content.

Another system with similarities to the sequence characteristics of DnaJB6 is the nuclear pore complex (NPC). Phenylalanines in disordered FG-repeat regions of nucleoporins in the NPC have been shown to be important for forming dynamic interactions with nuclear transport factor [49,50]. Interestingly, FG-repeat regions of nucleoporins also interact with each other [51], meaning that this type of interaction *could* be a mode of intersubunit interaction in DnaJB6 oligomers.

1.5.5 Structural modelling of DnaJB6

The structure of full length DnaJB6 has not been experimentally determined. In a 2018 article by Söderberg et al., the protein structure prediction software Robetta (a version of Rosetta) was used to generate *de novo* structure predictions of DnaJB6, and the best structural model was chosen based on chemical-crosslinking mass spectrometry restraints [44]. The proposed structure is compactly folded and does not resemble the elongated structure of canonical J-proteins. Based on this structure, a DnaJB6 dimer model was also proposed (figure 1.8). However, the structural model of DnaJB6 has not been further experimentally validated and the existence of a DnaJB6 dimer has not been experimentally confirmed.

The proposed DnaJB6 structure does not contain a long intrinsically disordered region in the SBD as predicted (figure 1.7a), but predicts a globular fold. This inconsistency in prediction of the DnaJB6 SBD structure provides incentive for structural investigation of the SBD.

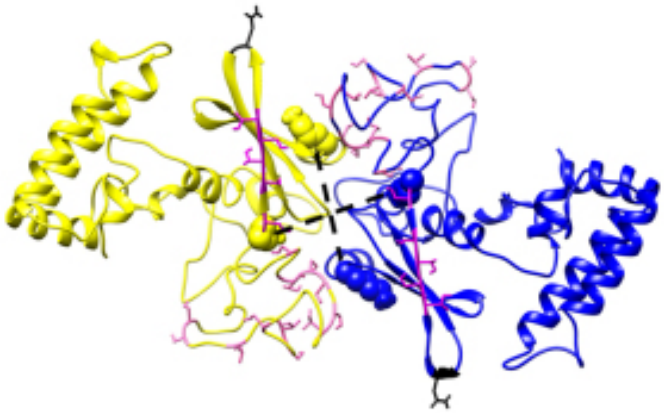

Figure 1.8: Structure of DnaJB6 dimer based on Robetta modelling with chemical crosslinking mass spectrometry (MS) restraints (figure from Söderberg et al. 2018 [44]). Structures of DnaJB6 were modelled using Robetta. A monomer structure was selected based on chemical crosslinking MS restraints. Monomers were docked into the shown dimer structure using HADDOCK with restraints from K189-K189 and K232-K232 crosslinks. Residues K189 and K232 are shown as spheres with the inter-subunit crosslinks indicated with dashed lines. Functionally important S/T-residues are shown in pink. Residues N199, G200 are shown in black.

1.6 Aims

1.6.1 Structural characterization by NMR

The SBD of DnaJB6 is an interesting target for study, as it differs in sequence from the domains of canonical J-proteins [17] and is predicted to be mostly disordered (figure 1.7a). The SBD is possibly observable by NMR spectroscopy due to the predicted flexibility, despite the formation of large oligomers with otherwise poor relaxation properties.

An aim of this project is to obtain a ^{1}H-^{15}N correlation spectrum of DnaJB6 under oligomeric conditions. This is to be done as a "proof of concept", showing that future study of full length DnaJB6 by NMR is possible. Additionally, such a spectrum may allow for preliminary structural characterization using previously obtained assignments from a DnaJB6 residue 1-130 construct (not a part of this work) and identification of certain residue types based on chemical shift.

1.6.2 Oligomerization

An aim of this project is to determine which oligomeric species are populated in the polydisperse distribution of DnaJB6 oligomers. This will be investigated by native mass spectrometry (MS).

Inspired by similarity to the sequence characteristics of FG-repeat regions of nucleoporins and liquid/liquid phase separating proteins, another aim of this project is to investigate whether charge-blocks and phenylalanine content in a potentially intrinsically disordered G/F-rich region of DnaJB6 could be driving the association of oligomers.

The functional role of DnaJB6 oligomerization remains unknown. Another aim of this project is to determine whether oligomerization is a requirement for DnaJB6 holdase chaperone activity.

1.6.3 LGMD1D-associated mutations

The structural and functional effect of LGMD1D-associated mutations on DnaJB6 remains unknown. An aim of this project is to determine the structural effect of LGMD1D-associated mutations on the J-domain of DnaJB6 by using NMR to determine chemical shift perturbations (CSPs) caused by selected mutations. Another aim is to determine the effect of these mutations on stimulation of HSP70 ATPase activity.

1.6.4 Research questions

Structural characterization:

- Is it possible to characterize full length DnaJB6 under oligomeric conditions by NMR?

Oligomerization:

- Which oligomeric species are populated by DnaJB6?

- Are phenylalanine content and charge-blocks in the DnaJB6 sequence important for the oligomerization interaction?
- Is oligomerization necessary for DnaJB6 holdase activity?

LGMD1D-associated mutations:

- Do LGMD1D-associated mutations F89I, F91L and F93L perturb the structure of the J-domain?
- Do LGMD1D-associated mutations F89I, F91L and F93L affect the stimulation of HSP70 ATPase activity by DnaJB6?

2 Materials and methods

Contents

2.1 Constructs and cloning 21
2.1.1 Plasmid and constructs 21
2.1.2 Cloning 22
2.2 Protein expression and purification 24
2.2.1 Protein expression 24
2.2.2 Full length DnaJB6 purification 26
2.2.3 HSC70 and DnaJB6 residue 1-130 purification 27
2.2.4 SDS-PAGE 28
2.3 Protein characterization 28
2.3.1 Circular dichroism spectroscopy 28
2.3.2 Holdase activity assay 28
2.3.3 Dynamic light scattering 29
2.3.4 Native mass spectrometry 31
2.3.5 Nuclear magnetic resonance spectroscopy 31
2.3.6 ATPase activity assay 32

2.1 Constructs and cloning

2.1.1 Plasmid and constructs

All protein expression was performed with the plasmid vector pPSG-IBA105 (IBA Lifesciences). The vector encodes ampicillin resistance and allows for cloning of twin-Strep-tag fusion constructs under a bacteriophage T7 promoter.

All DnaJB6 constructs were expressed as twin-Strep-tag fusion constructs with a TEV protease cleavage site for removal of the Strep-tag. HSC70 was expressed as a twin-Strep-tag fusion construct, but without a TEV site for removal of the Strep-tag. The DnaJB6 N-terminal Strep-tag construct was used for early stages of the project. As C-terminal degradation products proved to be a problem, the DnaJB6 C-terminal Strep-tag construct was cloned to remove C-terminal degradation products in the purification. This construct was used in later stages of the project. DnaJB6 isoform b was used for all experiments. A schematic of all the constructs used in this work can be seen in figure 2.1.

The mutant constructs F6A, R5K and R5A were used for mutational study of the properties of oligomerization in DnaJB6 (figure 2.2). These mutations were introduced in the DnaJB6 N-terminal Strep-tag construct. LGMD1D-implicated mutations F89I, F91L and F93L were introduced in the DnaJB6 residue 1-130 construct.

Table 2.1: Protein constructs

Name	Amino acid boundary	Mutations
DnaJB6	1-241	None
DnaJB6 F6A	1-241	F140A, F144A, F150A, F157A, F164A, F180A
DnaJB6 R5K	1-241	R126K, R127K, R130K, R133K, R135K
DnaJB6 R5A	1-241	R126A, R127A, R130A, R133A, R135A
DnaJB6 1-130	1-130	None
DnaJB6 1-130 F89I	1-130	F89I
DnaJB6 1-130 F91L	1-130	F91L
DnaJB6 1-130 F93L	1-130	F93L
HSC70	1-646	None

Table of protein constructs showing construct name, amino acid boundary and mutations.

2.1.2 Cloning

- C-terminal Strep-tag DnaJB6 was cloned by three-fragment Gibson Assembly (NEB). DNA fragments were obtained from PCR with plasmid pPSG-IBA105 encoding DnaJB6 N-terminal Strep-tag as template.

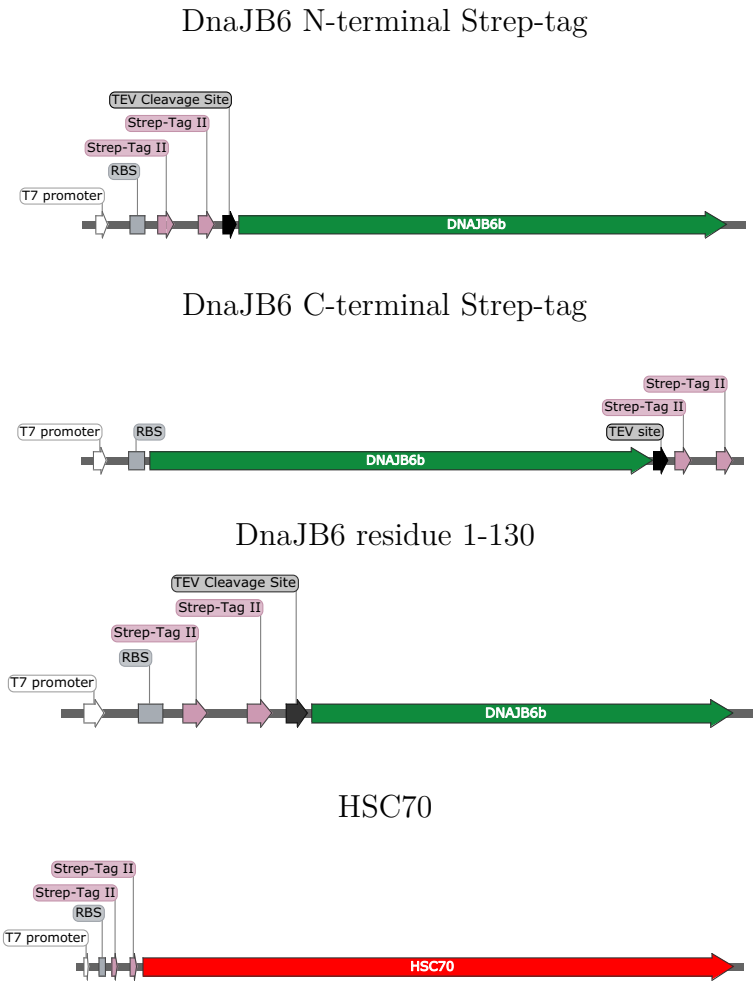

Figure 2.1: Protein constructs. Cartoon shows T7 promoter and ribosome binding site (RBS) used for protein expression. The open-reading-frame contains twin-Strep-tag, TEV-cleavage site and protein sequence.

- F6A, R5K and R5A constructs were cloned by two-fragment Gibson Assembly (NEB). Insert DNA fragment for F6A construct was ordered as a synthetic gene from GeneArt gene synthesis (Thermo Fisher). DNA fragments for R5K and R5A constructs were obtained from PCR with plasmid pPSG-IBA105 encoding DnaJB6 N-terminal Strep-tag as template.

- LGMD1D mutations F89I, F91L and F93L were introduced with GeneArt Site-Directed Mutagenesis (Thermo Fisher) with plasmid pPSG-IBA105 encoding DnaJB6 1-130 as template.

Figure 2.2: Mutational constructs of DnaJB6. F6A introduces 6 Phe-to-Ala mutations in the residue 139-188 region of the substrate binding domain. R5K introduces 5 Arg-to-Lys mutations in the residue 125-136 positive charge-block. R5A introduces 5 Arg-to-Ala mutations in the residue 125-136 positive charge-block.

All cloning was performed according to the manufacturer's manual for the respective cloning kit. All plasmids were sent for sequencing at Source Bioscience to confirm that cloning was successful.

2.2 Protein expression and purification

2.2.1 Protein expression

E. coli BL21(DE3) were transformed with plasmid by heat-shock transformation and plated on LB agar + 100 µg/mL ampicillin. Plates were incubated overnight at 37°C. A single colony was inoculated to start a 500 mL LB media + 100 µg/mL ampicillin primary culture, incubated overnight at 30°C. Primary culture was transferred to 1 L LB media + 100 µg/mL ampicillin secondary cultures to reach $OD_{600} = 0.1$. Secondary cultures were incubated at 37°C until $OD_{600} = 0.8$ and protein expression was induced with 1 mM isopropyl β-D-1-thiogalactopyranoside (IPTG).

For isotope labelling with ^{15}N, secondary cultures were pelleted by centrifugation at 10,980 x g (5500 RPM) for 15 minutes in a JLA-8.1000 rotor (Beckman Coulter). Four 1 L cultures were washed in 1 L M9 minimal media (salts only), centrifuged

Table 2.2: Primers for generation of DNA constructs

DnaJB6 with C-terminal Strep-tag:	
Strep-tag forward	5'-TGCTGCGCTTGGATAACAAGGAAAACCTG TACTTCCAGGGTGCCAGCGCATGGAGTCATC CTCAATTCGAG-3'
Strep-tag reverse	5'-GGGTGGCTCCCTTAGCTCCCTTATCCCAT TCCGGATTTTTCGAACTGCG-3'
DnaJB6 forward	5'-TTTAAGAAGGAGATATACAAATGGTGGAT TACTATGAAGTTCTAGGCGTGC-3'
DnaJB6 reverse	5'-CTTGTTATCCAAGCGCAGCAGCTG-3'
Plasmid forward	5'-GGGAGCTAAGGGAGCCACCCGCAAG-3'
Plasmid reverse	5'-TTGTATATCTCCTTCTTAAAGTTAAACAA AATTATTTCTAGAGGGAAACC-3'
DnaJB6 R5A and R5K:	
R5A forward	5'-TTGAGGACTTCTTTGGGAATGCGGCGGGT CCCGCGGGAAGCGCGAGCGCGGGGACGGGG TCGTTTTTCTC-3'
R5K forward	5'-TTGAGGACTTCTTTGGGAATAAAAAAGGT CCCAAAGGAAGCAAAAGCAAAGGGACGGGG TCGTTTTTCTC-3'
R5A and R5K reverse	5'-GTTGAAGTTGATATCGATTTGAAGTTGC-3'
Plasmid forward	5'-AAATCGATATCAACTTCAACTAAAATGGTT-3'
Plasmid reverse	5'-ATTCCCAAAGAAGTCCTCAAAAGG-3'
DnaJB6 F6A:	
Plasmid forward	5'-AAATCGATATCAACTTCAACTAAAATGGTT-3'
Plasmid reverse	5'-CGACCCCGTCCCTCGGCTTC-3'
DnaJB6 1-130 F89I, F91L and F93L:	
F89I forward	5'-ACAGTCCATTTGAAATTGGCTTCACATTCCG-3'
F89I reverse	5'-CGGAATGTGAAGCCAATTTCAAATGGACTGT-3'
F91L forward	5'-CATTTGAATTTGGCCTCACATTCCGTAACCC-3'
F91L reverse	5'-GGGTTACGGAATGTGAGGCCAAATTCAAATG-3'
F93L forward	5'-AATTTGGCTTCACACTCCGTAACCCAGATGA-3'
F93L reverse	5'-TCATCTGGGTTACGGAGTGTGAAGCCAAATT-3'

Primers used for PCR to generate DNA fragments used for cloning of DNA constructs.

again and resuspended in 1 L M9 minimal media with 1 g/L $^{15}NH_4Cl$. The culture was incubated for 15 minutes at 37°C before induction of protein expression with 2 mM IPTG.

After induction, cultures in LB media were incubated for 3 hours at 37°C for protein expression. Cultures in M9 minimal media for isotope labelling were incubated for 16 hours at 37°C for protein expression. Cultures were pelleted by centrifugation at 10,980 x g (5500 RPM) for 15 minutes in a JLA-8.1000 rotor (Beckman Coulter), supernatant was discarded and the cell pellet resuspended in 25 mL lysis buffer per 1 L culture (lysis buffer 1 for full length DnaJB6 and lysis

buffer 2 for DnaJB6 1-130 and HSC70). DNase I (Roche) and 10 mM $MgCl_2$ were added to resuspended cell pellets and resuspended cell pellets were stored at -80°C.

Table 2.3: Expression and purification buffers

DnaJB6 (full length):	
Lysis buffer 1	50 mM NaP_i, 500 mM NaCl, 8 M urea, 1 mM EDTA, 0.03% NaAzide, pH 8.0
Elution buffer 1	50 mM NaP_i, 500 mM NaCl, 4 M urea, 1 mM EDTA, 0.03% NaAzide, 50 mM biotin, pH 8.0
Standard buffer 1	20 mM NaP_i, 150 mM NaCl, 1 mM EDTA, 0.03% NaAzide, pH 8.0
TEV protease buffer	20 mM Tris-HCl, 300 mM NaCl, 5 mM DTT, 5% glycerol, pH 7.5
DnaJB6 (1-130) and HSC70:	
Lysis buffer 2	50 mM NaP_i, 300 mM NaCl, 1 mM EDTA, 0.03% NaAzide, pH 8.0
Standard buffer 2	20 mM NaP_i, 20 mM NaCl, 0.03% NaAzide, pH 7.2
Elution buffer 2	20 mM NaP_i, 20 mM NaCl, 0.03% NaAzide, 2.5 mM desthiobiotin, pH 7.2
TEV protease buffer	20 mM Tris-HCl, 300 mM NaCl, 5 mM DTT, 5% glycerol, pH 7.5

Table of buffers used in expression and purification of DnaJB6 (full length), DnaJB6 1-130 and HSC70.

2.2.2 Full length DnaJB6 purification

The frozen cell pellet was thawed and cell lysis was performed by sonication on ice with a QSonica Q700 sonicator. The lysate was cleared by ultracentrifugation at 234,998 x g (45,000 RPM) for 45 minutes in a Type 45 Ti rotor (Beckman Coulter). The cleared supernatant was purified by Strep-tag affinity chromatography with a StrepXT (IBA lifesciences) gravity flow column. The column was washed with 50 mL lysis buffer 1. Protein was eluted with 30 mL elution buffer 1. Flow-through, wash and elution fractions were collected and analyzed by SDS-PAGE. The elution fraction, containing DnaJB6, was dialyzed against 4 L standard buffer 1 for protein refolding. 0.5 mg TEV protease per 1 L biomass was added to the sample and the sample was transferred to dialysis against 4 L TEV protease buffer for 16 hours for cleavage of the Strep-tag. The sample was then run through a reverse Ni affinity chromatography gravity flow column to remove His-tagged TEV protease. The flow through from the reverse Ni column, containing DnaJB6, was dialyzed against 4 L standard buffer 1 and concentrated with a 10 kDa molecular weight cut-off

centrifugal filter. Protein concentration was determined by measuring absorbance at 280 nm with a nanodrop spectrophotometer (Thermo Fisher) (theoretical extinction coefficient ε= 0.015930 μM^{-1} cm^{-1} for construct with C-terminal Strep-tag, and ε= 0.014440 μM^{-1} cm^{-1} for construct with N-terminal Strep-tag). Sample purity was evaluated by SDS-PAGE.

2.2.3 HSC70 and DnaJB6 residue 1-130 purification

The frozen cell pellet was thawed and cell lysis was performed with a Constant Systems CF cell disruptor at 30 kpsi pressure. The lysate was cleared by ultra-centrifugation at 234,998 x g (45,000 RPM) for 45 minutes in a Type 45 Ti rotor (Beckman Coulter). The cleared supernatant was purified by Strep-tag affinity chromatography with a Strep-Tactin (IBA lifesciences) gravity flow column. The column was washed with 50 mL standard buffer 2. Protein was eluted with 30 mL elution buffer 2. Flow-through, wash and elution fractions were collected and analyzed by SDS-PAGE. For DnaJB6 1-130, 0.5 mg TEV protease per 1 L biomass was added to the elution fraction and the sample was transferred to dialysis against 4 L TEV protease buffer for 16 hours to cleave the Strep-tag. The sample was then run through a reverse Ni affinity chromatography gravity flow column to remove His-tagged TEV protease. This was not done for HSC70, as the HSC70 construct did not contain a TEV-cleavage site. The sample was concentrated with a 10 kDa (for DnaJB6) or 30 kDa (for HSC70) molecular weight cut-off centrifugal filter and purified by SEC with a Superdex S200 Increase 10/300 GL column (GE) in standard buffer 2. Fractions were collected and analyzed by SDS-PAGE. Fractions containing DnaJB6 or HSC70 were pooled. Protein concentration was determined by measuring absorbance at 280 nm with a nanodrop spectrophotometer (Thermo Fisher) (theoretical extinction coefficient ε= 0.014440 μM^{-1} cm^{-1} for DnaJB6 1-130

and ε= 0.044350 μM^{-1} cm^{-1} for HSC70). Sample purity was evaluated by SDS-PAGE. For samples to be used for ATPase activity assays, EDTA was left out of all buffers and NaP_i was replaced with HEPES.

2.2.4 SDS-PAGE

Bolt 12% Bis-Tris Plus (Invitrogen) gels were used with Bolt MES SDS running buffer (Novex) for SDS-PAGE. Samples were prepared as 5 µL protein sample and 5 µL NuPAGE LDS sample buffer (Novex). The molecular weight marker SeeBlue Plus2 (Thermo Fisher) was used. Gels were run at 200 V for 40 minutes and stained with InstantBlue Coomassie Blue (Expedeon).

2.3 Protein characterization

2.3.1 Circular dichroism spectroscopy

Circular dichroism (CD) spectroscopy was performed with a Jasco J-815 Spectropolarimeter with a Peltier temperature control unit in a 1 mM path-length quartz cuvette. Sample conditions were 10 µM protein in buffer 20 mM NaP_i, 20 mM NaCl, pH 7.2 at 20°C. 9 accumulations from 190 to 250 nm at a scan rate of 100 nm/minute were used for the final spectrum.

2.3.2 Holdase activity assay

DnaJB6 holdase activity was determined with an assay based on inducible insulin aggregation. Insulin aggregation was induced with DTT in the presence and absence of DnaJB6. Insulin aggregation was then followed over time by measuring light scattering at 360 nm with a Cary 50 UV-vis spectrophotometer (Agilent). Assays were carried out in a 400 µL reaction volume quartz cuvette. Absorbance (360 nm) was normalized so the sigmoidal curves have a baseline 0 and plateau 1.

Initial holdase activity assay was performed with 50 µM insulin induced by 25 mM DTT. The experiment was performed in the absence of DnaJB6 and with 5 and 25 µM full length DnaJB6. 25 µM DnaJB6 1-130 was used as a negative control. Assays were performed in triplicates. The assay was performed in buffer 20 mM NaP_i, 20 mM NaCl, pH 7.2 at room temperature.

Holdase activity assay under varying salt concentrations was performed with 75 µM insulin induced by 50 mM DTT. The assay was performed in buffer (20 mM NaP_i, 1 mM EDTA, 0.03% NaAzide, pH 7.2) with 150 mM, 750 mM and 1.5 M NaCl at room temperature. Each salt concentration was tested in the presence and absence of 50 µM DnaJB6.

2.3.3 Dynamic light scattering

DLS measurements were made with a Viscotek 802 instrument at 20°C. Samples were filtered in a 0.22 µm pore size cellulose acetate centrifugal filter prior to DLS experiments. The software OmniSIZE 3.0 was used for instrument control, calculation of sample viscosity and data processing. DLS was used to quantify the population of monomeric and oligomeric DnaJB6 in a sample. Examples of DLS spectra can be seen in appendix figure 3.9. As each experiment was internally normalized, DLS data was compared by integrating monomer and oligomer peaks to calculate the percentage population of monomer and oligomer:

$$\%monomeric = \frac{\int monomer\,peak}{\int monomer\,peak + \int oligomer\,peak}$$

$$\%oligomeric = \frac{\int oligomer\,peak}{\int monomer\,peak + \int oligomer\,peak}$$

Ionic strength

To test the dependence of DnaJB6 oligomerization on solvent ionic strength, DLS experiments were performed in buffer 20 mM NaP_i, 1 mM EDTA, 0.03% NaAzide, pH 8.0 with a range of NaCl concentrations. 3 M or 5 M NaCl buffer was mixed with 150 mM NaCl buffer and DnaJB6 sample to reach the desired NaCl concentration and a protein concentration of 50 µM DnaJB6. Samples were prepared in duplicates with NaCl concentrations from 150 mM to 1050 mM in steps of 100 mM. This was done for DnaJB6 wild type and the mutant constructs F6A, R5K and R5A.

Protein concentration

To test the dependence of DnaJB6 oligomerization on protein concentration, DLS experiments were performed at a range of DnaJB6 concentrations from 10 µM to 60 µM in steps of 10 µM in buffer 20 mM NaP_i, 150 mM NaCl, 1 mM EDTA, 0.03% NaAzide, pH 8.0. The experiment was performed in duplicates. This was done for DnaJB6 wild type and the mutant constructs F6A, R5K and R5A. For the F6A construct, measurements at protein concentrations of 100 and 150 µM were added, as the oligomeric state was not fully populated at 60 µM.

A logistic equation was fit (Levenberg–Marquardt algorithm) to the data describing oligomerization as a function of protein concentration:

$$f(x) = A2 + \frac{A1 - A2}{1 + (x/Kd)^p}$$

A dissociation constant K_d was determined from the fit, describing the equilibrium between monomer and all species of oligomer.

1,6-hexanediol

To test the dependence of DnaJB6 oligomerization on the presence of 1,6-hexanediol, DLS experiments were performed with 50 µM DnaJB6 in 20 mM NaP_i, 150 mM NaCl,

1 mM EDTA, 0.03% NaAzide, pH 8.0 with 1%, 4% and 8% (volume) 1,6-hexanediol. A negative control without 1,6-hexanediol was also prepared. After the addition of 1,6-hexanediol, samples were incubated on a rotary tube mixer at room temperature. DLS measurements were recorded at 20 minutes, 90 minutes and 23 hours.

2.3.4 Native mass spectrometry

Instrument control for native MS was performed by Dr. Shane Chandler from the Benesch Group (Department of Chemistry, University of Oxford). To optimize sample conditions for native MS, buffer exchange of the DnaJB6 sample was attempted in a centrifugal filter unit to 200 mM, 400 mM and 600 mM ammonium acetate pH 8.0, 200 mM ammonium acetate pH 7.2 and 200 mM ammonium bicarbonate pH 7.9, and by dialysis to ammonium acetate pH 8.0 and pH 7.2. The Native MS data presented here was collected on a Water's Instruments Synapt G1 mass spectrometer with a sample of 30 µM DnaJB6 in buffer 200 mM ammonium acetate pH 7.2, buffer exchanged by dialysis. A mass spectrum was collected prior to and after collision induced dissociation (CID) of DnaJB6 oligomers. The software MassLynx 4.1 (Water's Instruments) was used for data processing. Peak assignment was performed with the software UniDec [52], and assignments were subsequently inspected manually with the help of Dr. Shane Chandler.

2.3.5 Nuclear magnetic resonance spectroscopy

NMR experiments with full length DnaJB6 were performed with a Bruker Avance II 750 MHz (^{1}H) spectrometer with a TCI cryoprobe. NMR experiments with DnaJB6 residue 1-130 were performed with a Bruker Avance III HD 950 MHz (^{1}H) spectrometer. The BEST-TROSY (Band-selective excitation short-transient transverse relaxation optimized spectroscopy) pulse sequence [53, 54] was used for all experiments. The software NMRpipe [55] was used for data processing and the

software NMRFx Viewer [56] for data analysis.

The ^{1}H-^{15}N heteronuclear single quantum coherence (HSQC) spectrum of the DnaJB6 1-130 construct had been assigned previously by Dr. Felipe Ossa in the Schnell Group (Department of Biochemistry, University of Oxford). Assignments were transferred to the ^{1}H-^{15}N BEST-TROSY spectrum of DnaJB6 1-130 based on overlay with the ^{1}H-^{15}N HSQC spectrum of DnaJB6 1-130. Chemical shift perturbations (CSPs) from DnaJB6 1-130 F89I, F91L and F93L were calculated based on overlay of the ^{1}H-^{15}N BEST-TROSY spectra of the mutants with that of wild type DnaJB6 1-130. CSPs were determined using a minimal shift approach, where the mutant peak nearest to the given wild type peak was chosen for calculation of the CSP. CSPs were calculated as:

$$\sqrt{(Hppm_{\mathrm{mut}} - Hppm_{\mathrm{WT}})^2 + \frac{(Nppm_{\mathrm{mut}} - Nppm_{\mathrm{WT}})^2}{6.5}}$$

where H and N are the ^{1}H and ^{15}N chemical shifts and the value 6.5 is an empirically determined factor to normalized the chemical shift differences in the ^{15}N-dimension to the those in the ^{1}H-dimension [57].

Homology model to plot CSPs

A homology model of DnaJB6 1-130 was generated based on the structure of DnaJ2 from *T. thermophilus* [23] using PHYRE2 [58]. CSPs from the mutations F89I, F91L and F93L were plotted onto the homology model structure using PyMOL.

2.3.6 ATPase activity assay

HSC70 ATPase activity was assayed with a colorimetric ATPase activity assay kit (Expedeon, Product code: 601-0120). The manufacturer's protocol was followed with the modification that the quantities of all reagents was halved, resulting in a total reaction volume of 100 µL. 1 µM (in KCl buffer) or 2 µM (in NaCl buffer)

HSC70 was incubated with 0.5 mM (in KCl buffer) or 1 mM (in NaCl buffer) ATP in the presence and abscence of 25 µM DnaJB6 1-130 for 1 hour at 37°C. The ATP hydrolysis reaction was quenched and incubated at room temperature with the dye malachite green, which develops green color based on P_i concentration. After 30 minutes, absorbance at 620 nm was measured with a SpectraMax M3 micro plate reader (Molecular Devices) to determine the level of ATPase activity. The ATPase activity assay was performed in buffer 20 mM HEPES, 0.03% NaAzide, pH 7.2 with 50 mM KCl or 50 mM NaCl. Samples were dialyzed against 4 L of their respective buffers prior to use in the ATPase activity assay. ATPase reactions were carried out in 96-well plates (Corning). A negative control without protein was measured with each plate and subtracted from other measurements. The experiment was performed in triplicates within each plate.

3 Results

Contents

3.1 Expression and purification 35
3.1.1 Full length DnaJB6 35
3.1.2 DnaJB6 residue 1-130 37
3.1.3 HSC70 37
3.2 DnaJB6 is folded and active 39
3.3 Oligomeric full length DnaJB6 by NMR 40
3.4 Oligomerization 45
3.4.1 Native mass spectrometry 45
3.4.2 Mutational study of interactions in oligomerization . . . 49
3.4.3 The effect of 1,6-hexanediol on oligomerzation 54
3.4.4 Oligomerization and holdase activity 55
3.5 LGMD1D mutations and the G/F-rich region 57
3.5.1 Chemical shift perturbations in the J-domain 57
3.5.2 Stimulation of HSP70 ATPase activity 64

3.1 Expression and purification

3.1.1 Full length DnaJB6

At the beginning of this project, an expression and purification method for DnaJB6 1-130 and HSC70 had already been established in the Schnell Group (Department of Biochemistry, University of Oxford). However, the purification of full length DnaJB6

was not yet established. Initial attempts at purifying full length DnaJB6 were based on the purification protocol published by Månsson et al. [35], in which DnaJB6 was expressed into *E. coli* inclusion bodies and purified under denaturing conditions. When this method was attempted, DnaJB6 was not expressed in inclusion bodies, but remained in the cleared supernatant after ultracentrifugation of the cell lysate. However, DnaJB6 was successfully purified from the lysate by Strep-tag affinity chromatography, after which a SEC step was attempted. Only about 10% of protein was being recovered after SEC, perhaps due to unspecific interactions with the resin of the SEC column (Superdex S200 Increase 10/300 GL (GE)) or unpredictable migration on the column. As a result, the SEC purification step was removed from the purification. Additionally, urea concentration, NaCl concentration and pH were adjusted through multiple purifications. The final expression and purification protocol can be found in Materials and methods (2.2.1 and 2.2.2).

With this purification protocol, produced samples of full length DnaJB6 were pure enough for most experiments. However, some C-terminal degradation products remained in the final samples. This proved a problem for NMR experiments with oligomeric DnaJB6, where peaks from monomeric degradation products were much more intense than those from large, slowly tumbling oligomers. A DnaJB6 construct with a C-terminal Strep-tag was cloned, for which C-terminal degradation would remove the Strep-tag and allow for separation by Strep-tag affinity chromatography. This construct was successfully expressed and purified, resulting in higher protein purity and successfully removing the previously observed NMR signals from degradation products. SDS-PAGE gels from purification of full length DnaJB6 with N-terminal and C-terminal Strep-tag can be seen in figure 3.1.

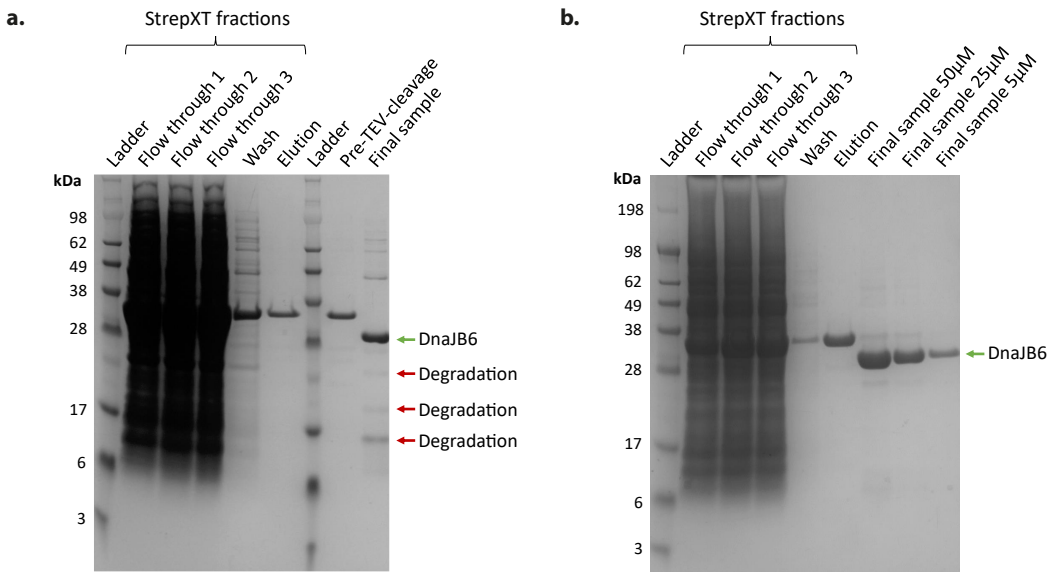

Figure 3.1: SDS-PAGE gels of DnaJB6 purification. DnaJB6 and degradation products are labelled. **a.** Samples from purification of DnaJB6 with N-terminal Strep-tag. **b.** Samples from purification of DnaJB6 with C-terminal Strep-tag. Gel: Bolt 12% Bis-Tris Plus gel (Invitrogen) run in Bolt MES SDS running buffer (Novex). Ladder: SeeBlue Plus2 (Thermo Fisher). Stained with Coomassie Blue (Expedeon).

3.1.2 DnaJB6 residue 1-130

The expression and purification protocol for DnaJB6 residue 1-130 can be found in Materials and methods (2.2.1 and 2.2.3). DnaJB6 1-130 eluted from SEC in a single peak. The SEC chromatogram and fractions pooled to obtain the final sample can be seen in figure 3.2.

3.1.3 HSC70

The expression and purification protocol for HSC70 can be found in Materials and methods (2.2.1 and 2.2.3). HSC70 eluted from SEC in overlapping peaks due to multiple oligomeric states of HSC70. The SEC chromatogram and fractions pooled to obtain the final sample can be seen in figure 3.2.

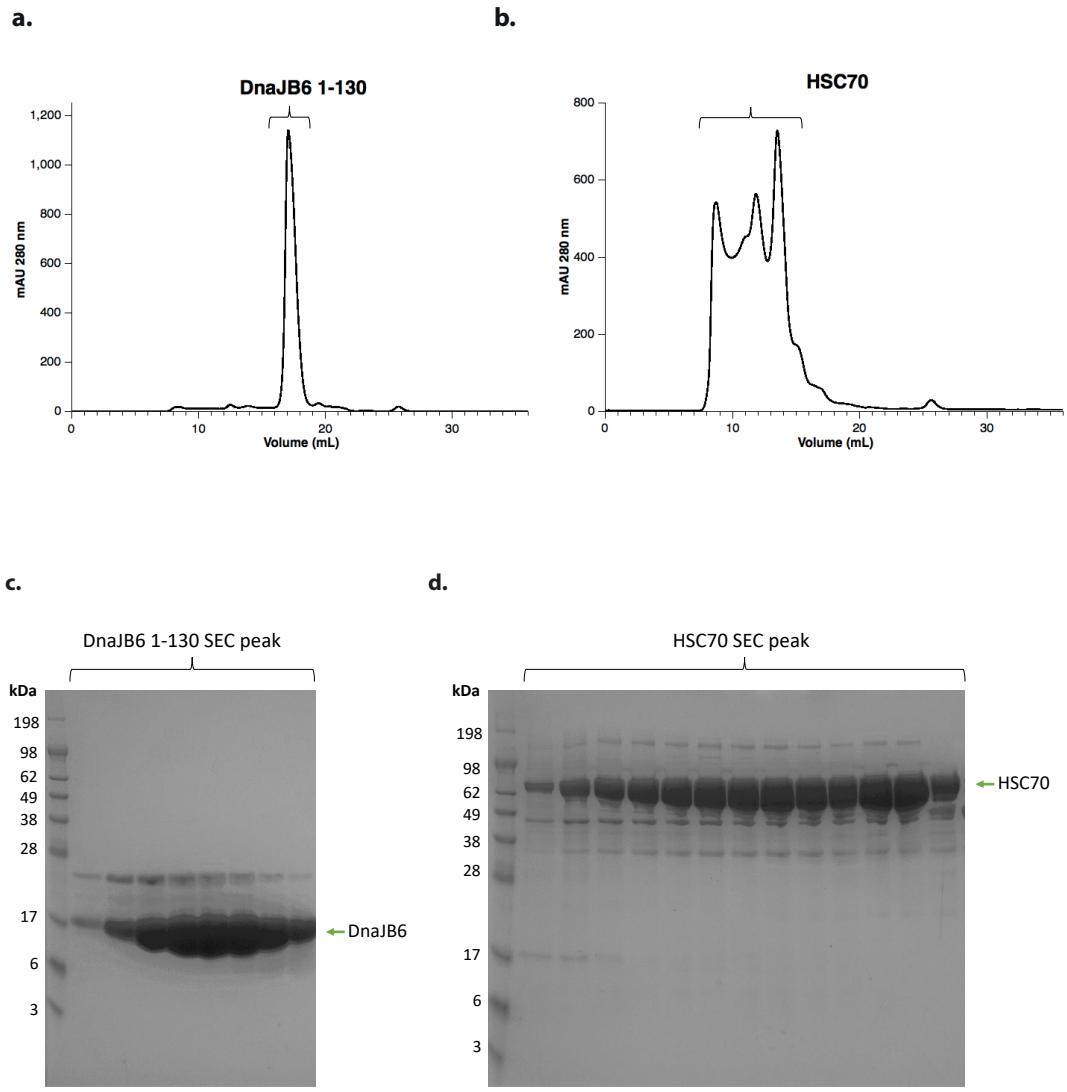

Figure 3.2: Size exclusion chromatography (SEC) traces and SDS-PAGE gels of DnaJB6 1-130 and HSC70 purifications. **a and b.** Chromatograms from SEC of DnaJB6 1-130 (a.) and HSC70 (b.) with a Superdex S200 Increase 10/300 GL column (GE). HSC70 elutes as multiple overlapped peaks due to oligomerization. SEC running buffer was 20 mM NaP_i, 20 mM NaCl, 0.03% NaAzide, pH 7.2. **c and d.** SDS-PAGE gels of peak fractions from SEC with DnaJB6 1-130 (c.) and HSC70 (d.) as labelled in figure a and b. Gel: Bolt 12% Bis-Tris Plus gel (Invitrogen) run in Bolt MES SDS running buffer (Novex). Ladder: SeeBlue Plus2 (Thermo Fisher). Stained with Coomassie Blue (Expedeon).

3.2 DnaJB6 is folded and active

As DnaJB6 was purified under denaturing conditions and refolded, it was important to ensure that the produced protein was correctly folded and active.

A far-UV CD-spectrum of DnaJB6 was recorded (figure 3.3). It indicates that the protein contains α-helix, and does not resemble the spectrum of a peptide in random coil.

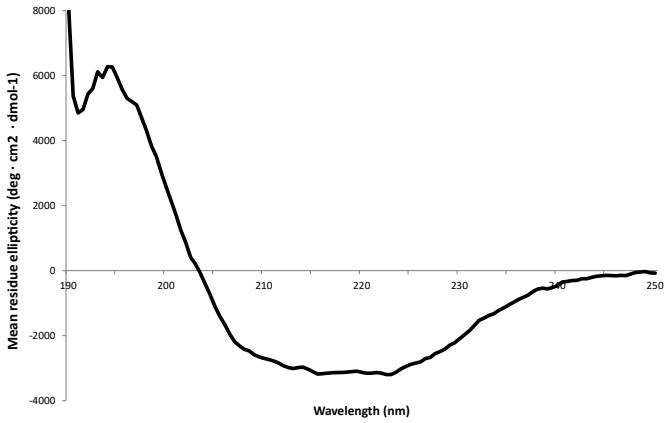

Figure 3.3: Far-UV circular dichroism (CD) spectrum of DnaJB6. Recorded with a Jasco J-815 Spectropolarimeter with a Peltier temperature control unit. Sample conditions were 10 µM DnaJB6 in 20 mM NaP_i, 20 mM NaCl, pH 7.2 at 20°C. Spectrum is the product of 9 accumulations from 190 to 250 nm at a scan rate of 100 nm/minute.

The holdase chaperone activity of DnaJB6 was determined using an assay based on inducible insulin aggregation (figure 3.4). Bovine pancreatic insulin consisting of α and β chains joined by two disulfide bonds begins to aggregate upon reduction with DTT. This aggregation can be followed by measuring light scattering at 360 nm. Holdase chaperone activity for aggregating insulin decreases the aggregation rate. DnaJB6 in a 1:2 molar ratio with insulin has clear antiaggregation activity.

DnaJB6 was also shown to form polydisperse oligomers by DLS (figure 3.9). Together with the CD-spectrum and holdase activity, this is taken as evidence that the produced protein was correctly folded and functional.

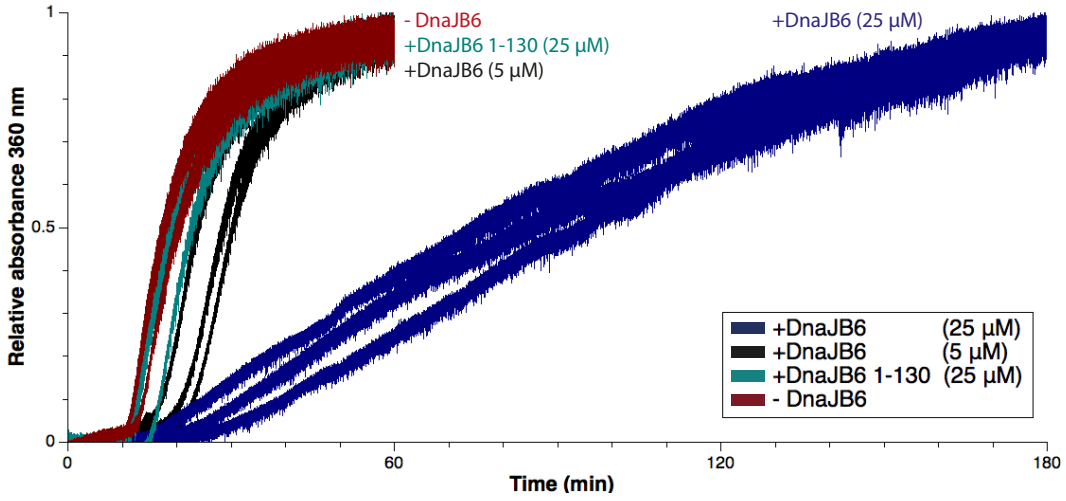

Figure 3.4: Holdase activity assay with DnaJB6. Aggregation of Bovine pancreatic insulin (Sigma-Aldrich) (50µM) was induced by DTT (25 mM) in the presence and absence of DnaJB6. Insulin aggregation was followed over time by measuring absorbance at 360 nm with a Cary 50 UV-vis spectrophotometer (Agilent). Assay was performed in 20 mM NaP_i, 20 mM NaCl, pH 7.2 at room temperature. Holdase assay was performed in triplicates with: red: no DnaJB6, Teal: DnaJB6 1-130 25 µM, Black: DnaJB6 5 µM, Navy: DnaJB6 25 µM.

3.3 Oligomeric full length DnaJB6 by NMR

The SBD of DnaJB6 remains structurally uncharacterized, despite being a functionally important region of the protein; the domain is responsible for interaction with substrate proteins, but is also predicted to contain the oligomerization site of DnaJB6 [34]. An aim of this project was to characterize full length and oligomeric DnaJB6 by NMR, to determine the structural characteristics of the SBD and CTD and as a "proof of concept" for future structural work on DnaJB6.

DnaJB6 forms large oligomeric complexes, which will have slow tumbling rates and therefore poor relaxation properties for NMR. However, the SBD of DnaJB6 is predicted to be intrinsically disordered. The internal dynamics of this region, if the disorder-prediction is correct, may allow for characterization by NMR despite the size of the oligomeric complexes. Indeed, this was the case; peaks were observable in

the ^{1}H-^{15}N correlation BEST-TROSY spectrum of full length DnaJB6 at oligomeric conditions (figure 3.5).

The spectrum shows higher contour level peaks of narrow ^{1}H dispersion, with some more disperse peaks appearing at a lower contour level. The spectrum can be interpreted as showing disordered or flexible regions, resulting in higher peaks of narrow dispersion, and a folded region or regions, resulting in lower peaks with a broader dispersion.

From the overlay of the full length DnaJB6 ^{1}H-^{15}N BEST-TROSY spectrum with that of DnaJB6 1-130, it is evident that many of the observable peaks are C-terminal of the residue 1-130 region (figure 3.6). Peaks with chemical shifts expected of Gly-residues and Ser/Thr-residues, not present in the spectrum of DnaJB6 1-130, show up in the spectrum of full length DnaJB6 (labelled in figure 3.5 and 3.6). This indicates that the G/F- and S/T-rich SBD does possess some flexibility. That these peaks are from G/S/T-residues in the SBD could be validated with assignment by mutation or truncation.

Additionally, a residue 75-80 poly-Gly region is observable in both the spectrum of full length DnaJB6 and DnaJB6 1-130 (labelled in figure 3.5 and 3.6). Because these peaks are present in the spectrum of full length DnaJB6, it indicates that this region is flexible, and may act as a flexible linker between the J-domain and the G/F-rich region. This has been confirmed in other work by Dr. Felipe Ossa — this region in the DnaJB6 1-130 construct has low values for the heteronuclear-NOE (Nuclear Overhauser Effect) indicating a high degree of flexibility (heternuclear-NOE is not part of this work).

A section of peaks with broader ^{1}H dispersion emerge at lower contour levels in the spectrum of full length DnaJB6 (figure 3.5). These peaks do not overlay with peaks from DnaJB6 1-130 (figure 3.6). While the low intensity of these peaks must be interpreted cautiously, it may indicate that that there is a folded region of DnaJB6 C-terminal of the residue 1-130 region, and as such outside the J-domain.

However, it is unknown whether there are substantial shifts of J-domain peaks in full length DnaJB6 compared with DnaJB6 1-130, so these peaks could be from the J-domain. A potential folded structure outside the J-domain could be a folded CTD, which is predicted to contain secondary structure, a folded region of the SBD or both. A C-terminal truncation construct could be used to determined whether these peaks are due to a folded CTD.

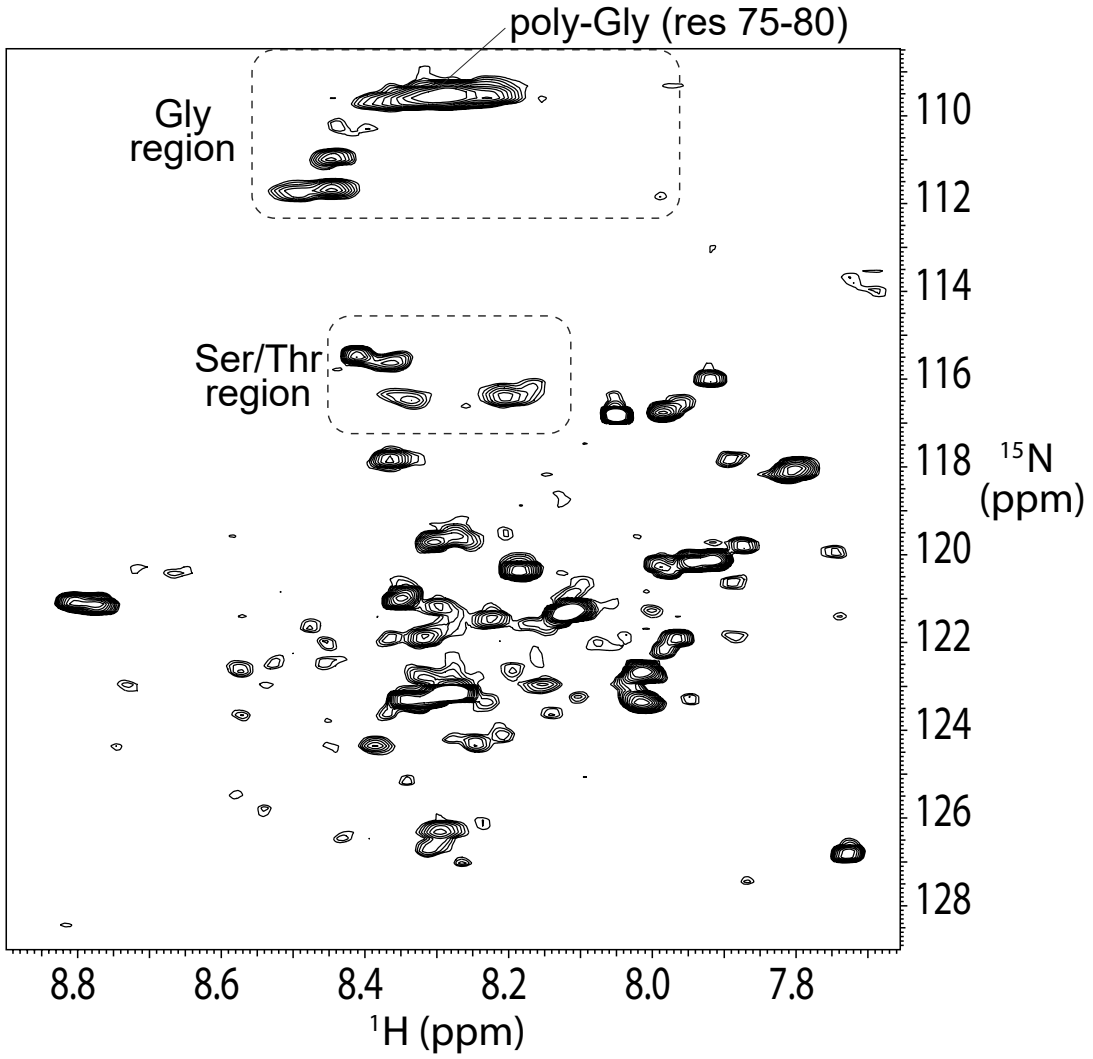

Figure 3.5: ^{1}H-^{15}N BEST-TROSY spectrum of ^{15}N-labelled DnaJB6. Peaks from Gly-, Ser- and Thr-residues are labelled based on chemical shifts. Residue 75-80 poly-Gly region is labelled based on assignment in DnaJB6 1-130. Spectrum was recorded on a Bruker Avance II 750 MHz (^{1}H) spectrometer with a TCI cryoprobe with the BEST-TROSY pulse sequence [53, 54]. Sample was 450 µM DnaJB6 in 20 mM NaP_i, 150 mM NaCl, 1 mM EDTA, 0.03% NaAzide, pH 7.2 at 15°C.

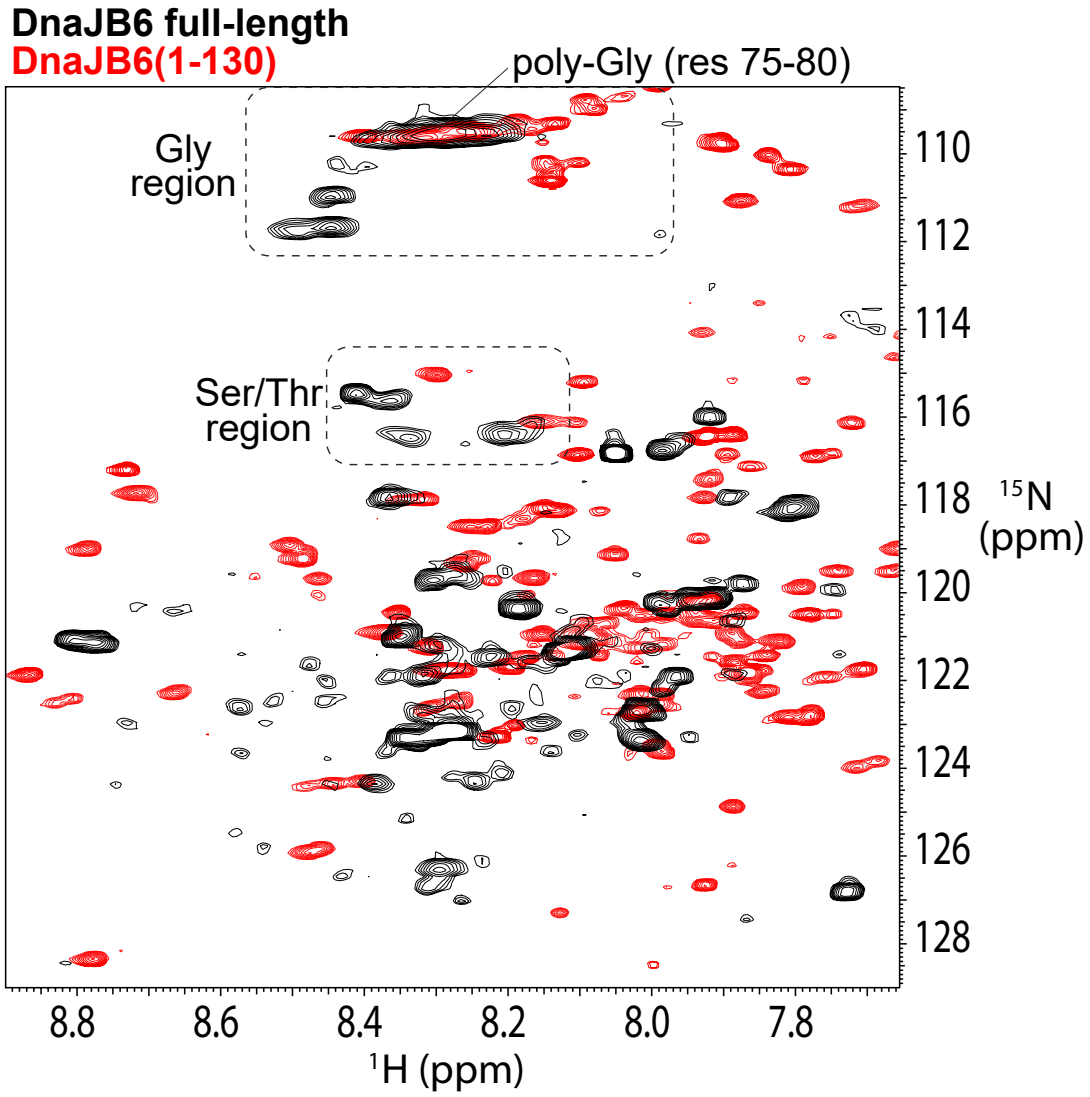

Figure 3.6: Overlay of ^{1}H-^{15}N BEST-TROSY spectra of ^{15}N-labelled DnaJB6 full length (black) and DnaJB6 1-130 (red). Peaks from Gly-, Ser- and Thr-residues are labelled based on chemical shifts. Residue 75-80 poly-Gly region is labelled based on assignment in DnaJB6 1-130. Spectrum of full length DnaJB6 was recorded on a Bruker Avance II 750 MHz (^{1}H) spectrometer with a TCI cryoprobe. Spectrum of DnaJB6 1-130 was recorded on a Bruker Avance III HD 950 MHz (^{1}H) spectrometer. The BEST-TROSY pulse sequence was used [53, 54]. DnaJB6 1-130 sample was 400 µM protein in 20 mM NaP_i, 20 mM NaCl, pH 7.2 at 25°C. DnaJB6 full length sample was 450 µM protein in 20 mM NaP_i, 150 mM NaCl, 1 mM EDTA, 0.03% NaAzide, pH 7.2 at 15°C.

3.4 Oligomerization

A main focus of this project was on characterizing the properties of polydisperse oligomerization of DnaJB6, addressing the questions: which oligomeric states are populated, which interactions drive oligomerization and is oligomerization necessary for holdase function?

3.4.1 Native mass spectrometry

Native MS was used to address the question of which oligomeric states are populated. The technique allows for identification of molecular species by mass in the gas phase under conditions where proteins can retain their native structure and oligomeric properties. If the resolution and signal-to-noise ratio is good enough, the relative population of each oligomeric species can be quantified. The technique CID was used to obtain a resolvable mass spectrum of DnaJB6. As used here, CID is a method of reducing the charge of the ionized oligomer species by collision with gas molecules and subsequent dissociation of a highly charged subunit [59]. As the mass to charge ratio (m/z) is the measured property of the ions, this charge reduction results in dispersion of the spectrum and higher resolution. This is necessary when dealing with polydisperse oligomers, as there will be a complex overlay of charge series from many oligomeric species. This technique has previously been used to determine the oligomeric species populated by another chaperone which forms oligomers in a polydisperse fashion, the small heat shock protein (sHSP) αB-crystallin [60].

An initial spectrum of "intact" DnaJB6 prior to CID was recorded (figure 3.7). The spectrum contains a bell-curve of many overlapping peaks, confirming that DnaJB6 forms polydisperse oligomers under the given experimental conditions.

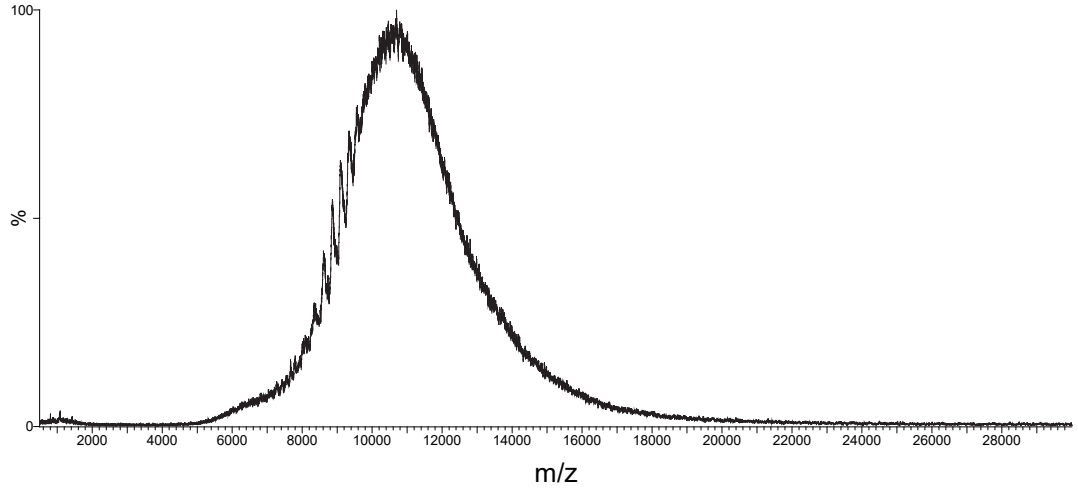

Figure 3.7: Native mass spectrometry (MS) of DnaJB6 polydisperse oligomers. MS spectrum was recorded on a Water's Instruments Synapt G1 mass spectrometer. Sample was 30 µM DnaJB6 in 200 mM ammonium acetate pH 7.2. Quadrupole was set to >7200 m/z, excluding lower mass species.

In the spectrum of "activated" DnaJB6 recorded with CID (figure 3.8), the oligomeric distribution can be resolved in two steps of the charge series. The observed masses correspond to 9-, 10-, 11-, 12-, 13- and 14-mer of 27 kDa DnaJB6 monomers. When accounting for the loss of a subunit by CID, this means that the oligomeric distribution is populated from 10-mer to 15-mer, with both even and odd oligomers populated. The spectrum has too low signal-to-noise ratio to accurately quantify the population of each oligomeric species.

The low-m/z monomer region of the spectrum contains a charge series of peaks corresponding to a mass of 27 kDa, confirming that the oligomers do consist of DnaJB6 subunits, which are dissociated by CID.

As the resolved distribution (figure 3.8) reveals that both even and odd oligomeric states are populated, this excludes a DnaJB6 dimer as the smallest subunit of oligomerization. As the signal-to-noise is low, the observed distribution does not exclude population of oligomers outside the 10-mer to 15-mer range. It does however

seem that the most populated species are in this range and that the polydisperse oligomeric distribution is centered on the 12-mer or 13-mer.

As described in Materials and methods (2.3.4), native MS was attempted with a variety of buffer conditions and buffer exchange methods. The results presented here were from one of the initial attempts at native MS. The experiment was attempted multiple times after this to test new buffer conditions and buffer exchange methods. However, this did not lead to an improvement in the quality of the data.

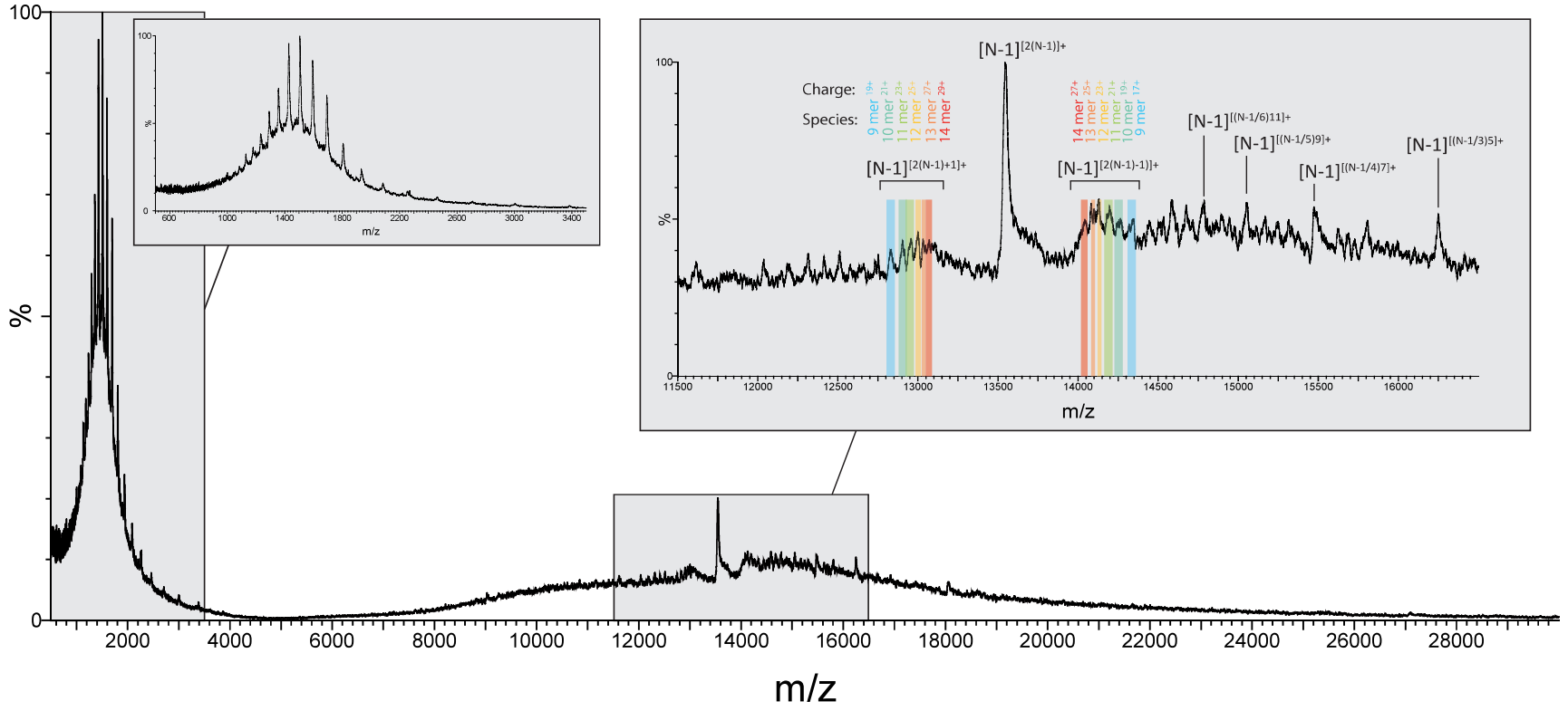

Figure 3.8: Native mass spectrometry (MS) of DnaJB6 with collision induced dissociation (CID). Insets show zoom of monomer region (left) and oligomer region (right). In the monomer region (left), peaks correspond to a 27 kDa DnaJB6 monomer. In the oligomer region (right), peaks corresponding to oligomeric species are highlighted with color and annotated with oligomer species and charge state. Peaks corresponding to commonly divisible charge states have been labelled >14500 m/z with [oligomer species]$^{[\text{charge state}]}$ (N = number of subunits before CID). Native MS was performed with a Water's Instruments Synapt G1 mass spectrometer. Sample was 30 µM DnaJB6 in 200 mM ammonium acetate, pH 7.2.

3.4.2 Mutational study of interactions in oligomerization

Certain sequence characteristics of the DnaJB6 SBD with a suspected role in the oligomerization interaction have been identified due to similarities to other systems. A pattern of positive and negative charge-blocks have been identified in the DnaJB6 sequence (figure 1.7b). Charge-blocks have previously been shown to be important in the interactions of the liquid-liquid phase separating protein Ddx4 [47]. Additionally, DnaJB6 contains a G/F-rich region in which Phe-residues may be important for DnaJB6 self-interaction, as observed in the interactions of the NPC nucleoporins [49–51]. The role of these sequence characteristics in DnaJB6 oligomerization were investigated by DLS with mutant variants of DnaJB6; the positive charge-block (residue 125-136) and the F-rich region (residue 139-188) in the suspected oligomerization site were chosen for mutational study (see figure 2.2 in Materials and methods for specific positions of mutations).

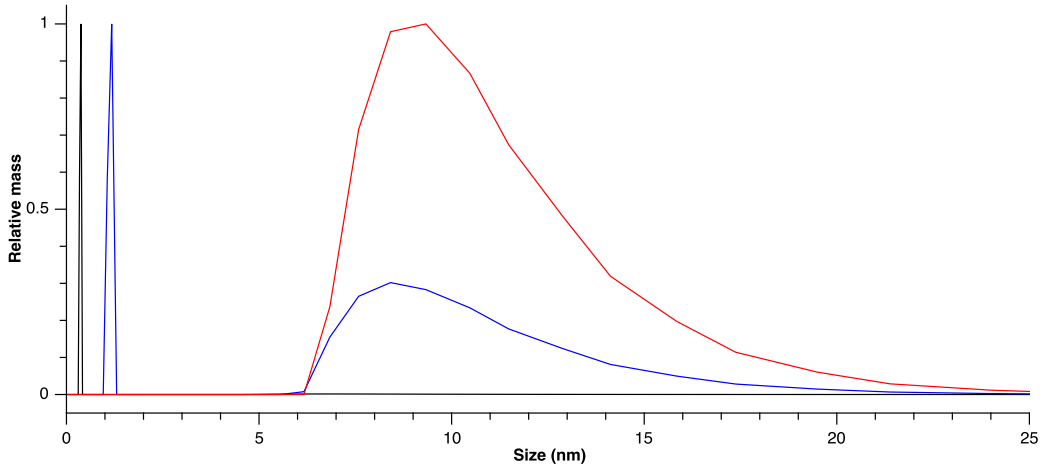

Figure 3.9: Example of dynamic light scattering to measure DnaJB6 oligomerization. A Viscotek 802 DLS instrument was used. Sample conditions were 20 mM NaP_i, 150 mM NaCl, 1 mM EDTA, 0.03% NaAzide, pH 8.0 at 20 °C with DnaJB6 concentrations Black: 10 µM, Blue: 40 µM, Red: 60 µM. Measurements are 10 runs of 10 seconds.

Two mutant constructs were prepared for investigation of the charge-block. Five Arg-residues in the residue 125-136 charge-block were mutated to Lys in one

construct (R5K), retaining positive charge but removing side chain pi-bonds, and Ala in another construct (R5A), also removing positive charge.

To investigate the role of Phe-content, a construct was prepared with every second of the twelve Phe-residues in the residue 139-188 region mutated to Ala (F6A). A construct with mutation of all Phe-residues in this region was also attempted, but the protein did not express in *E. coli*.

Oligomerization propensity of wild type DnaJB6 and the mutated variants described above was tested by DLS (figure 3.10 and 3.11). The relative population of DnaJB6 in the oligomeric and monomeric state was determined as a function of protein concentration (figure 3.10a) and solvent ionic strength (figure 3.10b).

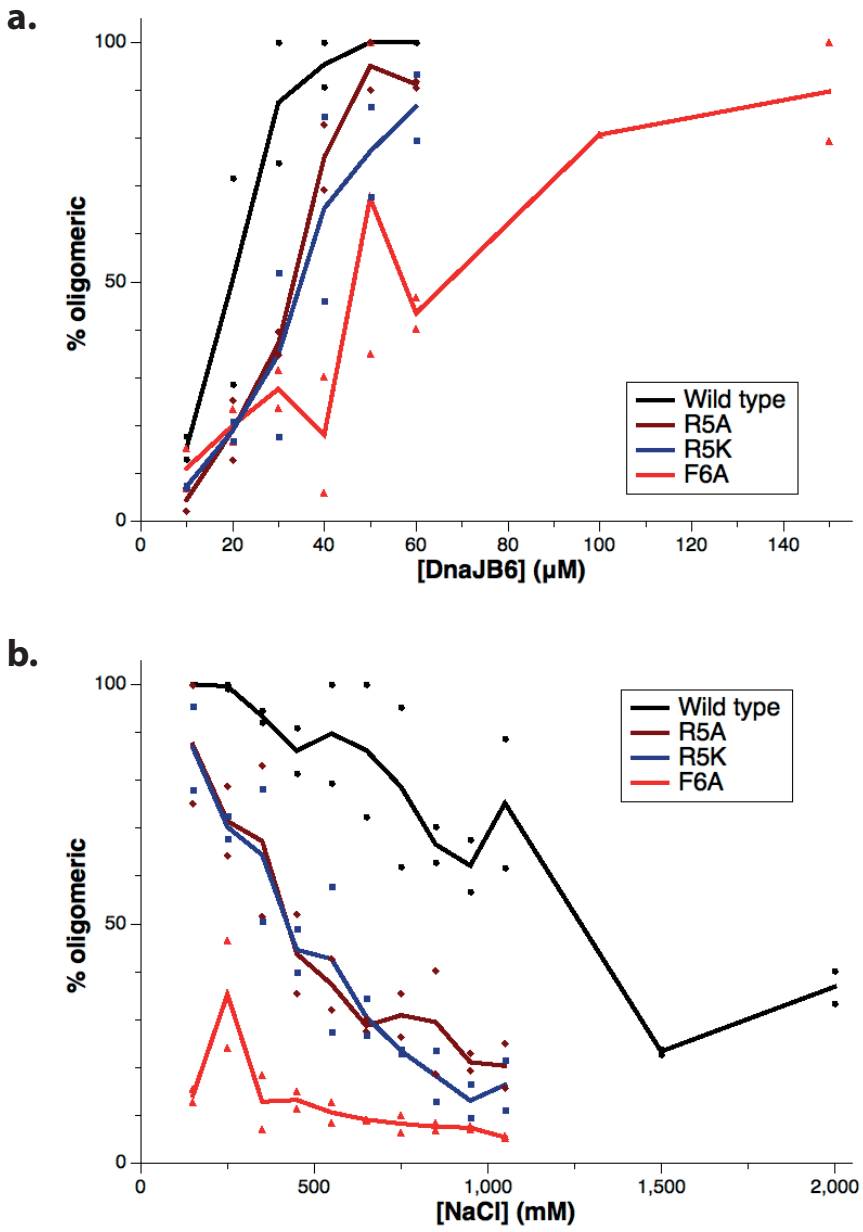

Figure 3.10: Mutational study of DnaJB6 oligomerization by dynamic light scattering (DLS). R5A and R5K introduce 5 Arg-to-Ala or Arg-to-Lys mutations in the residue 125-136 charge block. F6A introduces 6 Phe-to-Ala mutations in the residue 139-188 region (see figure 2.2). **a.** Oligomerization as a function of DnaJB6 concentration. **b.** Oligomerization as a function of NaCl concentration. A Viscotek 802 DLS instrument was used. Standard sample conditions were 50 µM DnaJB6 in 20 mM NaP_i, 150 mM NaCl, 1 mM EDTA, 0.03% NaAzide, pH 8.0 at 20°C, with protein and NaCl concentration varied in a. and b. respectively. DLS measurements were made in duplicates. Line plot shows average of duplicates and scatter plot shows individual measurements. "% oligomeric" reflects the number of DnaJB6 monomers on oligomeric form as a percentage of total monomers (see Materials and methods 2.3.3 for calculation).

A logistic function was fit to the data describing oligomerization as a function of protein concentration (figure 3.11). A dissociation constant K_d was determined from the fit, describing the equilibrium between monomer and all species of oligomer. It should be noted that the K_d is a product of many individual affinities of subunit binding at various stages of oligomer-assembly, and as such does not reflect a single binding affinity but rather an overall propensity for oligomerization.

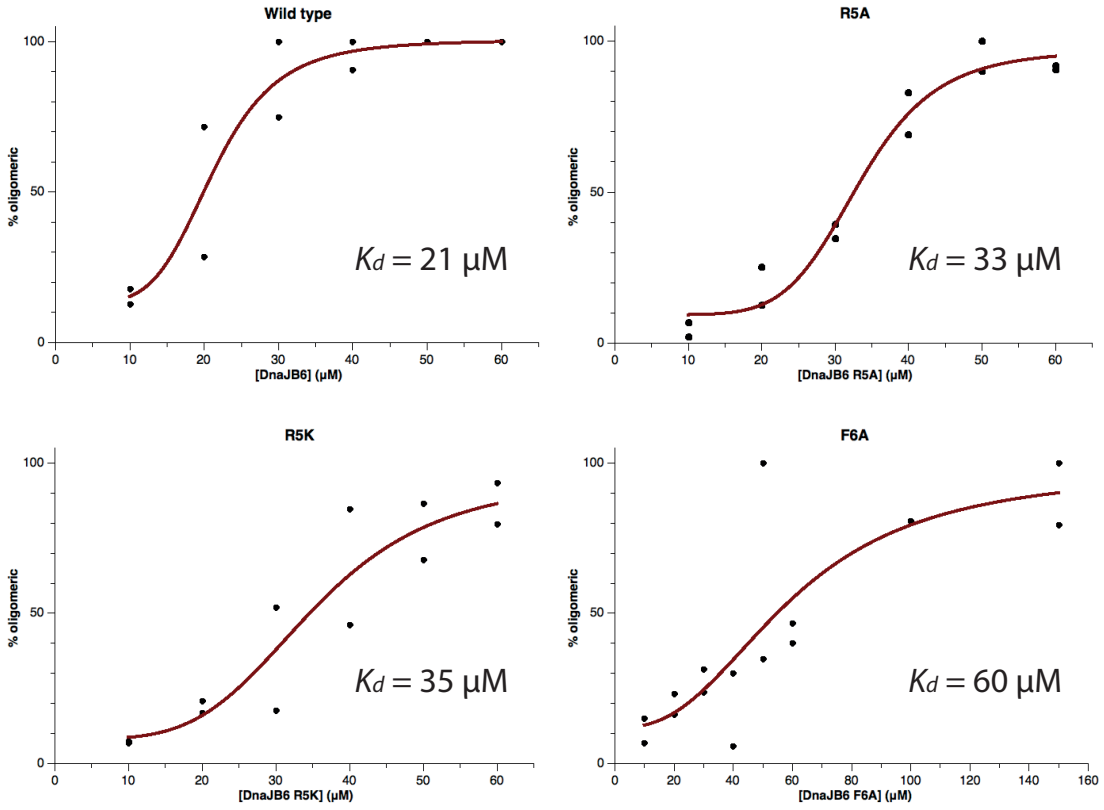

Figure 3.11: Oligomerization propensity of DnaJB6 mutant constructs by dynamic light scattering (DLS). R5A and R5K introduce 5 Arg-to-Ala or Arg-to-Lys mutations in the residue 125-136 charge block. F6A introduces 6 Phe-to-Ala mutations in the residue 139-188 region (see figure 2.2). Scatter plots show oligomerization as a function of DnaJB6 concentration (same data as figure 3.10a). Red line plot shows logistic fit (Levenberg–Marquardt algorithm) to determine K_d for oligomerization (see Materials and methods 2.3.3 for equation, see table 3.1 for error of fit). A Viscotek 802 DLS instrument was used. Sample conditions were 20 mM NaP_i, 150 mM NaCl, 1 mM EDTA, 0.03% NaAzide, pH 8.0 at 20°C. DLS measurements were made in duplicates. "% oligomeric" reflects the number of DnaJB6 monomers on oligomeric form as a percentage of total monomers (see Materials and methods 2.3.3 for calculation).

Table 3.1: Oligomerization propensities for DnaJB6 wild type and mutant constructs

DnaJB6 construct	K_d (oligomerization propensity)
Wild type	21 ± 2.23 µM
R5A	33 ± 1.61 µM
R5K	35 ± 6.86 µM
F6A	60 ± 22.6 µM

Table of oligomerization propensities (K_d) for DnaJB6 wild type and mutant constructs determined by dynamic light scattering (DLS). R5A and R5K introduce 5 Arg-to-Ala or Arg-to-Lys mutations in the residue 125-136 charge block. F6A introduces 6 Phe-to-Ala mutations in the residue 139-188 region (see figure 2.2). K_d was determined by logistic fit (Levenberg–Marquardt algorithm) to data in figure 3.11 (see Materials and methods 2.3.3 for equation). Error of fit for K_d is shown.

Wild type DnaJB6 has the highest oligomerization propensity. The charge-block mutants R5A and R5K have a slightly lower propensity for oligomerization than wild type. This is reflected both as a lower K_d, and as a lower ionic strength required for dissociation of oligomers. That oligomerization propensity is only slightly lowered compared to wild type makes it unclear whether the region has a significant role in the oligomerization interaction.

If electrostatic interactions of the positive charge-block were important for oligomerization, mutation to uncharged residues would be expected to decrease oligomerization propensity and also decrease the dependence of oligomerization on ionic strength. The mutant constructs R5A and R5K seem to have the same oligomerization propensity and dependence on NaCl concentration, indicating that the positive charge is not important.

The mutation of 6 Phe residues to Ala in the F6A construct has a significant effect on oligomerization propensity, with a 3-fold decrease in oligomerization propensity and a lower ionic strength necessary for dissociation of oligomers. It has been shown by Kakkar et al. that mutation of up to 18 Ser- and Thr-residues in the 132-195 region does not have a significant effect on oligomerization [36]. As such, the effect seen here by mutation of only 6 Phe residues indicates that phenylalanines in this region (residue 139-188) play a role in the oligomerization interaction.

3.4.3 The effect of 1,6-hexanediol on oligomerzation

As shown above, Phe-residues in the residue 132-195 region of DnaJB6 play a role in the oligomerization interaction. This interaction may be analogous to that of nucleoporins in the NPC, in which FG-repeats in a disordered region are important [49–51]. 1,6-hexanediol has been used previously to disrupt this interaction [51]. Additionally, 1,6-hexanediol has been used to dissolve phase separated membraneless organelles and liquid-liquid phase separated proteins, distinguishing between liquid-like phase separation and solid-like assemblies or solid aggregates [61]. As such, an effect of 1,6-hexanediol on DnaJB6 oligomerization could indicate that, as hypothesized, the DnaJB6 oligomerization interaction has characteristics similar to those of the nucleoporin interactions and the interactions of phase separating proteins.

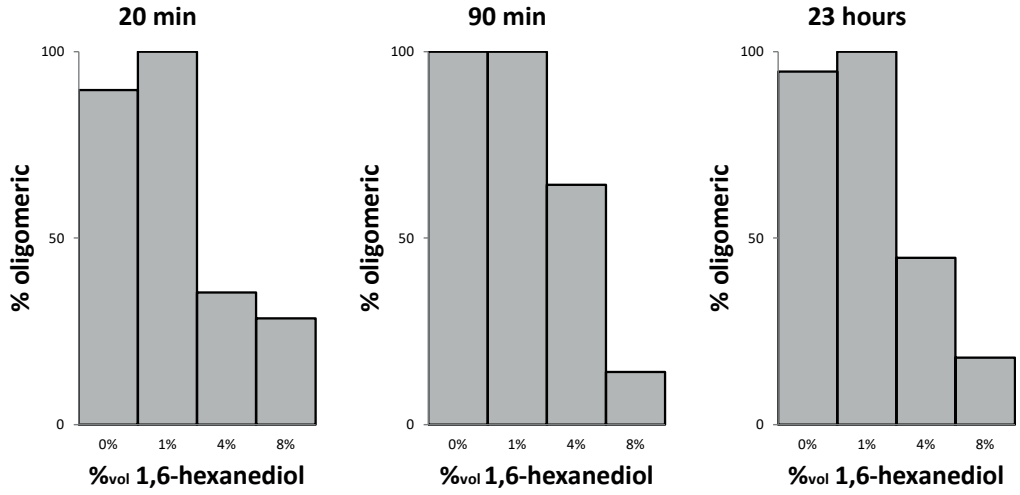

Figure 3.12: Effect of 1,6-hexanediol on DnaJB6 oligomerization by dynamic light scattering (DLS). DnaJB6 samples were incubated with 0%, 1%, 4% and 8% (volume) 1,6-hexanediol on a rotary mixer at room temperature and DLS measurements made at the indicated time-points. A Viscotek 802 DLS instrument was used. Sample conditions were 50 µM DnaJB6 in 20 mM NaP_i, 150 mM NaCl, 1 mM EDTA, 0.03% NaAzide, pH 8.0 with varied 1,6-hexanediol concentration. "% oligomeric" reflects the number of DnaJB6 monomers on oligomeric form as a percentage of total monomers (see Materials and methods 2.3.3 for calculation).

To test this, DnaJB6 was incubated with 1,6-hexanediol and oligomerization was measured by DLS at multiple time points (figure 3.12). With 1% 1,6-hexanediol, DnaJB6 fully retains oligomerization, but with 4% and 8% 1,6-hexanediol oligomerization is significantly disrupted. There does not seem to be a significant time-dependence of this effect, based on the time points used here. Interestingly, the interaction between nucleoporin FG-domains is disrupted at a concentration between 2.5% and 5% 1,6-hexanediol [51], matching with the preservation of oligomerzation at 1% but not 4% 1,6-hexanediol observed here. This result suggests that the DnaJB6 oligomerization interaction has characteristics similar to the FG-domain interaction of nucleoporins and the interactions of phase separating proteins. However, the mechanism by which 1,6-hexanediol disrupts these interactions is not clear, so interpretation of the result presented here should be cautious; it does not confirm a transient or dynamic interaction as determined for nucleoporins and liquid/liquid phase separating proteins.

3.4.4 Oligomerization and holdase activity

It is unknown what the function of DnaJB6 oligomerization is. It would be unexpected that oligomerization is required for interaction with HSP70, as this function is retained in other J-proteins that do not form oligomers—indeed truncations of DnaJB6 that do not oligomerize are capable of stimulating HSP70 ATPase activity as shown later in this thesis and in previous work [33]. However, oligomerization could be required for substrate binding and chaperone activity. Alternatively, oligomerization may not be strictly necessary for DnaJB6 substrate binding or interaction with HSP70, but may function to provide a higher local concentration of DnaJB6 for these interactions.

DnaJB6 oligomerization is dependent on ionic strength, with the population shifting to primarily monomeric at 1.5 M NaCl (figure 3.10b). This feature provides a system with which to tune the oligomerization of DnaJB6. This was exploited

to test whether DnaJB6 retains holdase activity when the oligomer is dissociated at higher ionic strength. The holdase activity of DnaJB6 was measured at 150 mM, 750 mM and 1500 mM NaCl using the holdase activity assay based on insulin aggregation (figure 3.13). Holdase activity decreases at 750 mM NaCl and is almost entirely abolished at 1500 mM NaCl.

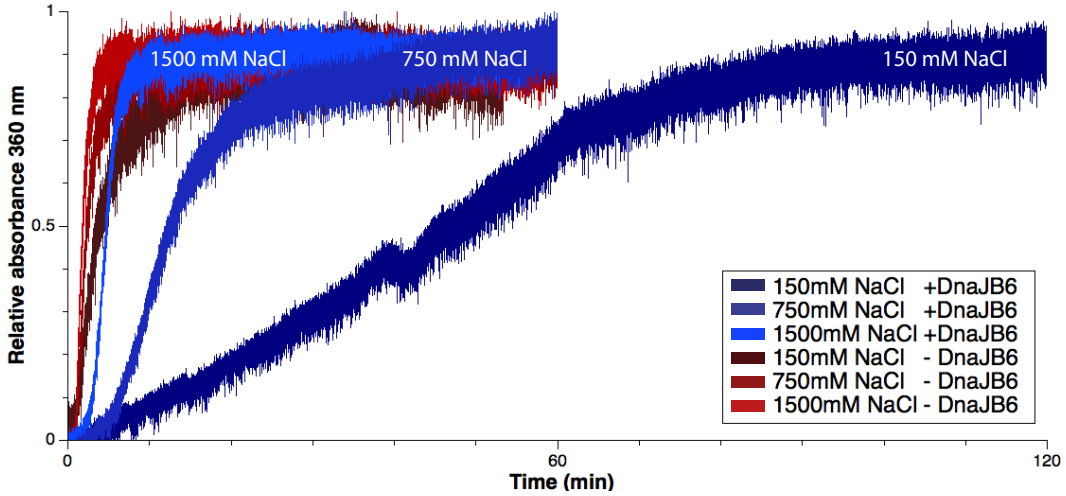

Figure 3.13: DnaJB6 holdase activity as a function of NaCl concentration. Aggregation of Bovine pancreatic insulin (75 µM) (Sigma-Aldrich) was induced by DTT (50 mM) in the presence and absence of DnaJB6 (50 µM) at various NaCl concentrations. Insulin aggregation was followed over time by measuring absorbance at 360 nm with a Cary 50 UV-vis spectrophotometer (Agilent). Assay was performed in 20 mM NaP_i, 1 mM EDTA, 0.03% NaAzide, pH 8.0 with 150 mM, 750 mM and 1500 mM NaCl at room temperature. See figure 3.10b for oligomerization state at given NaCl concentration. Measurements in the presence of DnaJB6 are labelled in white with NaCl concentration (negative control measurements not labelled).

It is striking that 750 mM NaCl, at which DnaJB6 is expected to be distributed in population between monomer and oligomer, results in an intermediate holdase activity level, while 1500 mM NaCl, at which DnaJB6 is expected to be mostly monomeric, results in no holdase activity. This correlation supports the hypothesis that the shift from oligomeric to monomeric DnaJB6 is the cause of decrease in activity.

However, the experiment does not isolate the decrease in activity as caused by decreased oligomerization. It should be noted that, even though the negative

controls without DnaJB6 present overlay quite well, there is a trend of a slight increase in aggregation rate with increasing NaCl concentration. This is the same trend as seen in the presence of DnaJB6. This raises the question of whether the effect seen here is actually due to an increased aggregation rate of insulin at higher salt and not a loss of DnaJB6 activity. Alternatively, it may be that ionic strength affects DnaJB6 substrate binding in a manner independent of oligomerization, resulting in loss of holdase activity.

The data presented here is an indication that oligomeric DnaJB6 is the active form of the protein in substrate binding and holdase activity, while the monomeric form is inactive, but the effect can not be directly attributed to oligomerization state; it may be due to other unknown effects of high NaCl concentration such as impaired substrate binding or increased rate of insulin aggregation.

3.5 LGMD1D mutations and the G/F-rich region

The function of the G/F-rich region in DnaJB6 is unknown. The mutations F89I, F91L and F93L associated with LGMD1D are located in this region and as such provide a framework for studying it. This project investigated the hypothesis that these mutations are in a region packed against the J-domain, and as such disrupt this interaction or perturb the J-domain structure resulting in lack of binding to HSP70 or loss of stimulation of HSP70 ATPase activity.

3.5.1 Chemical shift perturbations in the J-domain

Potential structural perturbation of the J-domain was investigated by NMR. This was done by recording ^{1}H-^{15}N BEST-TROSY spectra of wild type DnaJB6 1-130 and DnaJB6 1-130 with each mutation introduced (figure 3.14 and 3.15), from which CSPs caused by each mutation were calculated (figure 3.16). A CSP describes how much the chemical shifts of the observed nuclei has changed. As the chemical

shift depends on the chemical environment of the residue, the CSP describes a structural change in the protein [57].

The secondary structure of DnaJB6 1-130 was calculated from chemical shifts using TALOS in previous work performed by Dr. Felipe Ossa. The secondary structure matches that previously determined for J-domains and reveals an α-helix in the G/F-rich region which may be packing against the J-domain as seen in the *T. thermophilus* DnaJ2 structure [23]. Based on this, the *T. thermophilus* DnaJ2 structure was used to generate a homology model of DnaJB6 1-130 on which to plot the CSPs (figure 3.17). The TALOS data was also used to map the CSPs to the helices of the J-domain (figure 3.16).

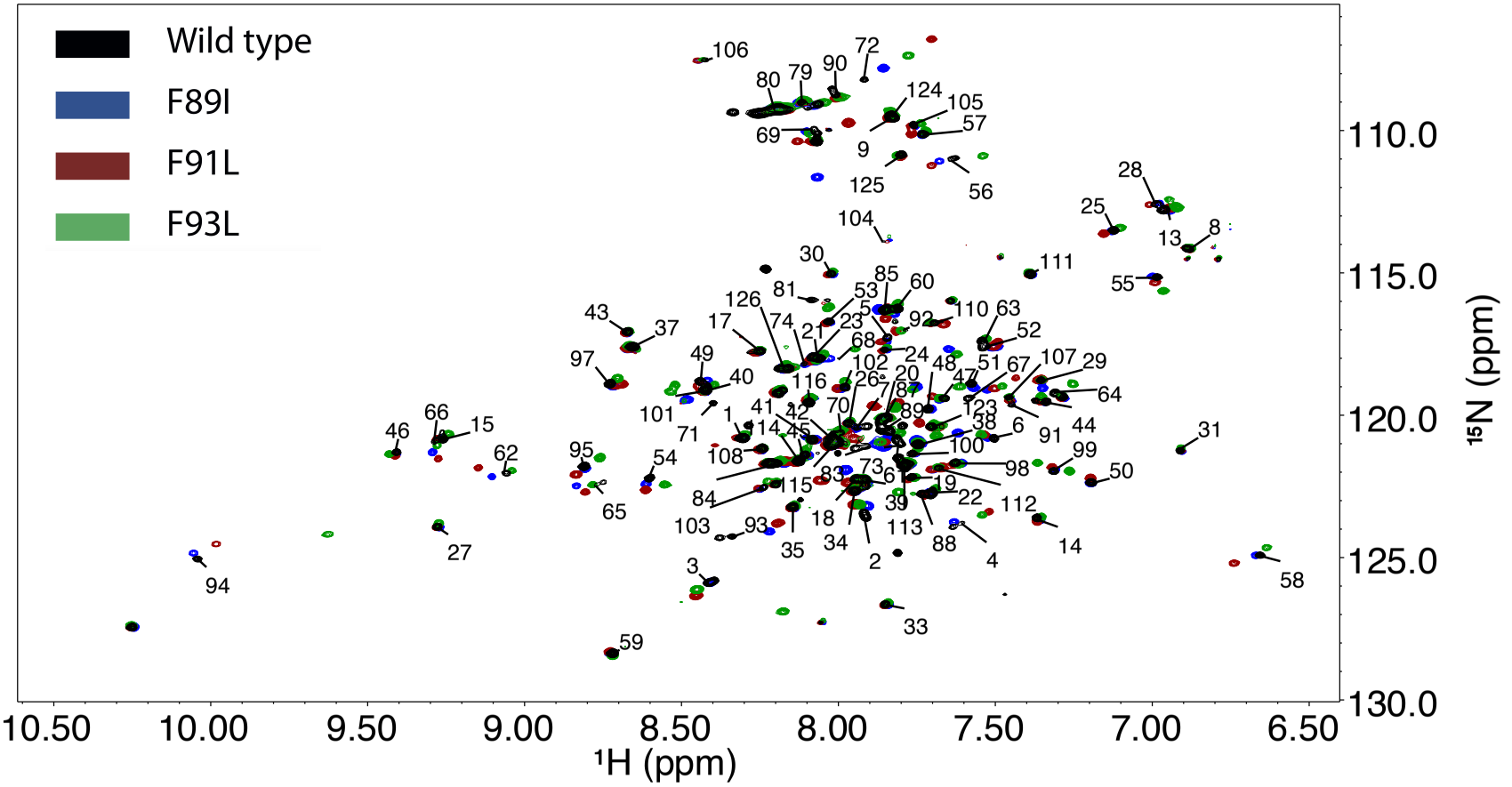

Figure 3.14: Overlay of ^{1}H-^{15}N BEST-TROSY spectra of ^{15}N-labelled DnaJB6 1-130 wild type and with LGMD1D-associated mutations F89I, F91L and F93L introduced. Spectra were recorded on a Bruker Avance III HD 950 MHz (^{1}H) spectrometer. The BEST-TROSY pulse sequence was used [53, 54]. Sample conditions were 300-500 µM protein in 20 mM NaP_i, 20 mM NaCl, pH 7.2 at 25°C. Wild type spectrum is labelled with peak assignments transferred from previously assigned ^{1}H-^{15}N HSQC of DnaJB6 1-130 wild type (not a part of this work).

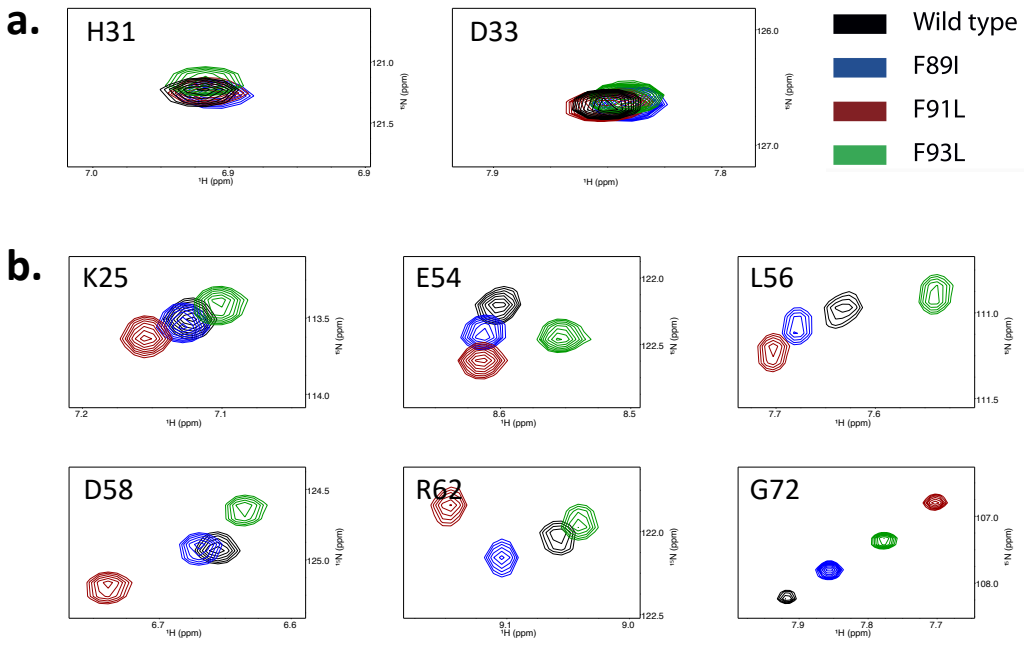

Figure 3.15: Zoom of peak shifts from overlay of ^{1}H-^{15}N BEST-TROSY spectra of ^{15}N-labelled DnaJB6 1-130 wild type and with LGMD1D-associated mutations F89I, F91L and F93L introduced (See full spectra in figure 3.14). **a.** Zoom of peaks from residues in the HPD-motif (residue 31 and 33). **b.** Zoom of other selected peaks. Spectra were recorded on a Bruker Avance III HD 950 MHz (^{1}H) spectrometer. The BEST-TROSY pulse sequence was used [53, 54]. Sample conditions were 300-500 µM protein in 20 mM NaP_i, 20 mM NaCl, pH 7.2 at 25°C. Peak assignments were transferred from previously assigned ^{1}H-^{15}N HSQC of DnaJB6 1-130 wild type (not a part of this work).

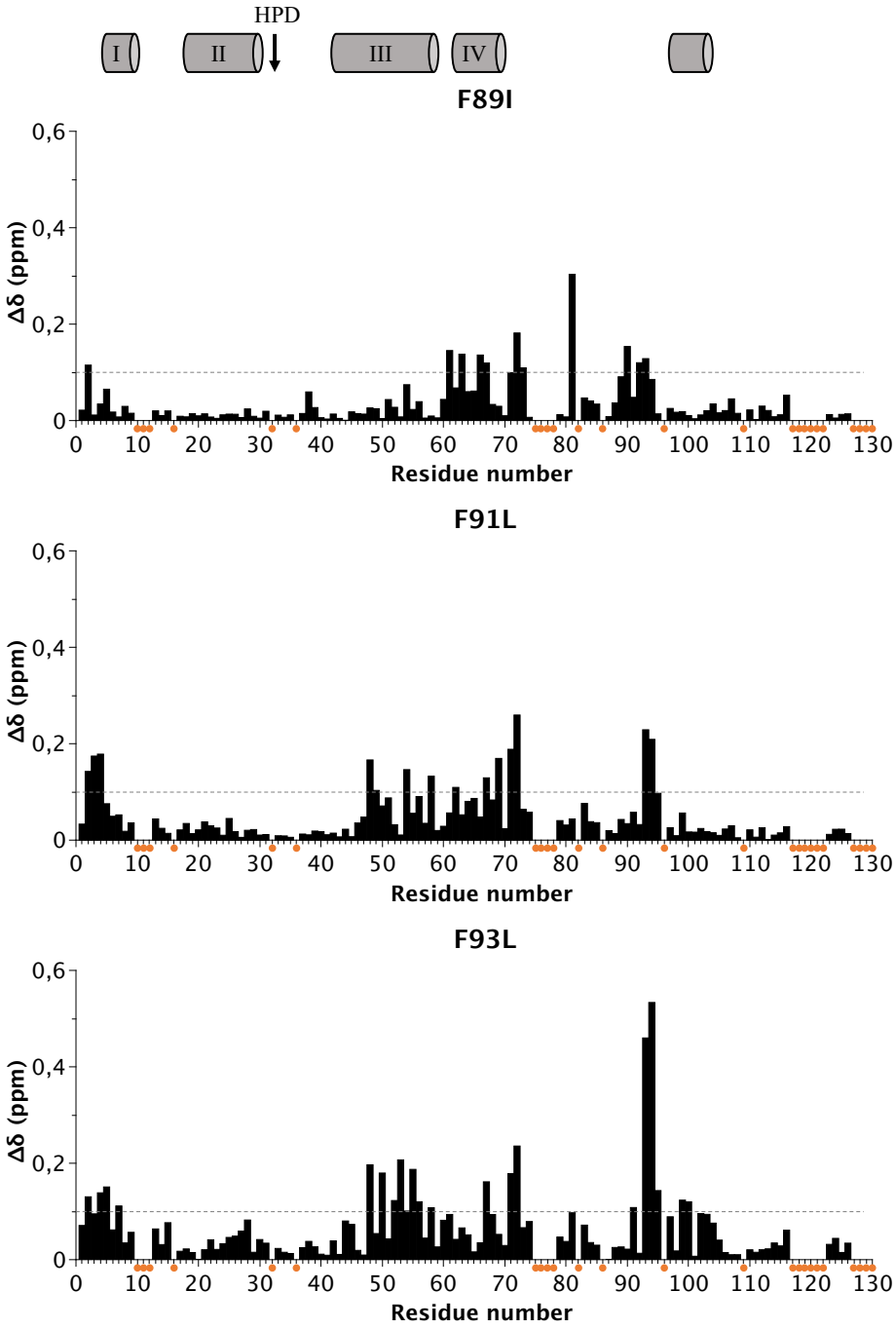

Figure 3.16: Chemical shift perturbations (CSPs) from LGMD1D-associated mutations F89I, F91L and F93L in DnaJB6 1-130. CSPs were calculated from overlay of ^{1}H-^{15}N BEST-TROSY spectra in figure 3.14 (see Materials and methods 2.3.5 for details). Grey cylinders represent α-helices based on previously obtained TALOS data on DnaJB6 1-130 (not a part of this work). J-domain helices are numbered. Residue 31-33 HPD-motif is labelled. Dotted grey line is arbitrarily placed at 0.1 ppm. Orange dots indicate unassigned residues for which CSPs have not been determined.

The largest CSPs are clustered in Helix I, III and IV of the J-domain, indicating that these helices are structurally perturbed by the mutations (figure 3.16 and 3.17). For the mutation F89I, helix III seems less perturbed than for F91L and F93L. The locations of the perturbations match with propagation from the mutation through helix IV/III to helix I, all located at the same end of the J-domain. Helix II and the HPD-motif are located at the other end of the J-domain, and are the least structurally perturbed region based on CSPs (see shift of HPD-motif peaks in figure 3.15a). This is the region of the J-domain known to interact with HSP70 and stimulate HSP70 ATPase activity [31], and as such the region hypothesized to be structurally perturbed by the LGMD1D-associated mutations. However, the data presented here indicates that structural disruption of helix II and the HPD-motif affecting HSP70 interactions are not the cause of the functional impairment by LGMD1D-associated mutations.

There seems to be a trend of F89I and F91L causing peaks to shift in the same direction, with F93L causing shifts in a different direction (figure 3.15). This may be related to F93L being in a unique position of the G/F-rich region; F93L is in the top of the helix rather than the extended region where F89I and 91L are found. However, there are examples of peaks where this is not the case, e.g. N74.

The largest CSPs would be expected to be clustered at the mutation site and surrounding residues, as mutation would have through-bond effects on this region. However, this is only the case for F93L, not for F89I and F91L. The lack of larger CSPs at the mutation site could be due to the minimal shift approach used to calculate CSPs. If, upon mutation, a peak shifts far away from the wild type position, another peak from a different residue may be selected as the minimal shift neighbor, if this is closer to the wild type peak. The minimal shift approach is thus conservative in determination of the magnitude of CSPs, but may result in underestimated CSPs for residues that experience large perturbation.

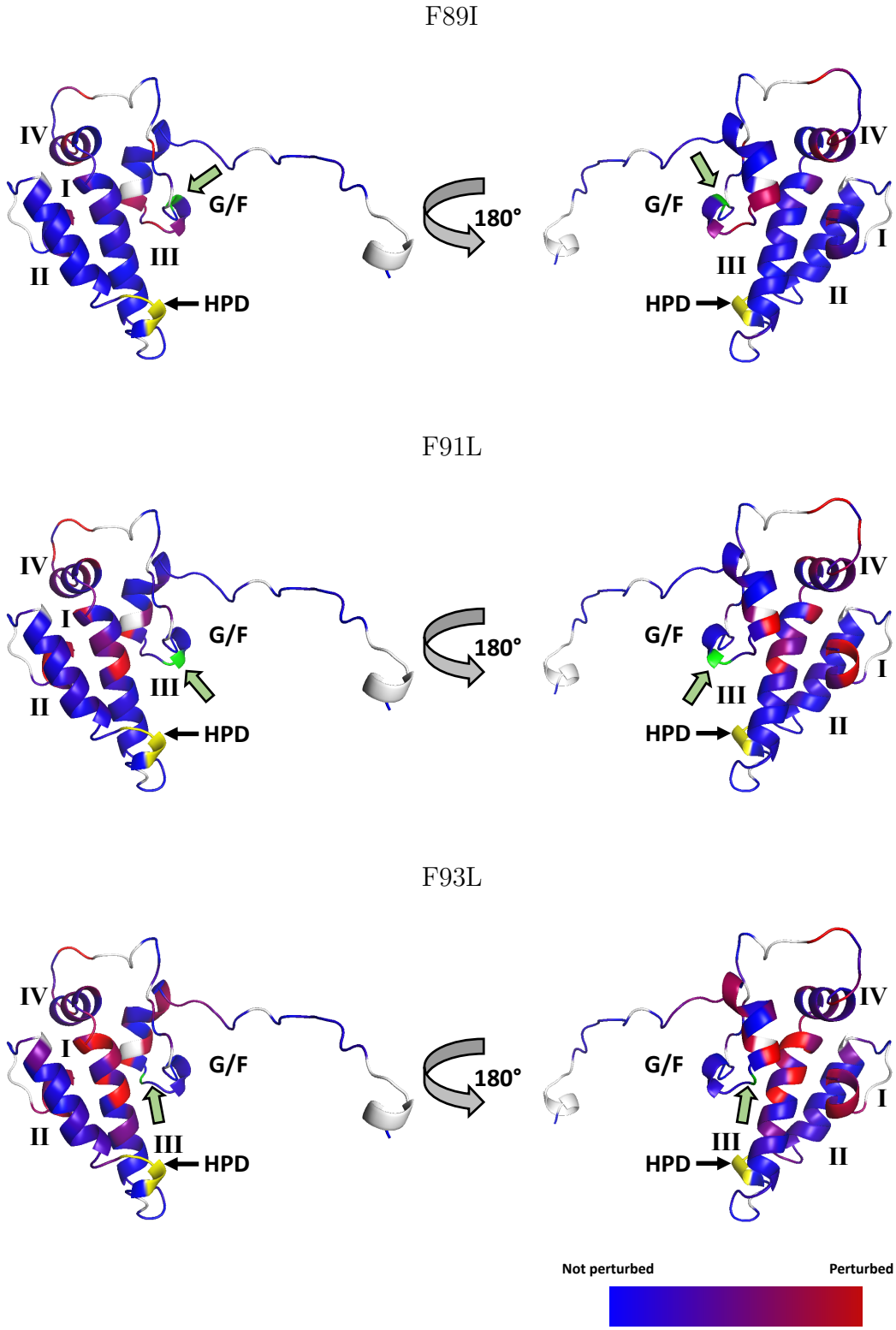

Figure 3.17: Chemical shift perturbations (CSPs) from LGMD1D-associated mutations (figure 3.16) plotted on homology model of DnaJB6 1-130. Homology model of DnaJB6 1-130 was generated with PHYRE2 based on structure of *T. thermophilus* DnaJ2 [23]. Blue: not perturbed, Red: most perturbed, Green: mutation, Yellow: HPD-motif, White: CSP not determined. Mutation position is labelled with green arrow. J-domain helices, residue 31-33 HPD-motif and G/F-rich region are labelled.

3.5.2 Stimulation of HSP70 ATPase activity

In order to investigate whether HSP70 ATPase stimulation is affected by LGMD1D-associated mutations, a colorimetric ATPase activity assay was used. ATPase activity of the ubiquitously expressed human house-keeping HSP70, HSC70, was tested in the presence and absence of DnaJB6 1-130 wild type and with LGMD1D-associated mutations introduced (figure 3.18). It has been proposed that Hsc70 activity depends on the presence of potassium ions, so the experiment was repeated in buffer with 50 mM NaCl and in buffer with NaCl replaced by 50 mM KCl [62]. It has previously been shown that a DnaJB6 residue 1-109 construct stimulates ATPase activity of HSP70 to a level comparable to the full length protein, taken to mean that DnaJB6 1-130 used here is a representative model of the protein [33].

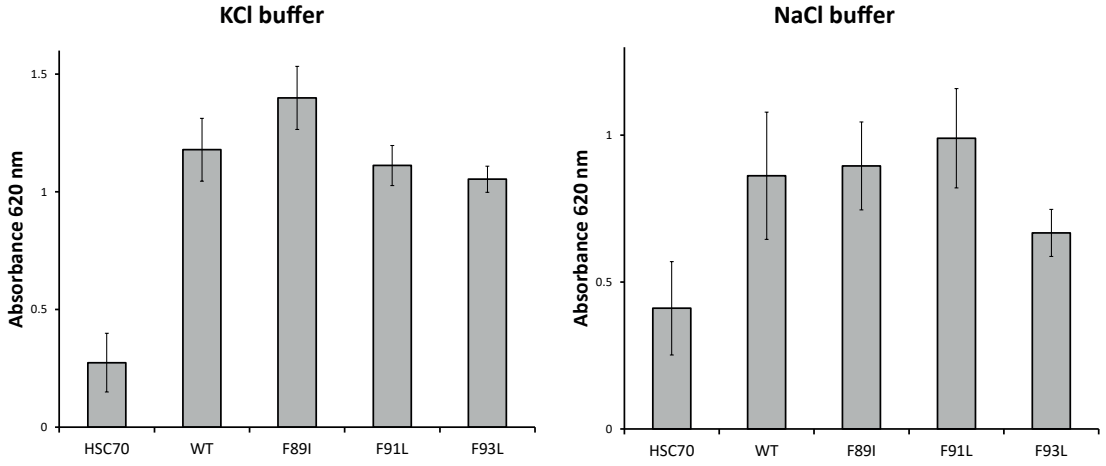

Figure 3.18: Effect of LGMD1D-associated mutations on DnaJB6 stimulation of HSC70 ATPase activity. ATPase activity of HSC70 alone and in the presence of wild type, F89I, F91L and F93L DnaJB6 1-130 was measured using a colorimetric ATPase activity assay (Expedeon). Samples were incubated for 1 hour at 37°C, reaction was quenched and after 30 minutes, absorbance at 620 nm, reflecting P_i concentration, was measured with a SpectraMax M3 micro plate reader (Molecular Devices). Experiment was performed in triplicates. Error bars are 2x standard deviation. KCl buffer samples: 1 µM HSC70, 25 µM DnaJB6 1-130, 0.5 mM ATP, 20 mM HEPES, 50 mM KCl, 0.03% NaAzide, pH 7.2. NaCl buffer samples: 2 µM HSC70, 25 µM DnaJB6 1-130, 1 mM ATP, 20 mM HEPES, 50 mM NaCl, 0.03% NaAzide, pH 7.2.

HSC70 shows a basal level of ATPase activity, which is stimulated by the presence of DnaJB6 as expected, with the presence of KCl resulting in a larger increase in activity. The introduction of LGMD1D-associated mutations F89I, F91L and F93L does not have a significant effect on the stimulation of HSC70 ATPase activity. Together with the structural data presented above, this indicates that HSP70 binding and stimulation of HSP70 ATPase activity are not the functions of DnaJB6 affected by LGMD1D-associated mutations.

4 Discussion

Contents

4.1 Structure 67
4.2 Oligomerization 69
4.2.1 Populated oligomeric species 69
4.2.2 Oligomerization interaction 70
4.2.3 Oligomerization and holdase activity 72
4.3 LGMD1D mutations and the G/F-rich region 73
4.3.1 Correlation with clinical severity 75
4.3.2 The functional effect of LGMD1D-associated mutations 75
4.4 Future work 76
4.4.1 Improvement of preliminary results 76
4.4.2 The functional effect of LGMD1D-associated mutation . 77
4.4.3 Oligomerization 78
4.4.4 Structural characterization 79
4.5 Conclusion 79

4.1 Structure

The structures of the SBDs of the B-type J-proteins human DnaJB1 and yeast Sis1 have been solved [21, 22]. However, DnaJB6 and its homolog DnaJB8 seem to have SBDs that differ from those of canonical B-type J-proteins [17]. Despite this, DnaJB6 remains largely structurally uncharacterized C-terminal of the conserved

J-domain. In this work, NMR was used to investigate the structural characteristics of full length DnaJB6 under oligomeric conditions.

DnaJB6 was expected to contain an intrinsically disordered region C-terminal of the J-domain, based on sequence-based prediction. The ^{1}H-^{15}N BEST-TROSY spectrum of full length DnaBJ6 presented here suggests that some residues of the protein are flexible, as they are clearly detectable at conditions where DnaJB6 forms large oligomeric complexes - it should be noted that there is a risk that a transient population of monomers or smaller oligomers are observed here. Additionally, the highest intensity peaks are narrowly dispersed in the ^{1}H-dimension, indicating a disordered region. As the peaks are not assigned, it is not clear exactly which regions are flexible, except for a poly-Gly region (residue 75-80), which has been assigned in the ^{1}H-^{15}N BEST-TROSY spectrum of DnaJB6 1-130. However, as there are peaks from Gly-residues and most likely Ser and Thr-residues, it seems likely that a region of the S/T-rich SBD is flexible.

A good way to confirm disorder or flexibility in DnaJB6 would be to record ^{1}H-^{15}N heteronuclear-NOEs. However, the samples of full length DnaJB6 at oligomeric conditions used here did not have sufficient signal intensity for this experiment.

The positions of the flexible residues observed in the spectrum of full length DnaJB6 could be determined by mutational assignment. A natural place to begin would be mutation of Ser/Thr-residues in the S/T-rich region of the SBD, in order to confirm whether the observable peaks labelled in figure 3.5 are indeed from Ser/Thr-residues and whether it is those of the SBD.

The spectrum also contains a layer of less intense peaks. These peaks are more disperse in the ^{1}H-dimension and have a lower signal intensity, indicating a folded region of the protein. These peaks do not overlay with peaks from DnaJB6 1-130, suggesting that DnaJB6 may also contain a folded domain C-terminal of the J-domain. Whether this is the postulated CTD predicted to begin at residue 196 or a folded region of the SBD could be confirmed by overlaying with the spectrum of

a C-terminal truncation construct or a construct containing only the CTD.

How does the characterization of DnaJB6 by NMR presented here fit with the proposed model by Söderberg et al. [44]? The structural model of DnaJB6 generated by Robetta is a compactly folded structure. While the NMR data presented here does not allow for conclusive characterization of intrinsic disorder in DnaJB6, it does suggest that the structure contains flexible regions, perhaps intrinsically disordered regions as predicted. It seems that the Robetta model does not account for this flexibility. It should be noted that Robetta/Rosetta structure prediction is based on well-folded structures. As such, the model of DnaJB6 may need adjustment to account for structural dynamics and disorder. However, further experimental evidence is required to fully confirm or reject the proposed structural model of DnaJB6.

4.2 Oligomerization

4.2.1 Populated oligomeric species

Results from native MS presented here confirm that DnaJB6 forms polydisperse homo-oligomers. The mass spectrum of DnaJB6 with CID remains preliminary, as the signal-to-noise is low. However, assignment of low intensity peaks in this spectrum indicates that species of 10-mer to 15-mer are present. Both odd and even steps are populated, showing that a potential DnaJB6 dimer is not the smallest subunit of the oligomer. However, DnaJB6 dimerization is not excluded, as equilibrium between oligomeric, dimeric and monomeric DnaJB6 is still possible. For example, the sHSP αB-crystallin is known to form dimers. For αB-crystallin, quantification of the oligomer populations revealed both even and odd oligomers were populated, with even oligomers slightly more populated than odd [60]. This may also be the case for DnaJB6, but is not revealed by the data presented here.

The theoretical minimum diameter of DnaJB6 oligomers can be calculated from molecular mass assuming a spherical oligomer structure with 1.37 g/cm^3 density [63]. This calculation gives a distribution of oligomers with a 8.5 nm to 9.8 nm diameter for a distribution from 10-mer to 15-mer of DnaJB6. Based on this, the distribution observed by DLS (figure 3.9) fits fairly well with the distribution observed by native MS, with the DLS distribution being broader than theoretically calculated, indicating that perhaps some species are not identified by native MS. The theoretical minimum diameter of the DnaJB6 monomer can be calculated in the same way. This gives a diameter of 2.0 nm. The monomeric peaks observed by DLS are smaller than this (figure 3.9) , which may be due to the high uncertainty of DLS measurements. Consistent with this, DnaJB6 monomer peaks shifted significantly between DLS measurements.

Previously published SAXS data on DnaJB6 [44] shows the existence of oligomers much larger than those observed here by native MS. A distribution of 34-mer to 55-mer was observed by SAXS. Perhaps these larger oligomeric species are also present in the native MS, but at a population too low to be observable with the low intensity signals presented here. Why are the smaller oligomers then not picked up by SAXS? Oligomers were separated by SEC previous to SAXS, and eluted in two peaks, where only the first eluted peak was characterized by SAXS. This could explain the lack of lower order oligomers in the SAXS data. Another possibility is that the ammonium acetate buffer used for native MS destabilizes the larger oligomers of DnaJB6. In any case, the native MS data presented here should be regarded as preliminary; better quality data is necessary to confidently determine the present species and for quantification of the population of each species.

4.2.2 Oligomerization interaction

A motif of charge-blocks with a neutral interspacer within a low-complexity G/F/S/T-rich region was investigated as the oligomerization site of DnaJB6. A residue 125-136

positive charge-block was chosen for mutational study, but did not exhibit a large effect on DnaJB6 oligomerization. However, mutation of 6 Phe-residues in the residue 139-188 region interspacing the charge-blocks resulted in a significant decrease in oligomerization propensity. This region is expected to contain the oligomerization site, based on previous work in DnaJB8 [34]. The data presented here supports this hypothesis. Whether it is the sequence motif of negative-positive-neutral-positive-negative charge-blocks that makes up the oligomerization site requires further study. It may be that it is phenylalanine content which drives the oligomer association, or perhaps a synergistic effect between the charge-block motif and phenylalanines. This could involve hydrophobic interactions or pi-pi/pi-cation interactions. Such an effect could be investigated by mutation of multiple such features together.

As discussed above, the NMR data presented in this work indicates that DnaJB6 possesses some flexibility in the oligomeric form, likely in the S/T-rich region. This same region is expected to contain the oligomerization site based on previous work in DnaJB8 [34] and the decrease of oligomerization propensity upon mutation of Phe-residues in this region observed here. How does flexibility in this region go hand in hand with participation in the oligomer interaction? One possibility is that a folded part of the S/T-rich region is responsible for the oligomerization interaction, while another part of this region does not participate in the interaction and as such remains flexible. Another possibility is that the SBD is indeed disordered in the oligomer, but is also the site of the oligomerization interaction, and is in a dynamic or fuzzy bound state. This would fit with a model of DnaJB6 oligomer formation that involves transient interactions analogous to the interactions of FG-repeat regions in nucleoporins [49–51]. The ability of 1,6-hexanediol to dissociate DnaJB6 oligomers further points towards an interaction-type similar to FG-nucleoporins and phase separating proteins. However, this is purely speculation; whether there is really

transient or fuzzy interactions at play in DnaJB6 oligomerization warrants further structural investigation and cannot be concluded from the data presented here.

It should be mentioned that, as the working hypothesis in this work was that DnaJB6 has properties similar to liquid/liquid phase separating proteins, DnaJB6 was investigated for liquid/liquid phase separation. This was done at protein concentration up to 400 µM in low salt condition (20 mM NaCl) with various Poly(ethylene glycol) (PEG) concentrations (up to 8 g/mL) as crowding agent. Phase separation was tested in a hanging drop on a siliconized glass cover slide by light microscopy, but droplets large enough to be detected by this experimental setup were not observed. This does not necessarily exclude potential liquid/liquid phase separation of DnaJB6 in a physiological context, as this may require other solvent conditions or the presence of certain interaction partners. The lack of observed liquid/liquid phase separation led to investigation of the discussed sequence characteristics in oligomerization.

4.2.3 Oligomerization and holdase activity

The functional role of oligomerization in DnaJB6 remains unknown. In this work, the effect of DnaJB6 oligomerization state on holdase activity was investigated by exploiting the ability of high ionic strength to dissociate DnaJB6 oligomers. The result indicates that DnaJB6 oligomers possess holdase activity, while the monomeric form does not. However, other effects of high ionic strength on the system are not known or controlled for, and as such the evidence is not conclusive. Experiments using orthogonal variables to control DnaJB6 oligomerization, for example Phe-mutations or 1,6-hexanediol as presented here, would allow for more confidence in this result.

Assuming that the decrease in holdase activity observed here is due to monomerization of DnaJB6, what could be the cause of an active oligomer and inactive monomer? Perhaps only the oligomeric form is active because the substrate binding

site is composed of the interface between multiple subunits. It has previously been proposed that the substrate binding site of DnaJB6 is composed of a cleft between two subunits in a homo-dimer [44]. Another possibility is that the role of DnaJB6 oligomerization is to form a cage-like structure in which substrate proteins can be bound, analogous to the mechanism of chaperonins.

4.3 LGMD1D mutations and the G/F-rich region

The LGMD1D-associated mutations F89I, F91L and F93L, located in the N-terminal end of the G/F-rich region of DnaJB6, cause structural perturbation of the J-domain as shown here by NMR. A possible cause of this effect on the J-domain is that the N-terminal G/F-rich region packs against the J-domain, as observed in *T. thermophilus* DnaJ2 [23]. Indeed, previously obtained TALOS data on DnaJB6 revealed that there is an α-helices in this region as in DnaJ2. Additionally, the NMR data on full length DnaJB6 presented here indicates that there is a flexible poly-Gly linker from residue 75 to 80. These observations fit well with the homology model of DnaJB6 based on DnaJ2 used here to structurally interpret CSPs from LGMD1D-associated mutations; in the homology model a coiled linker extends from the J-domain to a compact region packing against the J-domain in which the LGMD1D-associated mutations are located.

The CSPs in the J-domain can be rationalized in the context of the homology model; the structural perturbation propagates from the mutated region packing against the J-domain. Helix I, III and IV are structurally perturbed, whereas helix II and the HPD-motif, important for interaction with HSP70, are not [31]. This structural perturbation could be caused by disruption of the G/F-rich region's interaction with the J-domain or by changes in the interaction surface structurally propagating through the J-domain. Whatever the mechanism of perturbation, it does seem likely from the data presented here that the N-terminal part of the

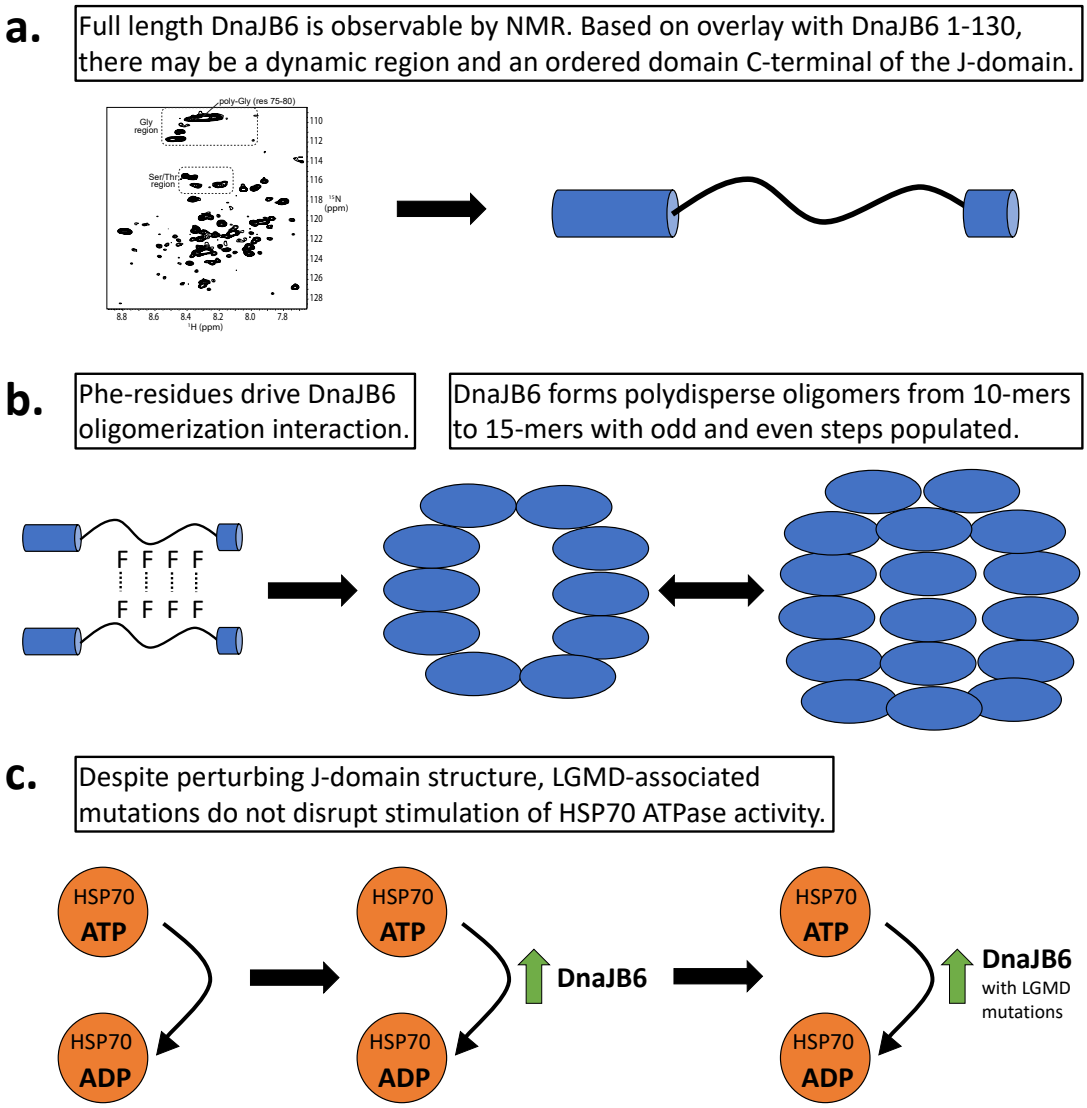

Figure 4.1: Summary of results. **a.** A ^{1}H-^{15}N BEST-TROSY NMR spectrum of full length DnaJB6 at oligomeric conditions was recorded. Sharp, narrow dispersion peaks indicate a dynamic region, while lower contour peaks indicate a folded domain. The peaks do not overlay with peaks from the DnaJB6 1-130 construct, indicating that these regions are C-terminal of the J-domain. **b.** Oligomerization of DnaJB6 was studied by DLS and native MS. Mutational study revealed that Phe-residues in the residue 139-188 region may play a role in the oligomerization interaction. Native MS revealed that DnaJB6 forms polydisperse oligomers from 10-mers to 15-mers, with both odd and even steps populated. **c.** LGMD1D-associated mutations F89I, F91L and F93L were characterized in the DnaJB6 1-130 construct. Determination of CSPs by NMR revealed that the J-domain is structurally perturbed by mutation, but not in helix II nor the HPD-motif. Consistent with this, stimulation of HSC70 ATPase activity by DnaJB6 was not affected by mutation.

G/F-rich region is packing against the J-domain in DnaJB6, as the locations of CSPs in the structure of the J-domain fit well with this model.

4.3.1 Correlation with clinical severity

The mutations F89I, F91L and F93L were chosen to represent different levels of LGMD1D clinical severity, in the order of F91L, F89I, F93L from most to least severe [40]. There does not seem to be a strict correlation with clinical severity in the magnitude or clustering of CSPs. However, F89I and F91L, but not F93L, seem to cause peaks to shift in the same direction. If, for this reason, F93L is excluded from the comparison, there is a correlation with clinical severity, with F91L causing larger CSPs than F89I.

These three mutations only represent three data points in a possible correlation. Characterization of more LGMD1D-associated mutations is necessary to determine whether clinical severity of LGMD1D can be structurally interpreted in DnaJB6.

4.3.2 The functional effect of LGMD1D-associated mutations

The introduction of LGMD1D-associated mutations F89I, F91L and F93L caused significant CSPs in the J-domain. Whether this had a functional effect on the J-domain's ability to stimulate ATPase activity in HSP70 was investigated. An impaired ability of DnaJB6 to stimulate HSP70 ATPase activity would make sense as a functional cause of the LGMD1D phenotype, which involves increased protein aggregation [40]. However, the mutations did not have a significant effect on the stimulation of ATPase activity in human HSC70. This result can be rationalized in the sense that helix II and the HPD-motif are the least structurally perturbed region of the J-domain. This region of the J-domain is responsible for interaction with HSP70, and the HPD-motif is required for stimulation of HSP70 ATPase activity [17, 31].

If the stimulation of HSP70 ATPase activity is not the affected function of DnaJB6, then what is? One theory is that the G/F-rich region plays a role in substrate hand-over from DnaJB6 to HSP70, working as a hydrophobic region which misfolded proteins can pass over from the substrate binding site. Perhaps functional substrate hand-over to HSP70 is impaired by the LGMD1D-associated mutations in the G/F-rich region. It has also been proposed that the G/F-rich region provides substrate specificity to J-proteins, as one study has shown that a chimeric construct of yeast Sis1 with an alternative G/F-rich region did not retain its original substrate specificity [64, 65]. If this is the case, the substrate specificity of DnaJB6 may be compromised by mutations in the G/F-rich region, possibly resulting in lack of specificity to important toxic substrates or saturation of DnaJB6 with unimportant substrates. Ultimately, any requirement for functional DnaJB6 could be affected by LGMD1D-associated mutations. These include oligomerization, localization, expression level, protein stability or unknown functions of DnaJB6. The work presented here indicates that the seemingly likely candidate of impaired HSP70 binding and stimulation of ATPase activity is *not* the function affected by LGMD1D-associated mutations in DnaJB6.

4.4 Future work

4.4.1 Improvement of preliminary results

Some of the results presented in this thesis are of a preliminary character. For example, the analysis of DnaJB6 oligomerization by native MS requires optimization, in order to quantify populated species. Optimization could involve screening of more buffer conditions than attempted here and exploration of other methods of buffer exchange. For each sample, MS conditions such as spray pressure, ionization voltage, gas and voltage for CID etc. would require optimization.

Another result which could be improved in quality is the quantification of oligomerization by DLS. DLS measurements were performed in duplicates for each condition. While the overall trends are clear, there is a large variance in the measurements for each data point, as is evident from figure 3.10. The quality of this data could be improved by increasing the number of measurements for each data point.

A ^{1}H-^{15}N correlation spectrum of full length oligomeric DnaJB6 was presented here. Peaks from many residues were not observable in the spectrum, as expected for a large protein. One way to improve the quality of this spectrum could be deuterium labelling of DnaJB6, which improves the relaxation properties of nuclei for biomolecular NMR [66] - deuteration may also allow for less sensitive NMR experiments to be performed. Additionally, interpretation of the spectrum could be improved with truncation and mutant constructs to assign peaks to regions of DnaJB6, e.g. the investigation of a folded CTD by C-terminal truncation and the assignment of peaks from S/T/G-residues to the SBD as discussed above.

It was shown here that disruption of oligomerization by increased ionic strength results in loss of DnaJB6 holdase chaperone activity. The effect of oligomerization state on holdase activity should be tested by tuning oligomerization with an orthogonal variable to ionic strength. This could for example be the introduction of mutations that disrupt oligomerization. Alternatively, the effect of 1,6-hexanediol on oligomerization presented here could also be used to control oligomerization when measuring holdase activity, requiring control experiments for the effect of 1,6-hexanediol on insulin aggregation.

4.4.2 The functional effect of LGMD1D-associated mutation

A potential future direction for study of DnaJB6 is to determine the functional effect of LGMD1D-associated mutations. This would entail the introduction of

the mutations in full length DnaJB6, as opposed to the DnaJB6 1-130 construct used here. The holdase activity could be measured to determine whether substrate binding and holdase activity is affected by the mutations. Whether substrate hand-over to HSP70 is affected could be tested by performing the holdase assay in the presence and absence of HSP70. If substrate hand-over is impaired by mutation, a smaller increase in chaperone activity upon addition of HSP70 would be expected. Stimulation of HSP70 ATPase activity could also be measured in the presence of substrate protein, to see if the substrate binding/release cycle is impaired.

Potential changes in the oligomerization properties of DnaJB6 with LGMD1D-associated mutations could be determined by native MS, if this is successfully optimized, and DLS. This could include characterization of which oligomeric species are populated and changes in oligomerization propensity. Furthermore, as the LGMD1D-associated mutations are dominant [40], it would be interesting to investigate whether the presence of wild type and LGMD1D-associated DnaJB6 (as would be observed in the heterozygotic state) results in hetero-oligomers with altered properties.

Overall structural change C-terminal of residue 1-130 caused by LGMD1D-associated mutations could be detected by recording ^{1}H-^{15}N correlation spectra of mutated full length DnaJB6 and overlaying with the spectrum of wild type DnaJB6.

4.4.3 Oligomerization

The oligomerization site and interaction in DnaJB6 could be further explored by mutational study. Deletion and C-terminal truncation constructs could be used to narrow down the position of the oligomerization site. Additionally, mutation of more charge-blocks (as defined in figure 1.7) and possibly combinations of charge-blocks to neutralize charge could clarify whether these do indeed contribute to the oligomerization interaction. A potential synergistic or additive effect of mutation of charge-blocks and phenylalanines could be investigate with mutant constructs

combining these mutations. Additionally, charged residues could be "scrambled" to neutralize blocks of charge in the sequence without affecting amino acid content, as done in the study of Ddx4 [47].

Establishing the relationship between oligomerization and holdase activity requires further work. The mutation of Phe-residues in the F6A construct, shown here to lower oligomerization propensity, is a first step towards obtaining a monomeric DnaJB6 mutant, which could be tested for holdase activity.

4.4.4 Structural characterization

Monomeric DnaJB6 should be characterizable by NMR, if a reliable way to disrupt oligomerization is found. The dependence of oligomerization on ionic strength, 1,6-hexanediol and mutation of Phe-residues shown in this work provide potential methods. Monomeric DnaJB6 should allow for assignment of the protein, making feasible dynamics measurements, determination of binding sites of interaction partners and potentially solving of the DnaJB6 monomer structure.

4.5 Conclusion

An expression and purification protocol for full length DnaJB6 was established based on previously published purifications. Produced DnaJB6 was confirmed to be correctly folded and functional, as demonstrated by CD-spectroscopy and a holdase activity assay based on inducible insulin aggregation.

Full length DnaJB6 was characterized by NMR. A ^{1}H-^{15}N correlation spectrum under conditions where DnaJB6 is oligomeric was recorded. The spectrum indicates that regions in the SBD or CTD of DnaJB6 are flexible, potentially disordered, and that there is a folded region C-terminal of the J-domain. Additionally, the spectrum indicates that the residue 75-80 poly-Gly region of DnaJB6 is a flexible

linker. However, these structural properties require further characterization.

The properties of polydisperse oligomerization of DnaJB6 were investigated. A preliminary native MS spectrum of DnaJB6 revealed a polydisperse distribution of oligomers from 10- to 15-mers with both odd and even oligomers populated. Mutation of 6 Phe-residues to Ala in the residue 139-188 region of DnaJB6 resulted in a decrease in oligomerization propensity, as characterized by DLS. Additionally, the mutation of 5 Arg-residues in the residue 125-136 positive charge-block to Lys and Ala resulted in a slight decrease in oligomerization propensity, but the significance of this result remains unclear. 1,6-hexanediol was shown by DLS to disrupt DnaJB6 oligomerization. Along with predicted intrinsic disorder, high G/F-content and the role of Phe-residues in the oligomerization interaction, this system seems analogous to the interactions of FG-repeat regions in nucleoporins of the NPC.

Holdase activity was measured as a function of ionic strength, disrupting DnaJB6 oligomerization. At monomeric conditions, DnaJB6 holdase activity was abolished, indicating that oligomerization is necessary for holdase activity. However, this finding requires verification by monomerization with an orthogonal variable to ionic strength.

The effect of LGMD1D-associated mutations F89I, F91L and F93L was investigated in a residue 1-130 truncation construct of DnaJB6. NMR was used to determine CSPs, revealing that the J-domain is structurally perturbed by these mutations. The positions of CSPs were structurally interpreted using previously obtained NMR data on DnaJB6 secondary structure and a homology model based on the structure of DnaJ2 from *T. thermophilus*. CSPs are clustered in helix I, III and IV, while helix II and the HPD-motif are less structurally perturbed.

The effect of LGMD1D-associated mutations on the stimulation of HSP70 ATPase activity by DnaJB6 was investigated. Stimulation of HSP70 ATPase activity

was not significantly affected by these mutations. This is consistent with helix II and the HPD-motif being the least structurally affected region of the J-domain from mutation. Which function of DnaJB6 is then affected by LGMD1D-associated mutations requires further investigation.

5
Appendix

DnaJB6 N-terminal strep tag:

WSHPQFEKGGGSGGGSGGSAWSHPQFEKSGMGENLYFQGAMVDYYEVLGVQRHASPE
DIKKAYRKLALKWHPDKNPENKEEAERKFKQVAEAYEVLSDAKKRDIYDKYGKEGLN
GGGGGGSHFDSPFEFGFTFRNPDDVFREFFGGRDPFSFDFFEDPFEDFFGNRRGPRG
SRSRGTGSFFSAFSGFPSFGSGFSSFDTGFTSFGSLGHGGLTSFSSTSFGGSGMGNF
KSISTSTKMVNGRKITTKRIVENGQERVEVEEDGQLKSLTINGKEQLLRLDNK

DnaJB6 C-terminal strep tag:

MVDYYEVLGVQRHASPEDIKKAYRKLALKWHPDKNPENKEEAERKFKQVAEAYEVLS
DAKKRDIYDKYGKEGLNGGGGGGSHFDSPFEFGFTFRNPDDVFREFFGGRDPFSFDF
FEDPFEDFFGNRRGPRGSRSRGTGSFFSAFSGFPSFGSGFSSFDTGFTSFGSLGHGG
LTSFSSTSFGGSGMGNFKSISTSTKMVNGRKITTKRIVENGQERVEVEEDGQLKSLT
INGKEQLLRLDNKENLYFQGASAWSHPQFEKGGGSGGGSGGSAWSHPQFEKSGMG

HSC70:

WSHPQFEKGGGSGGGSGGSAWSHPQFEKSGMRDAMSKGPAVGIDLGTTYSCVGVFQH
GKVEIIANDQGNRTTPSYVAFTDTERLIGDAAKNQVAMNPTNTVFDAKRLIGRRFDD
AVVQSDMKHWPFMVVNDAGRPKVQVEYKGETKSFYPEEVSSMVLTKMKEIAEAYLGK
TVTNAVVTVPAYFNDSQRQATKDAGTIAGLNVLRIINEPTAAAIAYGLDKKVGAERN
VLIFDLGGGTFDVSILTIEDGIFEVKSTAGDTHLGGEDFDNRMVNHFIAEFKRKHKK
DISENKRAVRRLRTACERAKRTLSSSTQASIEIDSLYEGIDFYTSITRARFEELNAD
LFRGTLDPVEKALRDAKLDKSQIHDIVLVGGSTRIPKIQKLLQDFFNGKELNKSINP
DEAVAYGAAVQAAILSGDKSENVQDLLLLDVTPLSLGIETAGGVMTVLIKRNTTIPT
KQTQTFTTYSDNQPGVLIQVYEGERAMTKDNNLLGKFELTGIPPAPRGVPQIEVTFD
IDANGILNVSAVDKSTGKENKITITNDKGRLSKEDIERMVQEAEKYKAEDEKQRDKV
SSKNSLESYAFNMKATVEDEKLQGKINDEDKQKILDKCNEIINWLDKNQTAEKEEFE
HQQKELEKVCNPIITKLYQSAGGMPGGMPGGFPGGGAPPSGGASSGPTIEEVD

DnaJB6 1-130:

WSHPQFEKGGGSGGGSGGSAWSHPQFEKSGMGENLYFQGAMVDYYEVLGVQRHASPE
DIKKAYRKLALKWHPDKNPENKEEAERKFKQVAEAYEVLSDAKKRDIYDKYGKEGLN
GGGGGGSHFDSPFEFGFTFRNPDDVFREFFGGRDPFSFDFFEDPFEDFFGNRRGPR

Strep-tag TEV-protease cleavage site Protein residue 1

Figure 5.1: Amino acid sequence of protein constructs with Strep-tag and TEV-cleavage site labelled.

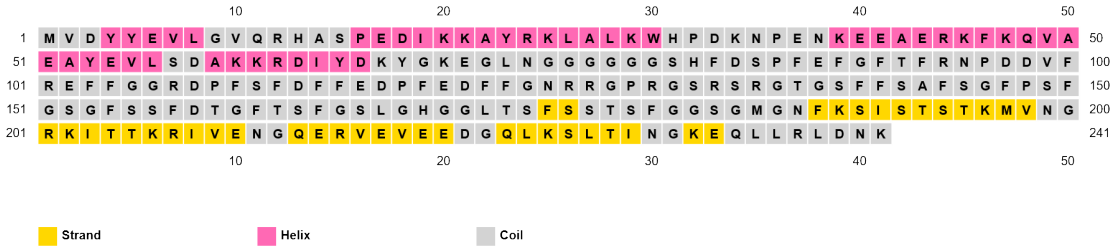

Figure 5.2: DnaJB6 amino acid sequence with secondary structure prediction (PSIPRED [67]).

Table 5.1: Alignments % sequence identity

	DnaJB6a	DnaJB6b	DnaJB1	DnaJB8
DnaJB6a	100	96.27	35.09	62.17
DnaJB6b	96.27	100	41.95	64.78
DnaJB1	35.09	41.95	100	35.35
DnaJB8	62.17	64.78	35.35	100

Table of % sequence identity between aligned amino acid sequences in figure 5.3.

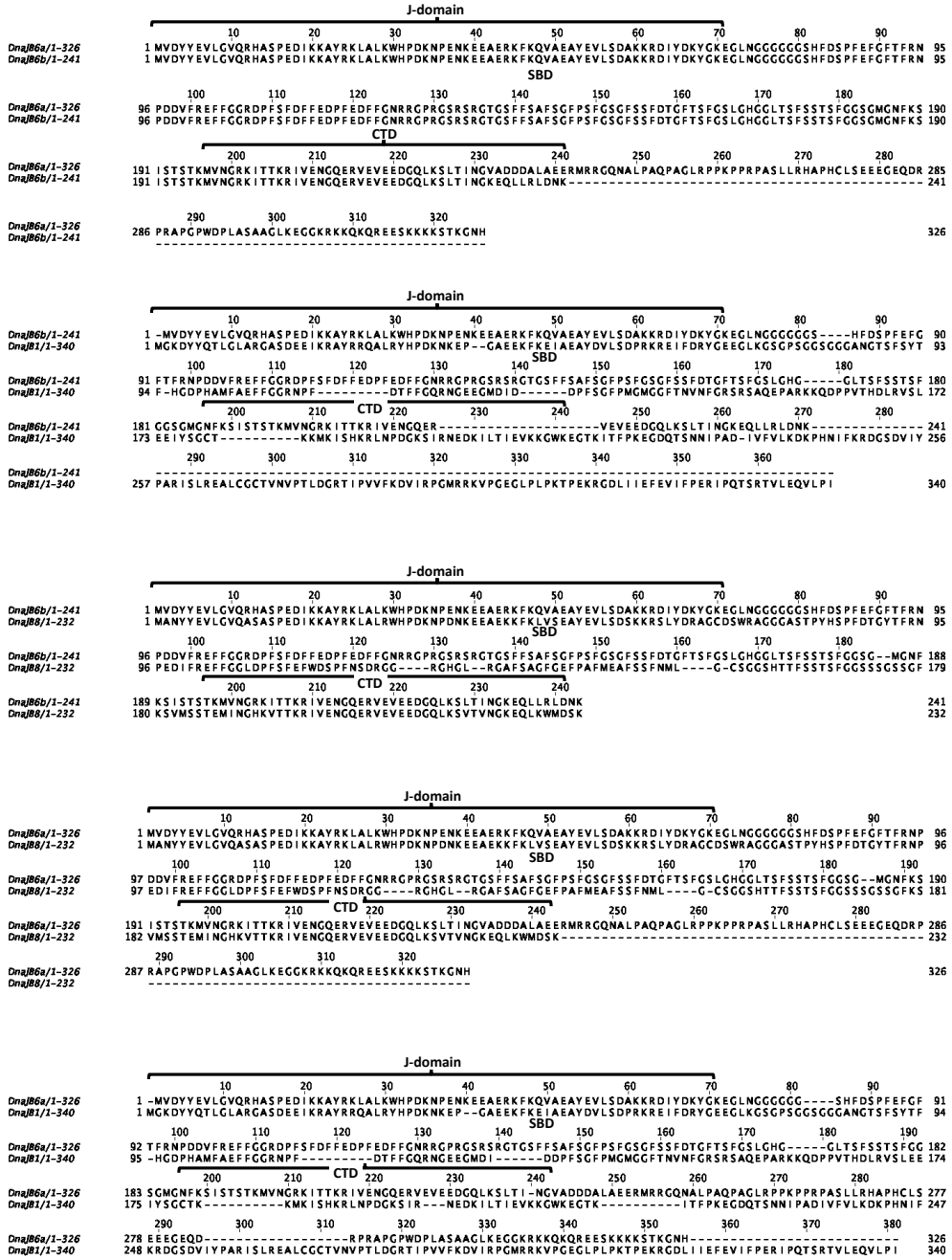

Figure 5.3: Protein sequence alignments. Alignments of amino acid sequences of human DnaJB6a and DnaJB6b to each other, DnaJB1 and DnaJB8. Sequence alignments were performed using ClustalΩ with default setting [68]. J-domain, substrate binding domain (SBD) and C-terminal domain (CTD) of DnaJB6 are labelled.

Bibliography

[1] David Balchin, Manajit Hayer-Hartl, and F Ulrich Hartl. In vivo aspects of protein folding and quality control. *Science*, 353(6294):aac4354, jul 2016.

[2] David J Brockwell and Sheena E Radford. Intermediates: ubiquitous species on folding energy landscapes? *Current opinion in structural biology*, 17(1):30–37, feb 2007.

[3] Aaron R Dinner, Andrej Šali, Lorna J Smith, Christopher M Dobson, and Martin Karplus. Understanding protein folding via free-energy surfaces from theory and experiment. *Trends in Biochemical Sciences*, 25(7):331–339, jul 2000.

[4] Anne Gershenson, Lila M Gierasch, Annalisa Pastore, and Sheena E Radford. Energy landscapes of functional proteins are inherently risky. *Nature chemical biology*, 10(11):884–891, nov 2014.

[5] Rina Rosenzweig, Nadinath B Nillegoda, Matthias P Mayer, and Bernd Bukau. The Hsp70 chaperone network. *Nature Reviews Molecular Cell Biology*, 2019.

[6] Yujin E Kim, Mark S Hipp, Andreas Bracher, Manajit Hayer-Hartl, and F Ulrich Hartl. Molecular Chaperone Functions in Protein Folding and Proteostasis. *Annual Review of Biochemistry*, 82(1):323–355, jun 2013.

[7] Robert Schinzel and Andrew Dillin. Endocrine aspects of organelle stress — cell non-autonomous signaling of mitochondria and the ER. *Current Opinion in Cell Biology*, 33:102–110, 2015.

[8] Rebecca C Taylor and Andrew Dillin. Aging as an event of proteostasis collapse. *Cold Spring Harbor perspectives in biology*, 3(5):a004440, may 2011.

[9] Clemens Scheufler, Achim Brinker, Gleb Bourenkov, Stefano Pegoraro, Luis Moroder, Hans Bartunik, F.Ulrich Hartl, and Ismail Moarefi. Structure of TPR Domain–Peptide Complexes: Critical Elements in the Assembly of the Hsp70–Hsp90 Multichaperone Machine. *Cell*, 101(2):199–210, 2000.

[10] J Höhfeld, D M Cyr, and C Patterson. From the cradle to the grave: molecular chaperones that may choose between folding and degradation. *EMBO reports*, 2(10):885–890, oct 2001.

[11] Szymon Ziętkiewicz, Agnieszka Lewandowska, Paweł Stocki, and Krzysztof Liberek. Hsp70 Chaperone Machine Remodels Protein Aggregates at the Initial Step of Hsp70-Hsp100-dependent Disaggregation. *Journal of Biological Chemistry*, 281(11):7022–7029, mar 2006.

[12] Szymon Żwirowski, Agnieszka Kłosowska, Igor Obuchowski, Nadinath B Nillegoda, Artur Piróg, Szymon Ziętkiewicz, Bernd Bukau, Axel Mogk, and Krzysztof Liberek. Hsp70 displaces small heat shock proteins from aggregates to initiate protein refolding. *The EMBO journal*, 36(6):783–796, mar 2017.

[13] Rui Sousa and Eileen M Lafer. Keep the traffic moving: mechanism of the Hsp70 motor. *Traffic (Copenhagen, Denmark)*, 7(12):1596–1603, dec 2006.

[14] Elizabeth A Craig. Hsp70 at the membrane: driving protein translocation. *BMC biology*, 16(1):11, jan 2018.

[15] Marta Stankiewicz, Rainer Nikolay, Vladimir Rybin, and Matthias P Mayer. CHIP participates in protein triage decisions by preferentially ubiquitinating Hsp70-bound substrates. *The FEBS Journal*, 277(16):3353–3367, aug 2010.

[16] M P Mayer and B Bukau. Hsp70 chaperones: cellular functions and molecular mechanism. *Cellular and molecular life sciences : CMLS*, 62(6):670–684, mar 2005.

[17] Harm H. Kampinga and Elizabeth A. Craig. The HSP70 chaperone machinery: J proteins as drivers of functional specificity. *Nature Reviews Molecular Cell Biology*, 11(8):579–592, 2010.

[18] Roman Kityk, Jürgen Kopp, and Matthias P Mayer. Molecular Mechanism of J-Domain-Triggered ATP Hydrolysis by Hsp70 Chaperones. *Molecular Cell*, 69(2):227–237.e4, 2018.

[19] Joyce Tsai and Michael G Douglas. A Conserved HPD Sequence of the J-domain Is Necessary for YDJ1 Stimulation of Hsp70 ATPase Activity at a Site Distinct from Substrate Binding *. *The Journal of Biological Chemistry*, 271(16):9347–9354, 1996.

[20] Jingzhi Li, Xinguo Qian, and Bingdong Sha. Heat shock protein 40: structural studies and their functional implications. *Protein and peptide letters*, 16(6):606–612, 2009.

[21] Junbin Hu, Yunkun Wu, Jingzhi Li, Xinguo Qian, Zhengqing Fu, and Bingdong Sha. The crystal structure of the putative peptide-binding fragment from the human Hsp40 protein Hdj1. *BMC structural biology*, 8:3, jan 2008.

[22] Bingdong Sha, Soojin Lee, and Douglas M Cyr. The crystal structure of the peptide-binding fragment from the yeast Hsp40 protein Sis1. *Structure*, 8(8):799–807, aug 2000.

[23] Elisabeth Hartmann, Ralf Seidel, Robert L Shoeman, and Sabine Zimmermann. Combining crystallography and EPR : crystal and solution structures of the multidomain cochaperone DnaJ research papers. *Biological Crystallography*, D69:1540–1552, 2013.

[24] K Huang, J M Flanagan, and J H Prestegard. The influence of C-terminal extension on the structure of the "J-domain" in E. coli DnaJ. *Protein science : a publication of the Protein Society*, 8(1):203–214, jan 1999.

[25] Glaucia M S Pinheiro, Gisele C Amorim, Anwar Iqbal, Fabio C L Almeida, and C H I Ramos. Solution NMR investigation on the structure and function of the isolated J-

domain from Sis1 : Evidence of transient inter-domain interactions in the full-length protein. *Archives of Biochemistry and Biophysics*, 669(February):71–79, 2019.

[26] Jaime L Stark, Kamiya Mehla, Nina Chaika, Thomas B Acton, Rong Xiao, Pankaj K Singh, Gaetano T Montelione, and Robert Powers. Structure and function of human DnaJ homologue subfamily a member 1 (DNAJA1) and its relationship to pancreatic cancer. *Biochemistry*, 53(8):1360–1372, mar 2014.

[27] M K Greene, K Maskos, and S J Landry. Role of the J-domain in the cooperation of Hsp40 with Hsp70. *Proceedings of the National Academy of Sciences of the United States of America*, 95(11):6108–6113, may 1998.

[28] Won-Chul Suh, William F Burkholder, Chi Zen Lu, Xun Zhao, Max E Gottesman, and Carol A Gross. Interaction of the Hsp70 molecular chaperone, DnaK, with its cochaperone DnaJ. *Proceedings of the National Academy of Sciences*, 95(26):15223 LP – 15228, dec 1998.

[29] Atta Ahmad, Akash Bhattacharya, Ramsay A McDonald, Melissa Cordes, Benjamin Ellington, Eric B Bertelsen, and Erik R P Zuiderweg. Heat shock protein 70 kDa chaperone/DnaJ cochaperone complex employs an unusual dynamic interface. *Proceedings of the National Academy of Sciences of the United States of America*, 108(47):18966–18971, nov 2011.

[30] Jin Hae Kim, T Reid Alderson, Ronnie O Frederick, and John L Markley. Nucleotide-dependent interactions within a specialized Hsp70/Hsp40 complex involved in Fe-S cluster biogenesis. *Journal of the American Chemical Society*, 136(33):11586–11589, aug 2014.

[31] Thomas Reid Alderson, Jin Hae Kim, and John Lute Markley. Dynamical Structures of Hsp70 and Hsp70-Hsp40 Complexes. *Structure (London, England : 1993)*, 24(7):1014–1030, jul 2016.

[32] Naohiko Seki, Atsushi Hattori, Akiko Hayashi, Sumie Kozuma, Nobuyuki Miyajima, and Toshiyuki Saito. Cloning, tissue expression, and chromosomal assignment of human MRJ gene for a member of the DNAJ protein family. *Journal Of Human Genetics*, 44:185, may 1999.

[33] Jen-Zen Chuang, Hui Zhou, Meicai Zhu, Shi-Hua Li, Xiao-Jiang Li, and Ching-Hwa Sung. Characterization of a Brain-enriched Chaperone, MRJ, That Inhibits Huntingtin Aggregation and Toxicity Independently. *Journal of Biological Chemistry*, 277(22):19831–19838, may 2002.

[34] Maria A.W.H. van Waarde, Ron P. Dirks, Henderika M.J. Oosterveld-Hut, Vaishali Kakkar, Harm H. Kampinga, Nicolette H. Lubsen, Maria A. Rujano, Natalia Govorukhina, and Jurre Hageman. A DNAJB Chaperone Subfamily with HDAC-Dependent Activities Suppresses Toxic Protein Aggregation. *Molecular Cell*, 37(3):355–369, 2010.

[35] Cecilia Månsson, Vaishali Kakkar, Elodie Monsellier, Yannick Sourigues, Johan Härmark, Harm H. Kampinga, Ronald Melki, and Cecilia Emanuelsson. DNAJB6 is a peptide-binding chaperone which can suppress amyloid fibrillation of polyglutamine peptides at substoichiometric molar ratios. *Cell Stress and Chaperones*, 19(2):227–239, 2014.

[36] Niels J. Kloosterhuis, Harm H. Kampinga, Sara Linse, Cecilia Månsson, Bart van de Sluis, Cecilia Emanuelsson, Marianne van der Zwaag, Christopher M. Dobson, Salam Al-Karadaghi, Gillian P. Bates, Remco T.P. van Cruchten, Eduardo P. de Mattos, Tuomas P.J. Knowles, Steven Bergink, Vaishali Kakkar, Ronald Melki, Maria A.W.H. van Waarde, Paolo Arosio, and Jan M. van Deursen. The S/T-Rich Motif in the DNAJB6 Chaperone Delays Polyglutamine Aggregation and the Onset of Disease in a Mouse Model. *Molecular Cell*, 62(2):272–283, 2016.

[37] Cecilia Månsson, Remco T.P. Van Cruchten, Ulrich Weininger, Xiaoting Yang, Risto Cukalevski, Paolo Arosio, Christopher M. Dobson, Tuomas Knowles, Mikael Akke, Sara Linse, and Cecilia Emanuelsson. Conserved S/T Residues of the Human Chaperone DNAJB6 Are Required for Effective Inhibition of Aβ42 Amyloid Fibril Formation. *Biochemistry*, 57(32):4891–4892, 2018.

[38] Francesco A. Aprile, Emma Källstig, Galina Limorenko, Michele Vendruscolo, David Ron, and Christian Hansen. The molecular chaperones DNAJB6 and Hsp70 cooperate to suppress α-synuclein aggregation. *Scientific Reports*, 7(1):1–11, 2017.

[39] Vijay Kumar, Neha Sami, Tara Kashav, Asimul Islam, Faizan Ahmad, and Md. Imtaiyaz Hassan. Protein aggregation and neurodegenerative diseases: From theory to therapy. *European Journal of Medicinal Chemistry*, 124:1105–1120, 2016.

[40] Maria Barbara Pasanisi, Simona Saredi, Marina Mora, Lorenzo Maggi, Simona Zanotti, and Alessandra Ruggieri. DNAJB6 Myopathies: Focused Review on an Emerging and Expanding Group of Myopathies. *Frontiers in Molecular Biosciences*, 3(September), 2016.

[41] Jaakko Sarparanta, Per Harald Jonson, Christelle Golzio, Satu Sandell, Helena Luque, Mark Screen, Kristin McDonald, Jeffrey M Stajich, Ibrahim Mahjneh, Anna Vihola, Olayinka Raheem, Sini Penttilä, Sara Lehtinen, Sanna Huovinen, Johanna Palmio, Giorgio Tasca, Enzo Ricci, Peter Hackman, Michael Hauser, Nicholas Katsanis, and Bjarne Udd. Mutations affecting the cytoplasmic functions of the co-chaperone DNAJB6 cause limb-girdle muscular dystrophy. *Nature genetics*, 44(4):450–S2, feb 2012.

[42] Songqing Li, Peipei Zhang, Brian D Freibaum, Nam Chul Kim, Amandine Molliex, Anderson P Kanagaraj, Ichiro Yabe, Shinya Tanaka, Hidenao Sasaki, Eric D Ross, J Paul Taylor, and Hong Joo Kim. Genetic interaction of hnRNPA2B1 and DNAJB6 in a Drosophila model of multisystem proteinopathy. *Human Molecular Genetics*, 25(5):936–950, 2016.

[43] Rocio Bengoechea, Sara K Pittman, Elizabeth P Tuck, Heather L True, and Conrad C Weihl. Myofibrillar disruption and RNA-binding protein aggregation in a mouse model of limb-girdle muscular dystrophy 1D. *Human molecular genetics*, 24(23):6588–6602, dec 2015.

[44] Morten Rasmussen, Christopher A. G. Söderberg, Johan Härmark, Sreekanth Rajan, Gudrun Rutsdottir, Katja Bernfur, Cecilia Emanuelsson, Salam Al-Karadaghi, Peter Höjrup, Hans Hebert, and Cecilia Månsson. Structural modelling of the DNAJB6 oligomeric chaperone shows a peptide-binding cleft lined with conserved S/T-residues at the dimer interface. *Scientific Reports*, 8(1):1–15, 2018.

[45] Bin Xue, Roland L Dunbrack, Robert W Williams, A Keith Dunker, and Vladimir N Uversky. PONDR-FIT: a meta-predictor of intrinsically disordered amino acids. *Biochimica et biophysica acta*, 1804(4):996–1010, apr 2010.

[46] Steven Boeynaems, Simon Alberti, Nicolas L Fawzi, Tanja Mittag, Magdalini Polymenidou, Frederic Rousseau, Joost Schymkowitz, James Shorter, and Benjamin Wolozin. Protein Phase Separation : A New Phase in Cell Biology. *Trends in Cell Biology*, 28(6):420–435, 2018.

[47] Timothy J Nott, Evangelia Petsalaki, Julie D Forman-kay, Andrew J Baldwin, Timothy J Nott, Evangelia Petsalaki, Patrick Farber, Dylan Jervis, Eden Fussner, Anne Plochowietz, Timothy D Craggs, David P Bazett-jones, Tony Pawson, Julie D Forman-kay, and Andrew J Baldwin. Phase Transition of a Disordered Nuage Protein Generates Environmentally Responsive Article Phase Transition of a Disordered Nuage Protein Generates Environmentally Responsive Membraneless Organelles. *Molecular Cell*, 57(5):936–947, 2015.

[48] Robert McCoy Vernon, Paul Andrew Chong, Alaji Bah, Hong Lin, Patrick Farber, Brian Tsang, Tae Hun Kim, and Julie Deborah Forman-Kay. Pi-Pi contacts are an overlooked protein feature relevant to phase separation. *eLife*, 7:1–48, 2018.

[49] Sigrid Milles, Davide Mercadante, Iker Valle Aramburu, Malene Ringkjøbing Jensen, Niccolò Banterle, Christine Koehler, Swati Tyagi, Jane Clarke, Sarah L Shammas, Martin Blackledge, Frauke Gräter, and Edward A Lemke. Plasticity of an ultrafast interaction between nucleoporins and nuclear transport receptors. *Cell*, 163(3):734–745, oct 2015.

[50] Loren E Hough, Kaushik Dutta, Samuel Sparks, Deniz B Temel, Alia Kamal, Jaclyn Tetenbaum-Novatt, Michael P Rout, and David Cowburn. The molecular mechanism of nuclear transport revealed by atomic-scale measurements. *eLife*, 4:e10027, sep 2015.

[51] Samir S Patel, Brian J Belmont, Joshua M Sante, and Michael F Rexach. Natively Unfolded Nucleoporins Gate Protein Diffusion across the Nuclear Pore Complex. *Cell*, 129(1):83–96, apr 2007.

[52] Michael T Marty, Andrew J Baldwin, Erik G Marklund, Georg K A Hochberg, Justin L P Benesch, and Carol V Robinson. Bayesian deconvolution of mass and ion mobility spectra: from binary interactions to polydisperse ensembles. *Analytical chemistry*, 87(8):4370–4376, apr 2015.

[53] Ewen Lescop, Paul Schanda, and Bernhard Brutscher. A set of BEST triple-resonance experiments for time-optimized protein resonance assignment. *Journal of Magnetic Resonance*, 187(1):163–169, 2007.

[54] Thomas Schulte-Herbrüggen and Ole Winneche Sørensen. Clean TROSY: Compensation for Relaxation-Induced Artifacts. *Journal of Magnetic Resonance*, 144(1):123–128, 2000.

[55] Frank Delaglio, Stephan Grzesiek, Geerten W Vuister, Guang Zhu, John Pfeifer, and Ad Bax. NMRPipe: A multidimensional spectral processing system based on UNIX pipes. *Journal of Biomolecular NMR*, 6(3):277–293, 1995.

[56] Michael Norris, Bayard Fetler, Jan Marchant, and Bruce A Johnson. NMRFx Processor: a cross-platform NMR data processing program. *Journal of Biomolecular NMR*, 65(3):205–216, 2016.

[57] Frank H Schumann, Hubert Riepl, Till Maurer, Wolfram Gronwald, Klaus-Peter Neidig, and Hans Robert Kalbitzer. Combined chemical shift changes and amino acid specific chemical shift mapping of protein–protein interactions. *Journal of Biomolecular NMR*, 39(4):275–289, 2007.

[58] Lawrence A Kelley, Stefans Mezulis, Christopher M Yates, Mark N Wass, and Michael J E Sternberg. The Phyre2 web portal for protein modeling , prediction and analysis. *Nature Protocols*, 10(6):845–858, 2015.

[59] Justin L P Benesch. Collisional Activation of Protein Complexes: Picking Up the Pieces. *Journal of the American Society for Mass Spectrometry*, 20(3):341–348, 2009.

[60] Georg K A Hochberg and Justin L P Benesch. Dynamical structure of a B-crystallin. *Progress in Biophysics and Molecular Biology*, 115:11–20, 2014.

[61] Sonja Kroschwald, Shovamayee Maharana, and Simon Alberti. Hexanediol: a chemical probe to investigate the material properties of membrane-less compartments. *Matters*, may 2017.

[62] Melanie C O'Brien and David B McKay. How Potassium Affects the Activity of the Molecular Chaperone Hsc70: I. POTASSIUM IS REQUIRED FOR OPTIMAL ATPase ACTIVITY . *Journal of Biological Chemistry*, 270(5):2247–2250, feb 1995.

[63] Harold P Erickson. Size and shape of protein molecules at the nanometer level determined by sedimentation, gel filtration, and electron microscopy. *Biological procedures online*, 11:32–51, may 2009.

[64] W Yan and E A Craig. The glycine-phenylalanine-rich region determines the specificity of the yeast Hsp40 Sis1. *Molecular and cellular biology*, 19(11):7751–7758, nov 1999.

[65] Judit Perales-Calvo, Arturo Muga, and Fernando Moro. Role of DnaJ G/F-rich domain in conformational recognition and binding of protein substrates. *The Journal of biological chemistry*, 285(44):34231–34239, oct 2010.

[66] Michael Sattler and Stephen W Fesik. Use of deuterium labeling in NMR: overcoming a sizeable problem. *Structure*, 4(11):1245–1249, 1996.

[67] David T Jones. Protein secondary structure prediction based on position-specific scoring matrices by G. Von Heijne. *Journal of Molecular Biology*, 292(2):195–202, 1999.

[68] Fabian Sievers, Andreas Wilm, David Dineen, Toby J Gibson, Kevin Karplus, Weizhong Li, Rodrigo Lopez, Hamish McWilliam, Michael Remmert, Johannes Söding, Julie D Thompson, and Desmond G Higgins. Fast, scalable generation of high-quality protein multiple sequence alignments using Clustal Omega. *Molecular Systems Biology*, 7(1):539, jan 2011.